UNIVERSITY OF
LIVERPOOL
Department of Chemistry

Polymer Routes Toward Designing Gold Nanostructures

Thesis submitted in accordance with the requirements of

the University of Liverpool for the degree of Doctor in Philosophy

by

Nicolas Schaeffer

January 2010

Supervizors:

Prof. Andrew I. Cooper
Dr. Raphaël Lévy

Examiners:

Prof. Mathias Brust
Prof. Wolfgang. Parak

Polymer Routes Toward Designing Gold Nanostructures.

Nicolas Schaeffer

Abstract

The formation of small metallic particles has been intensively investigated in the last few decades because of the unique properties that they exhibit on the nanometer scale. A handful of reliable and straightforward synthetic procedures are used routinely for their manufacture. The most widely applied procedures are variations of the Turkevich–Frens citrate reduction route that allow the manufacture of water–soluble, relatively monodisperse particles in the *c.a.* 5 to 50 nm range, or the Brust–Shiffrin method that leads, after reduction of a gold precursor in a two phases liquid/liquid system, to the formation of hydrophobic nanoparticles in the *c.a.* 3 to 8 nm. However, the controlled manufacture of well–defined water–soluble particles in the sub 5 nm scale is still challenging, and most of the reported methods for their preparation involve multip–step preparation or cumbersome size separation procedure, adding costly and time consuming stages to the synthesis. Thus, a simple, robust protocol for the gram-scale preparation of uniform colloidal gold below 5 nm is of broad practical value.

Herein, the synthesis of near monodisperse gold nanoparticles using series of water-soluble polymeric ligands containing a thiol and/or a thioether is described. The size of the so–formed particles can be adjusted between one and five nanometres by varying the polymer/gold ratio and the colloidal suspensions are stable in aqueous conditions because of the nature of their polymeric protective monolayer. Those polymeric structures have been optimized to control the growth of the particles, leading to an unprecedented narrow size distribution. The near monodispersity of the particles, their stability in aqueous conditions, and their one–pot synthesis all make this method an attractive and versatile synthetic route.

Furthermore, in extending the size–range tunability of some of those polymer stabilized gold nanoparticles to the sub 2 nm range, a transition between non–fluorescent and fluorescent nanoparticles is observed. This photophysical property is clearly size–dependant and fluorescence switching is detected for polymer-stabilized gold clusters below 1.7 nm in size. Detailed characterization indicates that the most fluorescent nanomaterial has a 3% quantum yield and is related to the presence of 1.1 nm gold core and a 6.9 nm hydrodynamic radius gold clusters and is not due to a polymer effect, nor to the formation of a gold(I) complex.

Acknowledgments

The author addresses his sincere gratitude to Pr. Andrew I. Cooper and Dr. Raphaël Lévy for supervising this project and to EPSRC for funding it.

Chapters 2 and 3 report the finalization of a research work started by Dr. Irshad Hussain, Dr. Zhenxin Wang and Dr. Bien Tan under the supervision of Pr. Andrew I. Cooper and Pr. Mathias Brust. The mass spectrometry data were obtained from the EPSRC National Mass Spectrometry Service Centre in Swansea, thanks to Dr. Mark F. Wyatt.

Numerous collaborators have been involved during the research carried out for the fourth Chapter; thus, Dr. Catherine Barentin and Dr. Laure Petit (Université Lyon I) are credited for the FRAP experiments, Pr. Brahim Lounis and Dr. Stéphane Berciaud (Université Bordeaux I) for the photothermal microscopy, Pr. Molly M. Stevens, Dr. Anna Laromaine (Imperial College London) and Dr. Calum Dickinson for HR–TEM studies, Dr. David G. Spiller for the fluorescence microscopy, and Dr. Sven Schroeder (University of Manchester) and Dr. Elizabeth Willneff for surface analysis, and Dr. Abbie Trewin for the simulation.

In a more general manner, the author also thanks all his coworkers, collaborators, and all those who, in their own ways, have been helping at different levels. Finally, M. Havelaar and P. Morris are greatly acknowledged; the redaction of this manuscript would have been hardly possible without them.

Contents

List of Figures

List of Tables

List of Abbreviations.

^{1}H NMR	Proton nuclear magnetic resonnance.
AIBN	2,2',N,N'–azobis(2-methylpropionitrile).
ATRP	Atom transfer radical polymerisation.
AuNP	Gold nanoparticle.
CTA	Chain transfer agent.
CTP	Chain transfer polymerization.
DAC	Di–ammonium hydrogen citrate.
DDT	Dodecane–1–thiol.
DHB	2,5-dihydroxybenzoic acid.
DLS	Dynamic light scattering.
DLVO	Derjaguin and Landau, Verwey and Overbeek.
DOS	Density of states.
EDT	2–ethanedithiol.
eV	Electronvolt.
EXAFS	Extended X–ray absorption fine structure.
FRAP	Fluorescence recovery after photobleaching.
GPC	Gel permeation chromatography.
HeptT	Heptane–1–thiol.
HR–TEM	High resolution transmission electron microscopy.
ICP–AES	Inductively coupled plasma atomic emission spectroscopy.
IR	Infra red.
IXB	Ion exchange beads.
kJ	Kilojoule.
LDI	Laser desorption/ionization .

M_n	Number average molecular weight.
M_w	Weight average molecular weight.
MALDI	Matrix–assisted laser desorption/ionizationi.
MAT	Mercaptoacetic acid.
MeO-PEG-SH	Thiol-terminated poly(ethylene glycol) monomethyl ether.
MES	2,2–mercaptoethylsulfide.
MS	Mass spectrometry.
NaOAc	Sodium acetate.
NDT	1,9–nonanedithiol.
nm	Nanometer.
ODT	Octadecane–1–thiol.
pAA	Polyacrylic acid.
PAMAM	Polyamidoamine.
PDI	Polydispersity index.
pDMAEMA	Polydimethylamino ethyl methacrylate.
pEGMA	Poly(ethyleneglycol)methacrylate.
PentT	Penatne–1–thiol.
pHEA	Polyhydroxyethyl acrylate.
pMAA	Polymethacrylic acid.
pNIPAM	poly(N–isopropylacrylamide).
PropT	Propane–1–thiol.
PTMP	Pentaerythritol tetrakis(3-mercaptopropionate).
pVP	Polyvinylpyrollidone.
pVSA	Polyvinylsulfonic acid.
QD	Quantum dot.
QY	Quantum yield.
SPR	Surface plasmon resonnance.
TEM	Transmission electron microscopy.
TFA	Triuoroacetic acid.
THAP	2,4,6-trihydroxy acetophenone.
THF	Tetrahydrofuran.

TOAB   Tetraoctylammonium bromide.

TOF   Time of flight.

UV   Ultra violet.

W   Watt.

XPS   X–ray photoelectron spectrooscopy.

Chapter 1

Introduction

1.1 "The world of neglected dimensions" [1]

THE GENESIS OF nanotechnology can be said to have started in 1959 with R.P. Feynman's lecture *"There's plenty of room at the bottom"* in which he described the possibility of building new mechanical, electronic and biological systems that might be created by manipulating materials at the atomic scale, and thus foresaw the beginning of a trend that helped scientists develop the fields of electronics, communications, genetics, biotechnology, materials design and much more through improving control of matter at the nanoscale.[1] However, the first occurrence of the term "nanotechnology" comes from N. Taniguchi who, in 1974. described a science that "consists of the processing of, separation, consolidation, and deformation of materials by one atom or by one molecule.[2,3]

Following Feynman's lecture, an increasing growth of research in the manipulation of matter at the nanometer scale has been observed, driven by the need of understanding the fundamental of the science and its potential applications in a wide range of applications, such as sensors,[4-6] catalysis,[7,8] solar cells,[9,10] fuel cells,[11] photonics and optoelectronics,[12] medical diagnostics,[13] cell labeling,[14-16] information storage,[17] nonlinear optics,[18,19] computer architecture,[20] and environmental protection[21,22] to name but a few.

Nowadays, nanotechnology can be described not only as an area of science in itself, but as various techniques and processes that have been developed for building structures at the nanometer scale, and which can be used in various scientific areas, such as physics,

---

[1]Wolfgang Ostwald (1883 - 1943) , *Die Welt der vernachlässigten Dimensionen*, **1914**
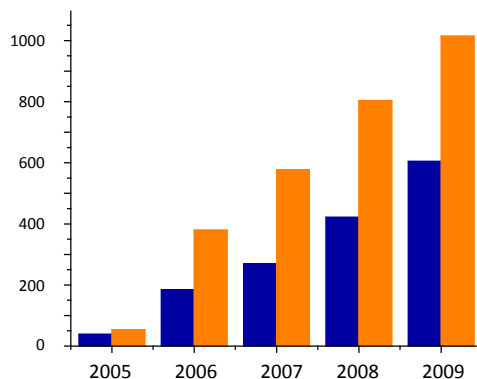
Figure 1.1: Growth in the number of manufacturer–identified, nanotechnology–enabled products listed on Project on Emerging Nanotechnologies Consumer Products Inventory from 2005 to 2009 (in orange) showing products under possible Consumer Product Safety Commission jurisdiction (blue). [26]

chemistry, engineering or biosciences, thus allowing an exchange of knowledge in the development of a broad interdisciplinary field. [23,24]

Over the last decades, the manufacture of various materials at the nanoscale (*i.e.* carbon nanotubes, fullerenes, nanoparticles, nanorods, *etc. . .*) [25] have been developed, some of them being already industrially produced and commercially available. Figure 1.1 shows the evolution of the "nanomarket" growth, depicting the number of "manufacturer–identified, nanotechnology–enabled products" inventoried by the official US Consumer Product Safety Commission and the Project on Emerging Nanotechnologies. [26]

Most applications reported in this inventory concern "first generation" of passive nanomaterials such as titanium dioxide in sunscreen, cosmetics and some food products; silver in food packaging, clothing, disinfectants and household appliances; zinc oxide in sunscreens and cosmetics, surface coatings, paints and outdoor furniture varnishes; and cerium oxide as a fuel catalyst. [26]

Due to the increasing interest in this field and its ability to be applied to different research and industrial areas, Taniguchi's definition was re–defined by the US National Nanotechnology Initiative Committee which described nanotechnology as a science which: [25]

- involves research and technology development at the 1nm – 100nm range.

- creates and uses structures that have novel properties because of their small size.

- builds on the ability to control or manipulate at the atomic scale.

The novelty of nanoscale materials arises from the fact that with decreasing size, the properties of materials change drastically from the bulk. The variations in the properties of nano–objects can be ascribed to two effects. The first is related to the number of surface atoms that is larger in nanoscaled structures than in the bulk, leading to dramatic differences of the materials surface properties. The second effect can be ascribed to the properties of the "inside" core of the structures that can exhibit quantum sized effects and unique electronic structure.[27,28] However the observed differences between nanostructures and their bulk counterparts are not only a result of scaling factor, but can result from different factors for different materials.[29–31]

1.2 The case of metallic and gold nanoparticles

Among all the materials that have been studied, particular attention has been focused on the synthesis and the study of noble metal and gold nanoparticles.[29]

Indeed, if gold, in its bulk state, is known to be one of the least reactive metal that can be found into the periodic classification, small aggregates of gold atoms exhibit interesting physical, optical and chemical properties due to the large amount of gold surface area available.[32]

Gold nanoparticles or colloids are made of the aggregation of a few metallic gold atoms (Au^0), the size of these aggregates ranging between a few hundreds to one nanometer (or even below). Those aggregates, to be stable in solution, are generally surrounded by a protective layer which purpose is to avoid further aggregation or coagulation between the particles. This layer, that can be a polymer, an organic or biologic molecule, play an important role as a stabilizing agent. It also governs some of the properties of the particles and of this layer depends the particles solubility, optical properties, and ability to integrate into larger nanostructures or connect to biomolecules.

Gold colloids have been widely studied due to their relative good stability at the nanoscale (less noble metals tend to be easily oxidized), their electronic conduction behavior, their optical properties and their unique surface chemistry that allows them to be used on their own, or as building blocks in bigger self–assembled structures.[28,33–35]

Overall, a good understanding and control of the essential properties of gold nanoparticles allows their use in number of potential applications to areas such as catalysis, biosciences, materials chemistry, optics, *etc...* [28,34]

1.3   Historical background on colloidal gold

Nanosized structures, and particularly metallic nanoparticles are known to have been used since at since the 4th century *B.C.* for decorative purpose with the romans using metal colloids to manufactur colored glasses and ceramics.[36] An archetypical artifact from this period is the Lycurgus cup that was made from soda lime glass containing gold and silver particles.[37,38] The cup has an optical dichroic effect that makes it appear red colored in transmission and green colored in reflected light due to the presence of the nanoparticles inside the glass (see Figure 1.2).[39,40] The use of gold colloids for decoration have probably first been described in the literature by the florentine glass maker, herbalist and alchemist Antonio Neri in 1612, in his treatise *L'Arte Vetraria* (the Art of Glass);[41,42] a glass colorant, named the "Purple of Cassius", resulting from the coagulation of gold particles and tin dioxide, became popular in the 17th century.[43]

The so–called "soluble gold" was also known in ancient Egypt and China for its curative purpose and was believed during the Middle Ages to be able to cure various disease (venereal diseases, dysentery, epilepsy, *etc...*). The therapeutical effects of gold colloids were reported for the first time in *"panacea aurea auro portabile"* by Francisci Antonii in 1618 in which he describes the formation of colloidal gold and its medical use.[44,45] Another report of the use of "drinkable gold" was described by Johann Kunckels in his book *"Aurum Potabile oder Gold Tinstur"* in which he mentions "drinkable gold that contains metallic gold in a neutral, slightly pink solution that exert curative properties for several diseases" and speculates on the structure of the gold compound to be "gold [that] must be present in such a degree of comminution that it is not visible to the human eye".[45–47] A more complete review on colloidal gold was published in the

Figure 1.2: The Lycurgus cup in transmission (right hand side) and reflected (left hand side) light.

17th century by Hans Heinrich Helcher, who notably commented on the need for gold colloid to be stabilized using boiled starch (see Section 1.4).[33,47,48] Finally, the first attempted explanation of the gold sols color was achieved in 1818 by Jeremias Benjamin Richters in *"Über die neueren Gegenstände in der Chemie"* (New chemical facts), where he suggested that the observed pink or purple sols contains gold in a "finest degree of subdivision", in comparison to yellow solutions formed after particles aggregation.[47,49]

However, more systematic study of the structure and the properties of colloidal gold may be told to have started in the second part of the 19th century with the research of Michael Faraday and the study of aqueous colloidal solutions of gold particles and the reported formation of deep red solutions of colloidal gold by reduction of an aqueous solution of chloroaurate ($AuCl_4^-$) using phosphorus in CS_2 and the description of particular interaction of light with metal particles depending on the state of polarization of the gold matter (see Figure 1.3). This investigation marked the foundation of modern colloid science.[50]

Nowadays, various methods for the preparation of gold colloids have been reported and reviewed.[34,35,51–53] In the past decades, the preparation of gold colloids of different sizes, shapes and functionalities have been the subject of a considerably increased number of books and reviews.[34,53–56] Some of the methods used routinely for the production of gold particles are described in Section 1.5.

Figure 1.3: Faraday's colloidal gold dispersed on a glass slide.

1.4 Stability of colloidal dispersions

The chemical stability of the particles is crucial to avoid degradation processes such as partial oxidation or undesired sintering of particles.

Indeed, small metal particles are unstable with respect to agglomeration to the bulk, and one of the most crucial aspect of colloid chemistry that have to be considered is the means by which such particle suspensions are stabilized in the medium in which they are dispersed.[34,35]

The behavior of small particles dispersion is mostly dependent of the Van der Waals attraction forces due to the polarization of the metal cores, and the Brownian motion (see Section 1.8.3).[35] Van der Waals forces are weak and are only significant for short inter–particles distances. However, since the Brownian motion ensure continuous colliding of the particles in the media, the combination of those two forces leads to irreversible aggregation and coagulation in the absence of repulsive forces to counteract these attractive forces. Such counteractions can be achieved by two means, that are an electrostatic stabilization by creating a distribution of charged species in the system and/or a steric stabilization which involves the adsorption of molecules or macromolecules onto the particles surfaces.

1.4.1 Electrostatic stabilization

Electrostatic stabilization is based on the coulombic repulsions forces created between the particles in solution when a double electrical layer is present at their surfaces. Gold surfaces are generally hydrophylic, thus, anionic species (citrates, hydroxyls, chlorides, *etc. . .*) are attracted to those surfaces. The so–called double layer is formed by those anions and the corresponding counter ions in solution. (see Figure 1.4a).
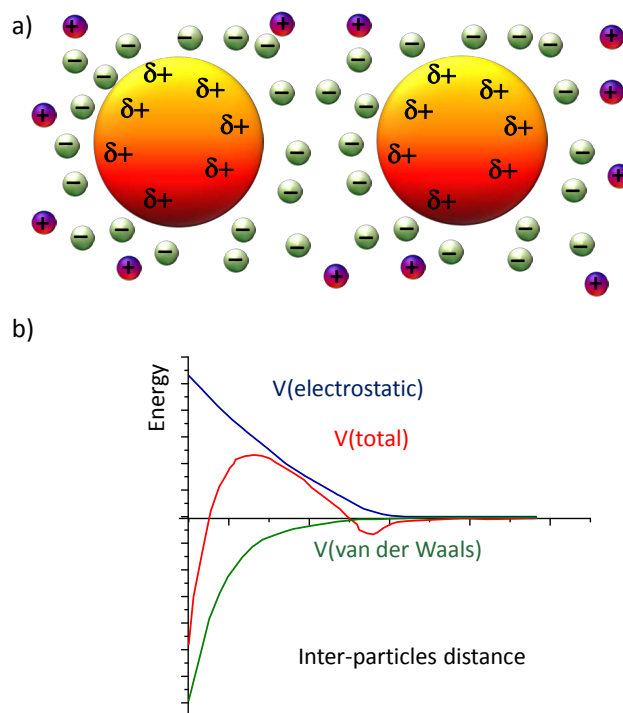
Figure 1.4: a) Electrostatic stabilization of colloidal gold and b) plot of the free energy against inter–particle distance for electrostatic stabilization.

The structure and stability of a colloidal dispersion is successfully described, in the case of a purely electrostatic stabilization, by the DLVO theory (Derjaguin, Landau and Verwey, Overbeek). This theory rely on the fact that the stability of a particle in solution is dependent on its total potential energy function V_T, with V_T being described as a balance between the two antagonist contributions of V_A the Van der Waals attractive forces and V_R the electrostatic repulsive forces.

The evolution of the total energy as a function of the inter–particles distance function is written as:

$$V_T = V_A - V_R = 2\pi\epsilon_0\epsilon_\tau r\varphi_0^2.e^{-\kappa D} - \frac{Ar}{12D} \tag{1.1}$$

where ϵ_0 is the permitivity of the vacuum, ϵ_τ is the permitivity of the medium in the diffusion layer, φ_0 the surface potential, κ^{-1} the double layer thickness, r the particle radius and D the inter–particles distance.

The plot of equation 1.1 presented in Figure 1.4b show that if two particles have a sufficiently high repulsion, the dispersion will resist flocculation and the colloidal system will be stable. However if a repulsion mechanism does not exist then flocculation or coagulation will eventually take place.

1.4.2 Steric stabilization

Steric (or polymeric) stabilization deals with the coordination of long organic molecules that can act as a protective layer on the gold surface. Metallic particles are thus separated from each other because of those chains which are preventing aggregation. The most commonly used species for steric stabilization all contains electronegative end–functionalities (nitrogen, phosphorus or suphur containing molecules)[28,34] that can adsorb onto the gold surface; such adsorption can be either due to weak physisorption or chemical bonding between the metallic atoms and the stabilizing molecule.

When two particles, their surfaces covered by a suitable stabilizer, approach to each other, the attached molecules or polymers interact with each other if the inter–particle distance becomes less than twice the thickness of the polymeric layer, assuming that the particles are dispersed in a good solvent (in which the stabilizer chains expand, see Figure 1.5a).

If the stabilizer coverage is high enough, the two molecular or polymeric layers are compressed, leading to a coiling up of the stabilizer and an increase of the overall free energy. For low surface coverage under the same conditions, the two stabilizer layers inter–penetrate each other so as to reduce the available space between polymer chains, leading to a reduction of entropy ΔS and again, to an increase of the free energy $\Delta G = \Delta H - \Delta S$.

In order to overcome those effects, the system will tend to repulse two particles so as the inter–particle distance is at least twice the thickness of the protective layer.

Furthermore, an osmotic effect takes place due to the high polymer concentration within the volume between two particles.

The variation of energy as a function of inter–particles distance is presented in Figure 1.5b).
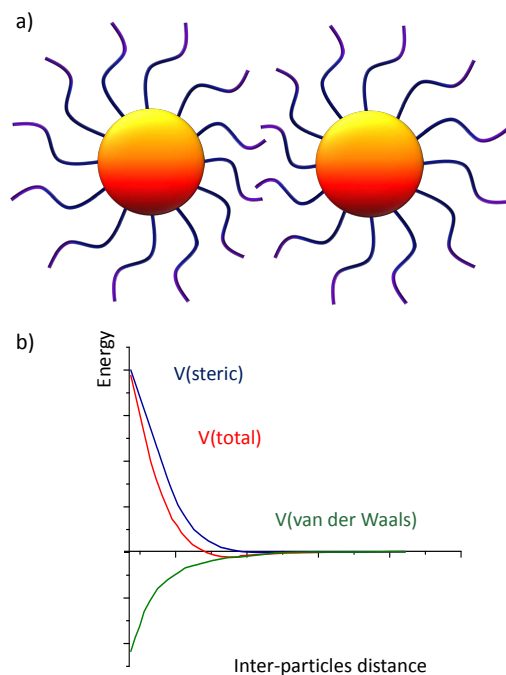
Figure 1.5: a) Steric stabilization of colloidal gold and b) plot of the free energy against inter–particle distance for steric stabilization.

1.4.3   Electrosteric stabilization

Colloidal stabilization can also be achieved by a combination of those two effects when a relatively long molecule or polymer that can bear charges is used as a stabilizer. This kind of electrosteric stabilization has been reported using long–chains alcohols,[57,58] surfactants[59,60] or organometalic species.[61,62]

1.5   Synthetic methods

There are many well–defined synthetic ways that are routinely used for the production of gold nanoparticles. Those methods can be classified in two series. The first series is the so–called top–down approach, that involves the sub–division of bulk material into smaller structures. This is generally achieved by physical processes, such as laser ablation[63,64] or gas deposition[65] for instance. However, those processes generally lead to the formation of relatively large, and non uniform particles, which is an important drawback for various applications.[66]

The second method, namely the "bottom–up" approach, deals with the controlled aggregation of atoms (or sometimes molecules) and the formation of smaller structures, with well–defined shapes and, in general, a relatively narrow size distribution (compared to the top–down approach).[67] The bottom–up approach is thus an interesting way for the reproducible manufacturing of well defined particles in the nanometer or sub–nanometer scale. It can be achieved by means of various chemical processes, such as thermal, sonochemical or photochemical decomposition of a gold precursor,[8,28,68–70] electrochemical reduction,[71–73] metal vapor synthesis,[74,75] or by chemical reduction of a metal salt.[76–79]

Because it's probably the easiest and most straightforward way of chemically producing gold particles, the chemical reduction of a gold salt in the presence of a suitable stabilizing agent has been widely employed and is the most popular method for producing gold nanoparticles. Different variations of this procedure have been developed, but all of them are based on the same principle, that is the reduction of a gold salt (containing in general gold atoms with an oxidation state of $+I$ or $+III$) to a zero–valent gold atom during the primary stage of the formation of gold particles, or their nucleation.[80] These metallic gold atoms are drawn to each other in solution due to the Van der Waals attraction forces, and collide to form small aggregates of metallic gold, or seeds. The size of those seeds is dependent on the redox potential of the gold and the reducer that is been used, a stronger reducing agent leading to smaller seeds.[80]

Many reducing agents have been used, but the most common ones are hydrides / borohydrides of alkali metals (such as $NaBh_4$ for instance). Those reducers have been extensively used for the synthesis of gold particles in aqueous conditions, or in a two–phases system. Their alkyl analogues have also been employed for the synthesis in an organic media.[78,81] H_2 and CO have also been used as gaseous reducing agents with various metal salts.[82,83] It has also been shown that some common solvents, such as alcohols, THF and DMF have the ability to reduce metallic salts.[84] Sodium citrate[79] and hydrazine[83,85] have also been used (see Sections 1.5.1 and 1.5.2).

The two methods which are currently predominantly used are the gold precursor reduction by citrates and the two–phase liquid–liquid system.

1.5.1 The Turkevich–Frens method

This synthesis have been discovered by Turkevich *et al.* in 1951[51] and further developed by Frens in 1973.[52] It is used to produce modestly monodisperse spherical gold nanoparticles suspended in water, their sizes ranging between 10 to 50 nm in diameter. Larger particles can be produced, but this comes at the cost of size dispersion and shape.[52]

This synthesis relies on the reduction of $HAuCl_4$ by trisodium citrate in water. The so–formed particles are stabilized electrostatically, the citrate molecules acting as both reducing agents and stabilizers.[86,87] This method is very often used even now when a rather loose shell of ligands is required around the gold core in order to prepare a precursor to "valuable" gold nanoparticles materials.

1.5.2 The Brust–Schiffrin method

After Schmid *et al.* first reported the formation of stable $Au_{55}(PPh_3)_{12}Cl_6$ clusters with a narrow size dispersion (1.4 ± 0.4 nm) for the study of a quantum–dot nanomaterial in 1981,[88] the synthesis of sub 5 nm gold particles remained unexplored for some years. However, after Giersig *et al.* described the stabilization of gold particles using alkanethiols of different chain lengths in 1993,,[89] Brust *et al.* published in 1994 the synthesis of thermally stable and air–stable gold particles of relatively narrow size dispersion and controlled size (ranging in diameter between 1.5 and 5.2 nm) for the first time. The technique of synthesis, inspired by Faraday's two–phase system[50] uses thiol–containing ligands that strongly bind to gold due to the soft character of both gold and sulphur. This synthesis consists on the transfer of $AuCl_4^-$ species from an aqueous phase to toluene by means of tetraoctylammonium bromide (TOAB) as a phase–transfer reagent, and the subsequent reduction of the gold by $NaBH_4$ in the presence of dodecanethiol (or thiol containing organic molecules).[78,81] Murray *et al.* have extended the solubility possibilities of these materials by using place–exchange reactions of one thiol for another.[90,91]

This synthetic method is now days routinely used for the preparation of small and stable metal particles dispersed in organic solvents.

1.5.3 Other methods

The two phase liquid–liquid method of synthesis has been extended to many other organo–soluble ligands, such as phosphines (PPh$_3$, tri–n–octylphosphine),[61,92] that prove to be a valuable alternative to thiols. Also, microemulsions involving the presence of amphiphiles as surfactants or block copolymers, in the presence or in the absence of thiol ligands, have been effectively used to obtain stable water– or oil–soluble particles.[59,60] The syntheses involve a two–phase system with a surfactant that causes the formation of the microemulsion or the micelle maintaining a favorable microenvironment, together with the extraction of metal ions from the aqueous phase to the organic phase. This dual role of the surfactant and the interaction between the thiol and the AuNP surface control the growth and stabilization of the AuNP or nanocrystal, yielding a relatively narrow size distribution.[93–95]

1.6 Nucleation, growth, size control and surface properties

The synthesis of gold nanoparricles involves three stages, that are a primary nucleation step that describes the aggregation of a few gold atoms due to the van der Waals attractive forces, a growth step, and a termination step driven by the adsorption of the capping agent.[34,79,96]

The nucleation and growth process are governed by two competing factors, that are bonding effects and electronic in origin (due to the filling of electronic or atomic shells) and the packing of gold atoms that is steric in nature.[97,98] These processes are kinetically and/or thermodynamically controlled and hence, sensitive to experimental conditions (concentrations of reactants, temperature, solvent, *etc* . . .)

The nucleation process describes the formation of simple polyhedral structures of low nuclearity, such as tetrahedrons or icosahedrons. Those primary clusters can be considered as building blocks for the growth mechanism and the formation of secondary clusters. The formation of those secondary clusters happens either by layer–by–layer addition of gold atoms onto the primary clusters, or by shell–by–shell growth, *i.e.* by condensation of primary clusters.[97,98] The growth process is terminated by the adsorption of the stabilizing molecule onto the so–formed gold surface.
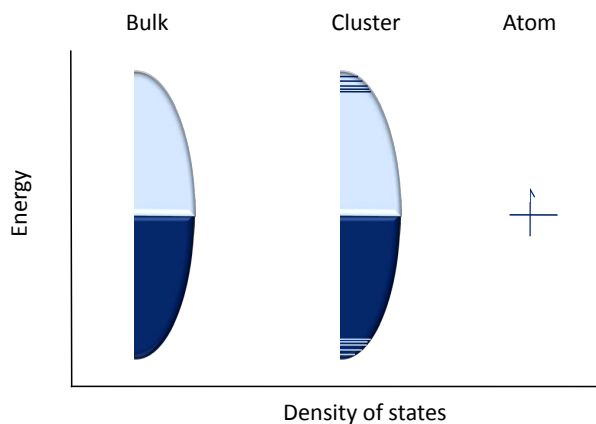
Figure 1.6: Density of states for metal clusters. The density of states is discrete at the band edges.

Hence, whatever the synthetic method that is used for the production of particles, the size of the so–formed particles depends on the relative concentration of stabilizing agent and their distribution in size tend to follow a Gaussian distribution, the dispersion in size being greatly dependent on the method used, and on the three stages described above.[96]

1.7   Physical and chemical properties

Optical and electronic properties of materials are strongly dependent of their electronic energy levels and density of states (DOS). For materials with their dimensions in the nanometer scale, those parameters vary as a function of their size, inducing dramatic changes in their behaviors compared with those of the bulk state.

1.7.1   Electronic properties and quantum size effect

The electronic structure of a small gold (or metal) cluster vary from the bulk and is dependent on the size of the considered cluster. In the case of particles or clusters small enough (typically below 2 nm),[99–101] the energy levels are discontinuous, by opposition to the bulk. The small size of the cluster leads to a confinement of the electron wave function, and the apparition of discrete energy states. The electronic energy between successive quantum levels δ is given by:
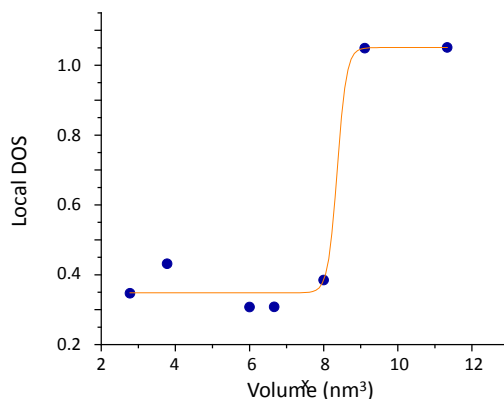
Figure 1.7: Variation of the nonmetallic band gap with nanocrystal volume for gold nanocrystals deposited on a graphite surface estimated by scanning tunneling spectroscopy.[102]

$$\delta = \frac{4E_F}{3n} \tag{1.2}$$

where E_F is the Fermi energy level and n the total number of valence electrons.

This particularity have a strong influence on the particles conductivity properties, making it behave as an insulator for $\delta < kT$ or as a conductor for $\delta > kT$ (with $k = 1.3810^{-23} J.K^{-1}$ the Boltzmann constant and T the temperature in kelvin).[103] The apparition of discrete energy states also have a strong effect on the magnetic properties of the particles.[94]

The electronic structure of metal particles of various sizes was studied by X–ray photoelectron spectroscopy and it has been observed that the binding energy (BE) of the metal clusters tend to increase when their size is decreased, such effect thought to be due to poor screening of the core hole created by the x–ray absorption and being a indication of the transition from metallic to non–metallic properties of the considered particles (see Section 1.8.6 and Sections 4.4.2.3 and 4.4.1 in Chapter 4).[104–107]

Information on the electronic gap of gold nanocrystals were obtained by STM study by Vinod *et al.* on gold crystals of varying size, and it has been shown that the transition between metallic to non–metallic particles occurs for sizes of approximately 1 nm (see Figure 1.7 and Chapter 4 Section 4.4.2.1).[102]
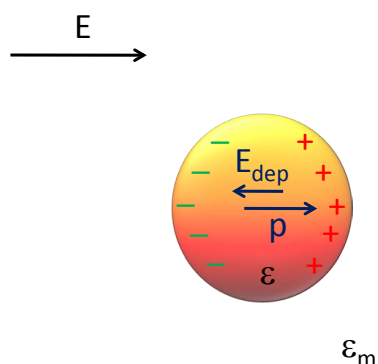
Figure 1.8: Interactions between a metallic sphere and an external electromagnetic field.

1.7.2 Optical response of a gold particle and surface plasmon resonance

The interactions between an electromagnetic field E and a small metallic sphere of dielectric constant ϵ_m in an homogeneous media of dielectric constant $_m$ have been described by the Mie theory.

The external electromagnetic field creates a force onto the electronic layer at the surface of the particle, polarizing this electronic shell and creating negative charges on one side of the particle (and thus, a positive charge on the other side) as described in Figure 1.8. A force E_{dep} is thus created to depolarize this anisotropic charge density. The two antagonist forces E and E_{dep} leads to an oscillation of the electronic shell around the particle (see Figure 1.9).[103] When the wavelength of this "electronic oscillation" is resonant with the applied electronic field, this one is then absorbed and this absorbance can be detected by spectroscopic methods. Such resonance is known as surface plasmon resonance (SPR, see Section 1.8.1).

The resonance wavelength is dependent on many parameters, that are the nature of the metallic sphere, the dielectric constant of the media, the size and shape of the particles.[108–110] The surface resonance plasmon of gold particles of various sizes is presented in Figure 4.7.
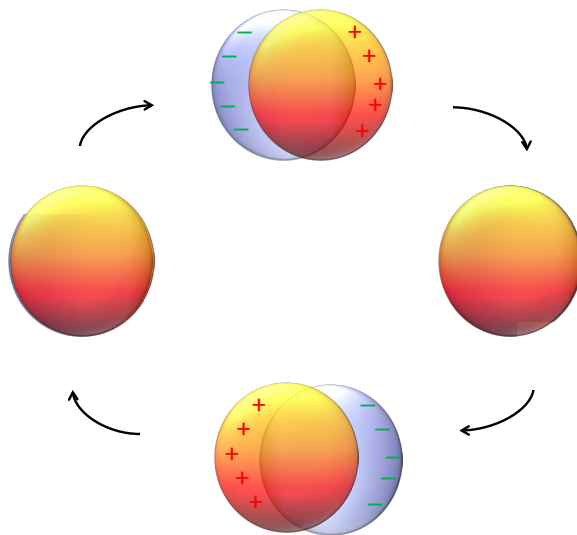
Figure 1.9: Representation of the surface resonance plasmon. The gray ares corresponds to the electronic layer surrounding the particle.

1.8 Analytical methods

Since the physical and chemical properties of nanostructures are mainly governed by their composition, structure, size, shape and surface properties, their accurate characterization is crucial for assessing those parameters and understanding their effect on the intrinsic properties of the materials. Thus, series of analytic tools have been developed for this purpose. Electron microscopes,[111] atomic force microscopy (AFM),[112] scanning probe microscopy (STM),[113] for example, can be used for structural analysis of nanomaterials. Spectroscopic techniques, such as UV visible absorption spectroscopy or Raman spectroscopy can also be used to reach information on the optical properties of the materials.[114–116] The various techniques used to characterize the structures mentioned in this manuscript are described below.

1.8.1 UV–visible spectroscopy

UV–visible absorption spectroscopy is widely used for the characterization of gold (or metallic) nanoparticles because they exhibit distinct colors (see Figure 1.10a) This is due to the absorption of the light by the oscillation of the particle's electronic layer (see Section 1.7.2) The resonance plasmon band (and thus, the color of the colloidal suspensions) is characteristic of the particles nature, size, shape or assembly,[28,117] on

a)

Particles diameter

3nm   9nm   22nm 48nm 99nm

b)
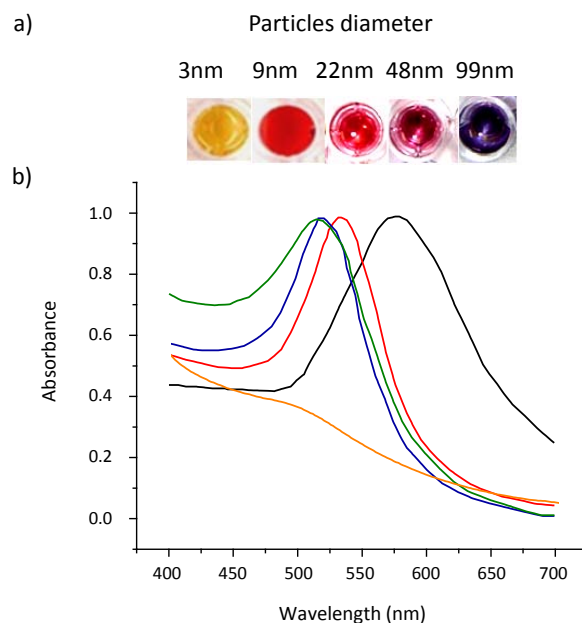
Figure 1.10: Typical UV–visible absorption spectra of aqueous suspensions of gold nanoparticles of 3nm (orange line), 9 nm (green line), 22 nm (blue line), 48 nm (red line) and 99 nm (black line)in diameter.

the refractive index of the surrounding medium[118] and on the nature of their protective layer.[119,120] The plasmon band intensity and broadness is dependent on the colloidal suspension concentration (and extinction coefficient) and its size dispersion respectively.[119,120] The resonance plasmon of gold particles of increasing size is presented in Figure 1.10b.[117]

Particles smaller than three nanometer in diameter does not show any plasmon band (Figure 1.10b, orange line). This difference in the UV–visible absorption profile stems from the discrete electronic energy levels that arise for small clusters (see Section 1.7.1).[121]

1.8.2   Transmission electron microscopy

Transmission electron microscopy (TEM) is a powerful imaging technique used to determine the shape and size of materials at the nanometer scale. Electron microscopes use in essence the same working principle than light microscopes, both techniques relying on the focusing an electron or a light beam through magnetic or optical lenses respectively.[111] The resolution r for both types of microscopes is defined by

$r = 0.61 \times \lambda \times \mu(\alpha)$ where λ is the wavelength of the incident beam, μ is the refractive index of the medium and α is the semi–angle of the microscope aperture.[122,123]

Since the wavelength of electrons is about ten thousand times smaller than the photons wavelength, the resolution of an electronic microscope is thus (in theory) about the same order higher than an optical microscope resolution, allowing imaging of nano–objects in the nanometer scale (however, TEM resolutions are limited by lenses aberration).[122]

In conventional TEM, a thin specimen is irradiated with an accelerated electron beam of uniform current density. Electrons are emitted from the electron gun and illuminate specimen through a two or three stage condenser lens system. The transmitted electron beam is magnified with a three or four stage lens system. TEM collects its data from electrons that are transmitted (or diffracted) through the sample. Materials for TEM must be thin enough (ly 10 to 100 nm) to transmit sufficient electrons such that sufficient intensity falls on the screen or photographic film to give an interpretable image in a reasonable time.[123]

1.8.3 Dynamic light scattering

Dynamic light scattering (DLS) is a fast and straightforward method to measuring the size of colloids in suspension. It involves the measuring of the radiations scattered at an angle $\theta = 90°$ originating from the passing of a laser beam through a dilute sample of colloidal suspension. Since the particles in suspension are in constant movement, due to molecules of solvent hitting them and creating the stochastic motion, or Brownian motion, and since their movement becomes faster with their size decreasing , the incident light at a wavelength λ is scattered after crossing the sample, with the scattered light having a time–dependent wavelength equal to $\lambda + \Delta\lambda$; the signal detected is an interferogram, due to the random motion of the particles in solution. Analysis of those interferences $\Delta\lambda$ yields to the diffusion coefficient of the suspensions, which in turn can be related to the particles hydrodynamic radii.[124,125]

One advantage of DLS over other size characterization methods such as TEM and SEM is this technique can study large samples of particle in solution. Consequently, in combination with TEM results, more complete information on the particle sizes can be

provided (see Chapter 3 Section 3.4.2).

1.8.4 Mass spectrometry

Mass spectrometry is seen as a useful tool for the characterization of gold clusters or their protective layer, and conventional laser desorption and electron impact mass spectrometry have been used for the characterization of cluster–like compounds. However, those techniques are severely limited due to the need of thermal stability and volatility of the analyte.

Atom bombardment mass spectrometry have been successfully applied on gold clusters.[126,127] In these techniques, the gold clusters and ligand shell are fragmented by a beam of rare gas atoms, the fragments been eventually discriminated and detected according to their $\frac{m}{z}$ values. The so–acquired spectra show multiple peaks corresponding to various isotopic combinations of gold, stabilizer and gold/stabilizer molecular formula. However, the fragmentation of the gold core do not allow the determination of its overall mass.

The successful way for assessing the mass and size of gold clusters and/or their protective layer rely on the soft ionization of those compounds. Matrix–assisted laser desorption/ionization mass spectrometry (MALDI MS) allow this type of ionization by using a suitable matrix and avoiding degradation of the analyte within the ionization chamber. Previous studies show that the major ionization effect is the loss of Au / Au–S moieties from the main fragment ion, thus leaving the metallic core intact for its mass analysis.[128,129] MALDI–MS is used for the structural analysis of a pMAA–PTMP polymer structure in Chapter 2 Section 2.3.5 and in Chapter 3 Section 3.3.1.5 for the analysis of pMAA–PTMP stabilized small clusters.

1.8.5 Fluorescence spectroscopy

Quantum dots (semi–conductor particles, or small metallic clusters) can undergo radiative desexcitation upon illumination, depending on their size, structure, or the nature of their protective layer.[130,131] Thus, fluorescence spectroscopy can be used for qualitative measurements of the average number of absorbed photons (excitation spectra) or re–emitted photons (emission spectra). It also allows the determination of the emissions and excitations wavelength, that can in turn be used to determine the energies
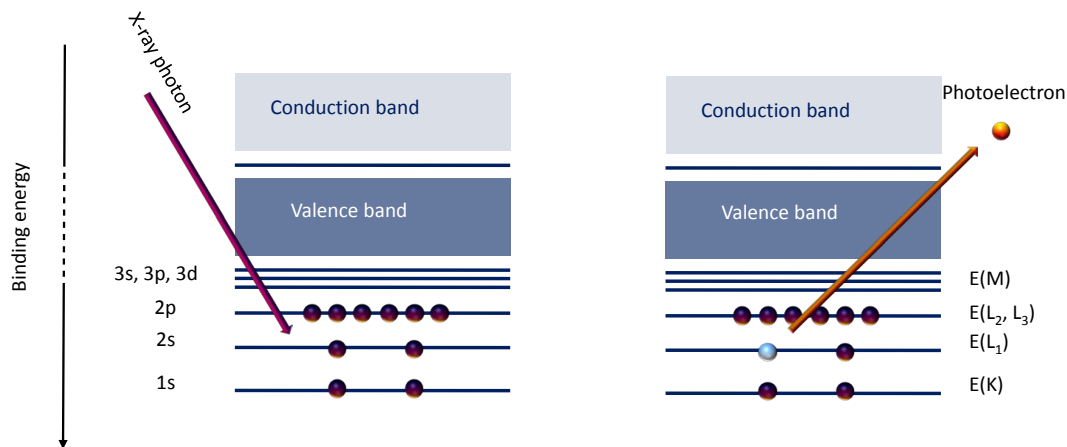
Figure 1.11: Schematic of photo–ionization during X–ray photoelectron spectroscopy

of the excitation/desexcitation processes, and thus help to determine the origin of the luminescence.

1.8.6   X–ray photoelectron spectroscopy

X–ray photoelectron spectroscopy consists in the blasting of a solid sample with X–ray photons, their energy being high enough to ionize the sample atoms and liberate a core electron in the vacuum.

The energy of the incoming X–ray beam is gradually increased; when it reaches a energy level high enough to ionize an core electron of an atom within the sample, the photo–ionization of the considered element occurs, due to the absorption of the X–ray photon and the excitation of this specific core electron. This photoelectron is thus released and can travel thought the surface to the vacuum, and hit a detector (see Figure 1.11).[132]

The x–ray photon energy needed to release an electron is characteristic of the electron binding energy (BE), and thus, of the considered element chemical nature and oxidation state.

X-ray photoelectron spectroscopy is a useful technique to investigate the overall charge state of metal clusters or particles and reach information on the clusters electronic structure since the binding energy shifts are sensitive to the local chemical environment, of the considered atom (see Chapter 4 Section 4.4.1).

1.8.7 Extended X–ray absorption fine structure

Extended X–ray absorption spectroscopy (XAS) is used to determine the radial proper-
ties of an element within the sample. A typical extended X–ray absorption fine structure
(EXAFS) experiment consists in blasting a sample with a monochromatic X–ray beam,
increasing gradually the photons energy. If the photon energy is below the absorption
edge of the elements present in the sample, it cannot excite the core electrons of this el-
ement. However, when the photon reaches energy values high enough to interact with a
core electron, a large absorption occurs, known as absorption edge. Like in XPS exper-
iments, this absorption leads to the formation of an hole in the core electronic structure
of the absorbing element, and the emission of a photoelectron which energy is equal to
the difference between the energy of the adsorbed photon and the binding energy of
the initial core state. These ejected photoelectrons have a relatively low kinetic energy
and interacts with other atoms surrounding the emitting elements, leading to a further
scattering events; this photoelectron can eventually be backscattered, depending on its
energy.[133,134]

The backscattered electron waves interfere with the forward–propagating waves, and
the resulting interference pattern shows up as a modulation of the measured absorption
coefficient, thereby causing the oscillation in the EXAFS spectra (see Figure 1.12).

The wavelength of the considered photoelectron is dependent on the energy and
phase of the backscattered wave that is present around the absorbing atom. This
wavelength varies as a function of the energy of the incoming photon, and the phase
and amplitude of the backscattered wave are dependent on the type of atom doing
the backscattering and the distance of the backscattering atom from the absorbing
atom.[135,136] Thus, from the evolution of the scattering wave, information on the chem-
ical coordination environment (oxidation state, inter–atom distance) of the absorbing
atom can be deduced.[137–139]

1.9 Using polymeric stabilizers

Amongst all the various methods for the formation and stabilization of gold nanoparti-
cles that have been studied, polymer embedded gold particles have received a particular
attention due to their physical and chemical characteristics, and their potential use in
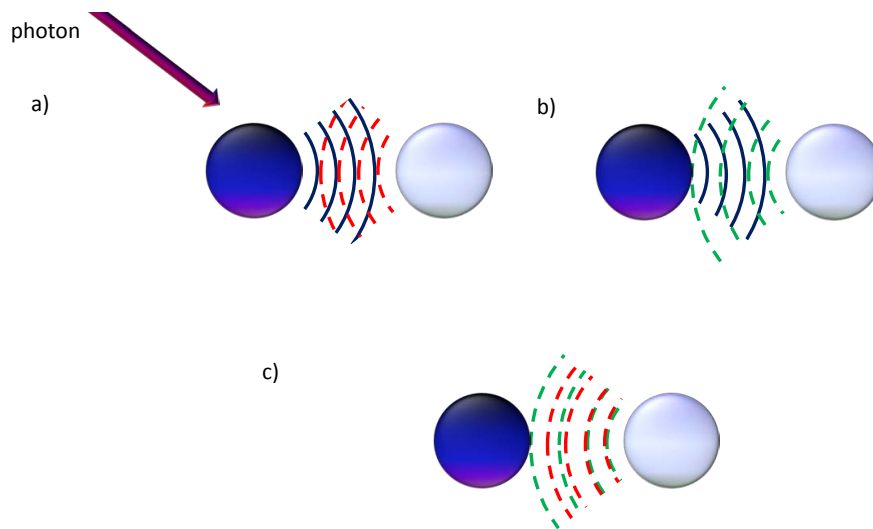
Figure 1.12: Schematic representation of the interactions between the emitted (blue) and two backscattered (red and green) photo–electron waves during EXAFS experiment and the creation of interferences (c) due to the backscattered electronic waves.

various applications.[140–142]

Indeed, gold–polymer composites are potentially useful as light color filters,[143] polarizers,[144,145] ultra–low refractive index materials,[146] nonlinear optical devices,[147] or optical sensors.[148]

However, synthetic routes for the production of core–shell composite metal nanoparticles with a polymer layer that may be physically or chemically bound to a metal core are still limited and the synthesis of monodisperse thiol–derivatized polymer embedded particles with controlled size and size distribution remains challenging.[95]

Most of the *"in situ"* reported methods for the synthesis of polymer embedded gold particles are variations of the Brust–Schiffrin method (see Section 1.5.2)[78,95] which lead to the formation of particles exhibiting a moderate size dispersion and can be applied to a limited number of alkanes or arenes compounds due to ligands solubility issues.[95] Furthermore, the particles size can only be slightly varied through varying the gold precursor concentration relatively to the stabilizing agent. Since gold particles properties are size dependent, the ability to fine–tune their dimensions is of critical importance.[77,95,140] For example, Carotenuto *et al.* have reported the mixing of polyvinyl pyrolidone (PVP) and ethyleneglycol with small quantities of concentrated solutions of $HAuCl_4$.[149,150] Such preparation leads to an Au–PVP composite that can then used

for the thiol–drerivatized gold preparation. Corbierre *et al.* also reported the synthesis of polystyrene–functionalized gold nanoparticles (PS–Au) by the covalent attachment of a thiol-terminated polystyrene prepared by anionic polymerization.[151] The use of few other polymeric structures have also been reported, such as polyethylene oxyde polypropylene oxide (star shape polymer structure,[152] or thiol end–functionalized polymer[153,154]), or poly(N–isopropylacrylamide).[155] However, those methods only allow a poor control on the size and size dispersion of the so–formed particles.

"Grafting from" approaches, *i.e.* the growth of a polymer chain from the gold surface carrying suitable polymerization–initiating species, have also been studied. Monomers have been polymerized from the particle surfaces via various polymerization processes. Oxazolines have been successfully polymerized at the surface of gold particles by cationic polymerization.[156] Polymethacrylic acid was also polymerized in a similar manner.[157] Low *et al.* reported the polymerization of various block co–polymers on gold surfaces by radical addition fragmentation (RAFT) polymerization has also been reported.[158] Atom transfer radical polymerization (ATRP) have also been used.[159]

However, those methods remains relatively expensive, time consuming, and are greatly dependent on the nanoparticles stability in the experimental polymerization conditions.

1.10 Thesis outline

The work presented hereby reports the synthesis of series of linear water–soluble polymer ligands, and the use of these ligands for the stabilization of gold nanoparticles in the aim to achieve good size control over the particles, and improved size dispersion.

Chapter 2 reports the synthesis and characterization of series of polymers prepared via chain–transfer polymerization, each series focusing on the variation of a specific parameter of the polymeric structure. The studied parameters comprise the nature of the polymer backbone (Section 2.3.1), the length and average molecular weight (M_n) of the polymer chains (Section 2.3.2), the hydrophobicity of the polymers functional end–groups (Section 2.3.3) and the use of multi–functional end–groups (Section 2.3.4).

The following Chapter (Chapter 3) treats of the formation and characterization of gold nanoparticles using the polymeric structures described in Chapter 2 as steric or

electrosteric stabilizers. Particles of different sizes are prepared by varying the relative concentrations of polymer to gold precursor, and are analyzed using a combination of techniques (*i.e.* UV–visible absorption spectroscopy, transmission electron microscopy, dynamic light scattering, and in one case, matrix assisted laser desorption/ionization mass spectrometry) to assess their size and dispersion in size.

Finally, Chapter 4 reports the formation of polymer coated gold nanoparticles exhibiting a strong size–dependent fluorescence for particles diameter between 1.1 and 1.7 nanometers. Particular attention have been given to control experiments and analysis of these materials to ensure the observed fluorescence originates from the gold particles and not from any byproduct, unreacted polymer or oligomeric polymer/gold species. Those particles exhibit a quantum efficiency of 3% and undergo photobleaching upon laser excitation. The possible origins of this luminescence are discussed in Section 4.4.2.

1.11   Bibliography

1. R.P. Feynman. *J. Microelectromechanical Syst.*, 1:60, 1992.

2. N. Taniguchi. *Proc. ICPE Tokyo*, 2:18, 1974.

3. A. Sandhu. *Nature Nanotech.*, 1:78, 2006.

4. C.M. Niemeyer. *Angew. Chem. Int. Ed.*, 40:4128, 2001.

5. D. Born J. Reichert W. Fritzsche A. Csaki, G. Maubach. *Single Mol.*, 3:275, 2002.

6. T. Pellegrino D. Zanchet C. Micheel S.C. Williams R. Boudreau M.A.L. Gros C.A. Larabell A.P. Alivisatos W.J. Parak, D. Gerion. *Nanotechnology*, 14:R15, 2003.

7. L.N. Lewis. *Chem. Rev.*, 93:2693, 1993.

8. H. Patin A. Roucoux, J. Schulz. *Chem. Rev.*, 102:3757, 2002.

9. M. Gratzel A. Hagfeldt. *Acc. Chem. Res.*, 33:269, 2000.

10. A.A. Ramos J.T. Bueno, N. Shchukina. *Nature*, 430:326, 2004.

11. M. Fichtner. *Adv. Eng. Mater.*, 7:443, 2005.

12. J.M. Steele C.E. Moran and N.J. Halas. *Nano. Lett.*, 4:1497, 2004.

13. C.A. Mirkin N.L. Rosi. *Chem. Rev.*, 105:1547, 2005.

14. P. Gin S. Weiss P.A. Alivisatos M. Bruchez Jr., M. Moronne. *Science*, 281:2013, 1998.

15. S. Nie W.C.W. Chan. *Science*, 281:2016, 1998.

16. C. Plank 16 R9-R25 (2005). W.J. Parak, T. Pellegrino. *Nanotechnology*, 16:R9, 2005.

17. E. Matijevic. *Ann. Rev. Mater. Sci.*, 15:483, 1985.

18. Y Wang. *Acc. Chem. Res.*, 24:133, 1991.

19. P.G. Kik H.A. Atwater S.A. Maier, M.L. Brongersma. *Phys.l Rev. B*, 65:1934081, 2002.

20. G.S. Snider R.S. Williams J.R. Heath, P.J. Kuekes. *Science*, 280:1716, 1998.

21. K.J. Klabunde Y.X. Li. *Langmuir*, 7:1388, 1991.

22. A. Volodin K.J. Klabunde O.B. Koper, I. Lagadic. *Chem. Mater.*, 9:2468, 1997.

23. C. Hayter. *Materials Science and Engineering*, C 23:703, 2003.

24. V. Young S.T. Gregory, J.G. Widdicombe. *Resp. Phys. and Neurobiol.*, 13:3, 2002.

25. E. Boysen E. R. Boker. *Nanotechnology for Dummies.* 2005.

26. D. Rejeski. Cpsc fy2010 agenda and priorities. Technical report, Consumer Product Safety Commission, 2009.

27. A.P. Alivisatos. *J. Phys. Chem.*, 100:13226, 1996.

28. D. Astruc M.C. Daniel. *Chem. Rev.*, 104:293, 2004.

29. K.J. Klabunde. *Nanoscale Materials in Chemistry.* Wiley Interscience, 2001.

30. C.T. Seto G.M. Whitesides, J.P. Mathias. *Science*, 254:1312, 1991.

31. G. Perec. *Substance*, 9:37, 1980.

32. M. Verhas P. Englebienne, A. VanHoonacker. *Spectroscopy*, 17:25, 2003.

33. Z. Gaburro D.L. Andrews. *Frontiers in Surface Nanophotonics*. Springer, 2006.

34. G. Schmid. *Clusters and Colloids*. VCH Weinheim, 1994.

35. M.A. Hayat. *Colloidal Gold, Principles, Methods and Applications*. Academic Press: New York, 1989.

36. L. Hunt. *Gold Bull.*, 9:134, 1976.

37. L. Stievano S. Calogero-Q.A. Pankhurst K.-P. Martinek F.E. Wagner, S. Haslbeck. *Nature*, 407:691, 2000.

38. M. Sax C. Iggitt I. Freestone, N. Meeks. *Gold Bull.*, 40:270, 2007. litterature about lycargus cup.

39. I.C. Freestone D.J. Barber. *Archaeometry*, 32:33, 1990.

40. R.H. Brill. *Comptes Rendus; VIIe Congres International du Verre*, page 223, 1985.

41. A. Neri. *L'arte Vetraria*. Nella Stamperia De Giunti, 1612.

42. P. Mulvaney. *MRS Bull.*, 26:1009, 2001.

43. G. Savage. *Glass and Glassware*. Octopus Book, 1975.

44. F. Antonii. *Panacea Aurea–Auro Potabile*. Bibliopolio Frobeniano, 1618.

45. S. Nlate D. Astruc M.C. Daniel, J.R. Aranzaes. *J. Inorg. and Organometal. Pol. and Mat.*, 15:107, 2005.

46. J. Kunckels. *Nuetliche Observationes oder Anmerkungen von Auro und Argento Potabili*. Schutzens, 1676.

47. H.S. Klickstein H.M. Leicester. *A Source Book in Chemistry, 1400–1900*. Oxford University Press, 1968.

48. H.H. Helcher. *Aurum Potabile oder Gold Tinstur*. J. Herbord Klossen, 1718.

49. J.B. Richters. *Über die Neueren Gegenstände der Chemie*. Breslau, 1791 – 1802.

50. M. Faraday. *Phil. Trans. R. Soc.*, 147:145, 1857.

51. J. Hillier J. Turkevich, P.C. Stevenson. *Disc. Faraday Soc.*, 11:55, 1951.

52. G. Frens. *Nat. Phys. Sci.*, 241:20, 1973.

53. G. Schmid. *Chem. rev.*, 92:1709, 1992.

54. R.W. Murray A.C. Tempelton, M.P. Wuelfing. *Acc. Chem. Res.*, 33:27, 2000.

55. C.J. Zhong J.E. Harris-R.W. Vachet M.R. Clak J.D. Londono S.J. Green J.J. Stokes G.D. Wignall G.L. Glish M.D. Porter N.D. Evans R.W. Murray M.J. Hostetler, J.E. Wingate. *Langmuir*, 14:17, 1998.

56. D.J. Schiffrin C.J. Kiely D. Bethell, M. Brust. *Electroanal. Chem.*, 409:137, 1996.

57. T. Chena H. Yua-C. Chena G. Jianga, L. Wang. *Mat. Chem. Phys.*, 98:1, 2006.

58. V.V.V.S. Subbaraoa A. Kasi Vishwanatha B.K. Dasa C.V.V. Satyanarayanab P.K. Khannaa, R. Gokhalea. *Mat. Chem. Phys.*, 92:229, 2005.

59. P.B. Davies T. Kawai, D.J. Neivandt. *J. Am. Chem. Soc.*, 122:12031, 2000.

60. C.M. Payne E.S. Day L.J.E. Anderson M. Zhong S. Lee K.M. Mayer T. Zal L. Adam C.P.N. Dinney R.A. Drezek J.L. West J.H. Hafner B.C. Rostro-Kohanloo, L.R. Bickford. *Nanotechnology*, 20:434005, 2009.

61. C. Battocchio I. Fratoddi E. Piscopiello L. Tapfer M.V. Russo F. Vitale, R. Vitaliano. *J. Organomet. Chem.*, 693:1043, 2008.

62. T. Yoshimura K. Esumi, S. Sarashina. *Langmuir*, 20:5189, 2004.

63. Y. Takeda T. Kondow F. Mafuné, J. Kohno. *J. Phys. Chem. B*, 105:5114, 2001.

64. E.A. Nevara N.A. Savastenkoa N.V. Tarasenko, A.V. Butsena. *App. Surf. Sc.*, 252:4439, 2006.

65. T. Yoshidaa E. Ozawaa Y. Kawakami, T. Setob. *App. Surf. Sc.*, 197:587, 2002.

66. D. Mandler I. Willner. *J. Am. Chem. Soc.*, 111:1330, 1989.

67. T. Yonezawa N. Toshima. *New J. Chem.*, 22:1179, 1998.

68. K. Meguro K. Esumi, T. Tano. *Langmuir*, 5:268, 1989.

69. M.O. Delcourt J.P. Chevalier J.L. Marignier, J. Belloni. *Nature*, 317:344, 1985.

70. C.A. Mirkin K.L. Kelly G.C. Schatz J.G. Zheng R.C. Jin, Y.W. Cao. *Science*, 294:1901, 2001.

71. W. Helbig M.T. Reetz. *J. Am. Chem. Soc.*, 116:7401, 1994.

72. S.A. Quaiser M.T. Reetz. *Angew. Chem. Int. Ed.*, 34:2240, 1995.

73. J.H. Song F. Kim and . P. Yang. *J. Am. Chem. Soc.*, 124:14316, 2002.

74. J.S. Ogden D. Young F.W. Benfield, M.L.H. Green. *Chem. Commun.*, page 866, 1973.

75. C.G. Francis H.X. Huber K. Molnar G.A. Ozin, M.P. Andrews. *Inorg. Chem.*, 29:1068, 1990.

76. C. Dickinson M.J. Rossensky A. Laromaine D.W. McComb M.M. Stevens Y. Wang L. Petit C. Barentin D.G. Spiller A.I. Cooper R. Levy N. Schaeffer, B. Tan. *Chem. Commun.*, 34:3986, 2008.

77. I. Hussain N. Schaeffer M.F. Wyatt M. Brust A.I. Cooper Z. Wang, B. Tan. *Langmuir*, 23:885, 2007.

78. D. Bethell D.J. Schiffrin R. Whyman M. Brust, M. Walker. *Chem. Commun.*, page 801, 1994.

79. J. Hillier J. Turkevich, P.P.C. Stevenson. *Disc. Faraday Soc.*, 11:55, 1951.

80. S. Wolf F. Granzer L. Woste T. Leisner, C. Rosche. *Surf. Rev. & Lett.*, 3:1105, 1996.

81. D. Bethell D.J. Schiffrin C. Kiely M. Brust, J. Fink. *Chem. Commun.*, page 1655, 1995.

82. D. Meisel K. Kopple, D. Meyerstein. *J. Phys. Chem.*, 84:870, 1980.

83. T.R. Webb C.A. McAuliffe C.K. Tan, V. Newberry. *Dalton Trans.*, page 1299, 1987.

84. K. Asakura M. Miyake N. Toshima P. Lu, T. Teranishi. *J. Phys. Chem.*, 103:9673.

85. K. Torigoe K. Meguro K. Esumi, N. Sato. *J. Coll. & Int. Sc.*, 149:295, 1992.

86. J. Turkevich. *Gold Bull.*, 18:125, 1985.

87. J. Turkevich. *Gold Bull.*, 18:86, 1985.

88. R. Boese F. Bamdermann S. Meyer G.H.M. Calis W.A. Vandervelden G. Schmid, R. Pfeil. *Chem. Ber. Recl.*, 14:3634, 1981.

89. P. Mulvaney M. Giersig. *Langmuir*, 9:3408, 1993.

90. J.J. Stokes R.W. Murray M.J. Hostetler, S.J. Green. *J. Am. Chem. Soc.*, 118:4212, 1998.

91. R.W. Murray M.J. Hostetler, A.C. Templeton. *Langmuir*, 15:3782, 1999.

92. S. Gladiali T. Bürgi C. Gautier, R. Taras. *Chirality*, 20:486, 2007.

93. R.L. Johnston. *Atomic and Molecular Clusters*. London press, 2002.

94. C.N.R. Rao P.P. Edwards, R.L Jonston. *Metal Clusters in Chemistry*. Wiley VCH Weinheim, 1999.

95. G. Carotenuto L. Nicolais. *Metal Polymer Nanocomposites*. Wiley Interscience, 2005.

96. D.G. Duff P.P. Edwards I. Gameson B.F.U. Johnson D.J. Smith A.I. Kirkland, D.E. Jefferson. *Proc. R. Soc. London A*, 440:589, 1993.

97. X.o Shi . 1990 112 (23) pp 8552Ű8562 B.K. Teo, H. Zhang. *J. Am. Chem. Soc*, 112:8552, 1990.

98. H.. Zhang D. Huang X. Shi B.K. Teo, M. Hong. *Chem. Commun.*, page 204, 1988.

99. R.W. Murray T. Huang. *J. Phys. Chem. B*, 105:12498, 2001.

100. T. Tsukuda Y. Negishi, K. Nobusada. *J. Am. Chem. Soc.*, 127:5261, 2005.

101. S. Sato H. Yao K. Kimura T. Tsukuda Y. Negishi, Y. Takasugi. *J. Am. Chem. Soc.*, 126:6518, 2004.

102. G. U. Kulkarni C. P. Vinod and 329 (1998). C. N. R. Rao, 289. *Chem. Phys. Lett.*, 289:329, 1998.

103. D.R. Huffman C.F. Bohren. *Absorption and Scattering of Light by Small Particle.* Wiley, New York, 1983.

104. P.P. Edwards W.J.H. Nelson N.D. Vargas D.C. Johnson, R.E. Benfield. *Nature*, 314:231, 1985.

105. lJj. deLongh G. Schmid M.N. Vargaftik I.I. Moiseev Y. Volokitin, J. Sinzig. *Nature*, 324:624, 1996.

106. D. D. Sarma C. N. R. Rao V. Vijayakrishnan, A. Chainani. *J. Phys. Chem.*, 96:8679, 1992.

107. G. N. Subanna H. N. Aiyer, V. Vijayakrishnan and C. N. R. Rao. *Surf. Sci.*, 313:392, 1994.

108. M. Verhas P. Englebienne, A. Van Hoonacker. *Spectroscopy*, 17:255, 2003.

109. F. Goettmann A. Moores. *New J. Chem.*, 30:1121, 2006.

110. P. Mulvaney S. Underwood. *Langmuir*, 10:3427, 1994.

111. M. Hoppert. *Microscopic Techniques in Biotechnology.* Wiley VCH, 2003.

112. D. Ricci P.C. Braga. *Atomic Force Microscopy: Biomedical Methods and Applications.* Humana press, 2004.

113. A. Kingon P.M. Vilarihno, Y. Rosenwacks. *Scanning Probe Microscopy: Characterization, Nanofabrication and Device Application of Functional Materials.* Kluwer academic, 2005.

114. R.A. Alvarez-Puebla L.M. Liz-Marzn M. Brust P. Aldeanueva-Potel, E. Faoucher. *Anal. Chem.*, 81:9233, 2009.

115. C.F. Zukoski D.L.V. Hyning. *Langmuir*, 14:7034, 1998.

116. M.J. Natan K.R. Brown. *Langmuir*, 14:726, 1998.

117. M.A. El-Sayed S. Eustis. *Chem. Soc. Rev.*, 35:209, 2005.

118. B. Schechter. *New Scientist,*, 78:31, 2003.

119. U. Kreibig M. Quinten. *Surface Science*, 172:557, 1986.

120. J.J. Shiang S.E. Henrichs J.R. Heath C.P. Collier, R.J. Saykally. *Science*, 277:1978, 1997.

121. M.A. El-Sayed S. Link. *J. Phys. Chem. B*, 103:8410, 1999.

122. F.J. Humphreys P.J. Goodhew. *Electron Microscopy and Analysis*. Taylor and Francis, 1988.

123. Z.L. Wang N. Yao. *Handbook of Microscopy for Nanotechnologies*. Kluwer Academic, 2005.

124. R. Pecora B.J. Berne. *Dynamic Light Scattering with Applications to Chemistry, Biology and Physics*. Dover publications Inc., 1999.

125. L. Duchesne D. Lasne N. Schaeffer-D.G. Fernig B. Lounis V. Octeau, L. Cognet. *ACS Nano*, 3:345, 2009.

126. B.D. Alexender J.A. casalnuova P.R. Gannon-S.M. Johnson E.A. Larka A.M. Meueting H. Pignolet P.D. Boyle, B.J. Johnson. *Inorg. Chem.*, 26:1346, 1987.

127. O.B. Shawkataly B.N. Green I. Lewis T. Blumenthal, M.I. Bruce. *J. Organomet. Chem.*, 269:C10, 1984.

128. A.J. Mills R.W. Murray R. Balasubramanian, R. Guo. *J. Am. Chem. Soc.*, 127:8126, 2005.

129. T.G. Schaaff. *Anal. Chem.*, 76:6187, 2004.

130. M. Manninen S. Reimann. *Rev. Modern Phys.*, 74:1283, 2002.

131. T.J. Bukowski; J.H. Simmons. *Sol. State Mat. Sc.*, 27:119, 2002.

132. S. Hufner. *Photoelectron Spectroscopy: Principles and Applications.* Springer, 2003.

133. R. Prins. *X–ray Absorption: Principles, Applications and Techniques of EXAFS, SEXAFS and XANES.* Wiley Interscience, 1988.

134. B.-K. Teodorescu. *EXAFS: Basic Principles and Data Analysis.* Springer, 1986.

135. P. Zhang T.K. Sham, P.-S.G. Kim. *Solid State Commun.*, 138:553, 2006.

136. G. Foranb D.B. Akolekara, S.K. Bhargavaa. *Rad. Phys. and Chem.*, 75:1948, 2006.

137. R. Litran D. Martínez-Martínez J. M. de la Fuente S. Penades A. Fernandez C. Lopez-Cartes, T. C. Rojas. *J. Phys. Chem. B*, 109:8761, 2005.

138. H. Kudo T. Miyanaga T. Nanke-T. Kobayashi Y. Suzuki, H. Makanae. *App. Phys. A*, 78:335, 2004.

139. M.N. Piancastelli M. De Crescenzi. *Electron Scattering and Related Spectroscopies.* Worls scientific publishing, 1996.

140. L. Nicolais G. Carotenuto. *Encyclopedia of Polymer Science and Technology.* Wiley, New York, 2003.

141. W. Caseri. *Macromol. Rapid Commun.*, 21:705, 2000.

142. M. Miyake T. Teranishi, M. Hosoe. *Adv. Mater.*, 9:61, 1997.

143. Y. Staedler K. Feldman G. Hahner-W.R. Caseri P. Smith A.G. deLeon, Y. Dirix. *Appl. Opt.*, 39:4847, 2001.

144. A.M. Kessinger C.A. Foss A.H. Lu, G.H. Lu. *J. Phys. Chem. B*, 101:9139, 1997.

145. W. Heffels C. Bastiansen W. Caseri-P. Smith Y. Dirix, C. Darribere. *Appl. Opt.*, 38:6581, 1999.

146. M. Caseri U.W. Suter P. Walther L. Zimmerman, M. Weibel. *Pol. Adv. Technol.*, 4:1, 1993.

147. R.W. Boyd G.L. Fisher. *Nanostructured Materials Clusters, Composites and thin Films.* V.M. Shalev and M. Moskovits, Washington DC, 1998.

148. J.S. Wilkinson R.D. Harris. *Sensors and Actuators*, 29:261, 1995.

149. L. Nicolais G. Carotenuto. *J. Mater. Chem.*, 13:1038, 2003.

150. M. Miyake T. Teranishi, I. Kiyokawa. *Adv. Mat.*, 10:596, 1998.

151. M. Sutton S.G.J. Mochrie M.B. Lurio-A. Ruhm M.B. Lennox M.K. Corbierre, N.S. Cameron. *J. Am. Chem. Soc.*, 123:10411, 2001.

152. U.S. Schubert J.F. Gohy M. Filali, M.A.R. Meier. *Langmuir*, 21:7995, 2005.

153. D.T. Miles R.W. Murray W.P. Wuelfing, S.M. Gross. *J. Am. Chem. Soc.*, 120:12969, 1998.

154. P.V. Braun R.G. Schimmin, A.B. Schoch. *Langmuir*, 20:5613, 2004.

155. H. Jiang E. Kauppinen H. Tenhu J. Shan, M. Nuopponen. *Macromolecules*, 36:4526, 2003.

156. A. Ulman Y.-M. Chou O. Nuyken R. Jordan, N. West. *Macromolecules*, 34:1606, 2001.

157. D.R. Walt T.K. Mandal, M.S. Fleming. *Nano Letters*, 2:3, 2002.

158. M.S. Donovan C.L. McCormick A.B. Lowe, B.S. Sumerlin. *J. Am. Chem. Soc.*, 124:11562, 2002.

159. H. Wurm M.L. Hallensleben S. Nuss, H. Bottcher. *Angew. Chem. Int. Ed.*, 40:4016, 2001.

Chapter 2

Design of Polymeric Stabilizers for Water–Soluble Gold Nanoparticles

2.1   Introduction

FUNCTIONALIZED METAL nanoparticles are of great interest in terms of their potential applications in biomedical, electronic or optical materials.[1–3] The formation of such materials has thus been of considerable interest since the first synthetic breakthroughs.[4,5]

Among the many new techniques used to produce gold particles, particular attention has been focused on metal nanoparticles stabilized by polymers in solution, or embedded in polymer matrices.[6] Interest in such systems is mainly due to the possibility of nanoparticles self–assembly driven by the intrinsic organizational properties of the polymeric stabilizers.[7–9]

Thus, several synthetic procedures for the synthesis of polymer–gold nanoparticles composites can be found in the literature. Those procedures can be classified into two main groups; the first synthetic route involves in the functionalization of the pre–formed particles by a polymer precursor, and the subsequent growth of polymer chains onto the gold surface.[10] For example, thiol–terminated polystyrene and poly(ethylene oxide)–poly(propylene oxide)–stabilized gold nanoparticles have been synthesized by grafting to approaches.[6,11] However, these techniques involve multiple steps prepara-

tions, making them time–consuming and not cost–effective. Furthermore, the limited number of polymer initiators that can be adsorbed onto the gold surface and the reaction conditions required for the subsequent growth of the polymeric chains are a limitation to the polymer structures that can be formed and may jeopardize the stability of the colloidal suspensions.

The second set of techniques consists on the *in–situ* preparation of gold particles stabilized within a polymeric matrix. These methods rely on the reduction of a gold precursor in the presence of a suitable polymer structure.[12–14] A number of research groups have investigated water-soluble polymers as stabilizing ligands for gold nanoparticles, particularly with the aim of achieving size-controlled nanoparticle synthesis. For example, poly(ethylene oxide)–poly(propylene oxide)–stabilized gold nanoparticles were prepared but were found to be quite polydisperse.[15] Star–shaped poly(ethylene oxide)-block-poly(caprolactone) ligands have also been developed.[16] These ligands led to rather better control over particle size distributions but did not achieve monodisperse samples. Thiol–terminated poly(ethylene oxide)–poly(propylene oxide) monomethyl ether (MeO–PEG–SH) stabilized gold nanoparticles[17,18] and poly(N–isopropylacrylamide)–monolayer–protected gold clusters[19] have been produced, and the MeO–PEG–SH route in particular can lead to well–defined (although not monodisperse) particles in water.[17,18]

More sophisticated structures have also been prepared. For example, poly(amido amine) dendritic polymer ligands[20] has not necessarily led to a greater degree of control over particle size and particle size distribution.

However, despite the potential uses of polymer embedded gold nanoparticles structures, only a few examples of polymer stabilized nanoparticles using linear polymer with a single anchor point as stabilizers can be found in the literature, and there is, in general, an incomplete understanding of the relationship between the structure and functional properties of linear polymeric ligands and their effect onto the gold particles growth and stabilization.

The chain transfer polymerization process allow the preparation of linear polymeric chains end–functionalized with a thioether containing end–group that can adsorb onto the gold surface (see Figure 2.1). This polymerization can be readily applied to a wide
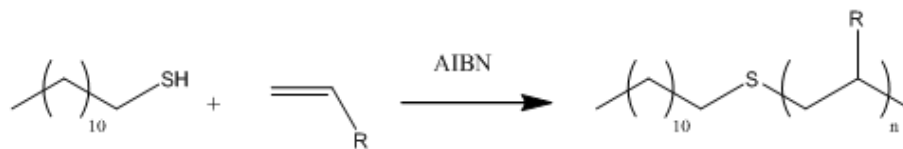
Figure 2.1: Scheme representing the gold particle polymeric capping agent synthesis by chain transfer polymerization.

range of monomeric species. Hence, it seems to be an interesting synthetic process for the systematic preparation of linear polymeric stabilizer for gold nanoparticles.

In this Chapter, a methodology for the preparation by chain transfer polymerization of series of water-soluble polymeric ligands containing a thiol and/or a thioether end–group is described. The ability of those polymeric ligands to stabilize gold particles is reviewed in Chapter 3.

2.2 Experimental

2.2.1 Materials

All monomers (methacrylic acid, acrylic acid, vinylpyrrolidone, vinylsulfonic acid, hydroxyethyl acrylate and poly(ethylene oxide)–poly(propylene oxide)methacrylate), chain transfer agents (propane–1–thiol, pentane–1–thiol, heptane–1–thiol, dodecane–1–thiol, octadecane–1–thiol, 1,9–nonanedithiol, 2–mercaptoacetic acid, 2–mercaptoethyl sulfide, pentaerythritiol tetra(3–mercaptopropionate) and 2–ethanedithiol), azobisisobutyronitrile (AIBN), polymethacrylic acid were purchased from Aldrich and used as received, unless otherwise described. Dialysis membranes (7000 Daltons cut–off) were purchased from Pierce Chemicals.

2.2.2 Methods

2.2.2.1 Polymeric stabilizer synthesis

The polymeric ligands were prepared as follows for a targeted molecular weight of approximately 3000 g/mol. The monomer (50 mmol), chain transfer agent (5 mmol) and AIBN (0.080 g, 0.50 mmol) were heated in ethanol (30 cm^3) under nitrogen at 75°C in a round–bottomed flask fitted with a reflux condenser (Radleys Carousel Reactor). The reaction was carried out for five hours under agitation. The resulting product

was precipitated into cold diethyl ether (100 cm^3), filtered using a Buchner funnel, and dried in vacuo at 45°C for 24 hours.

The preparation of pMAA–DDT polymeric ligands of various molecular weight was carried out using the same protocol, however, the chain–transfer agent concentration was varied from 5 mmol to 0.16mmol and the initiator and monomer concentrations were kept constant (0.50 mmol and 50 mmol respectively).

2.2.2.2   Polymeric stabilizer characterization

^{1}H NMR spectroscopy ^{1}H NMR spectra were recorded on a 400 MHz Bruker DPX-400 spectrometer using δ6–DMSO or D$_2$O as a solvent in a 5 mm quartz NMR tube. The chemical shifts of the different polymers are depicted in Table 2.1

Gel permeation chromatography   Gel permeation chromatography (GPC) was performed using a Polymer Laboratories system equipped with a PL–ELS 1000 evaporative light scattering detector and a series of PC mix gel columns 5 um MIXED C and D. THF was used as the eluent at a flow rate of 1.0 ml/min at 40°C. Calibration was carried out using EasiCal polystyrene standards (Polymer Laboratories). The polymer was first converted to the methyl ester using TMS–diazomethane reagent to render it soluble in THF.[21]

Mass spectrometry of PTMP end–functionalized pMAA   DHB and THAP matrix solutions were made to a concentration of 10 mg/mL in 1:1 (vol/vol) H$_2$O/MeCN. DHB solution was also made to the same concentration in MeOH. Aqueous matrix solutions were mixed with DAC solution (50 mg/mL in H$_2$O) in a 9:1 ratio. pMAA–PTMP solution was made to a concentration of 10 mg/mL in MeOH, and mixed with the matrix solutions in a 5μL:50μL ratio. One μL of NaOAc solution (10 mg/mL in MeOH) or 100% TFA was added as required. For IXB preparations, 0.5 mg of NH4$^+$ loaded IXB was added to 200 |muL of the pMAA–PTMP solution, which was agitated by vortex mixer (at slow speed) for 20 seconds, before mixing with matrix; 0.5 μL of the final mixture was spotted onto a stainless steel sample plate and dried in a stream of cool air. MALDI–TOF–MS data were acquired using an Applied Biosystems Voyager DE–STR spectrometer (Framingham, MA), which is equipped with a nitrogen laser

Polymer	solvent	^{1}H NMR chemical shifts
Monomer Series		
pMAA–DDT	δ_6 DMSO	end–group: 0.9(b) CH_3, 1.4 & 2.4 (CH_2); backbone: 1.7–2.1 (CH_2), 1.2 (CH_3) 12.3(b) COOH
pAA–DDT	δ_6 DMSO	end–group: 0.9(b) CH_3, 1.3 & 2.6 (CH_2); backbone: 1.5–1.8(b) (CH_2, CH), 11.9(b) (COOH)
pVP–DDT	δ_6 DMSO	end–group: 0.9(b) CH_3, 1.2 & 2.6 (CH_2); backbone: 1.6–2.1(b) (CH_2), 2.4&2.8&3.4(b) $(CH_2$ pyr.), 4.3 (OH)
pVSA–DDT	δ_6 DMSO	end–group: 0.8(b) CH_3, 1.4 & 2.5 (CH_2); backbone: 1.8–2.4(b) (CH_2), 3.6 (CH)
pHEA–DDT	δ_6 DMSO	end–group: 0.9(b) CH_3, 1.4 & 2.7 (CH_2); backbone: 1.7 & 2.0–2.4 (CH_2), 4.5 $(O-CH_2)$, 3.4–3.8(b) (CH_2-OH)
pEGMA–DDT	δ_6 DMSO	end–group: 0.9(b) CH_3, 1.3 & 2.6 (CH_2); backbone: 1.9 & 2.2–2.4 (CH_2), 3.3–3.5 $(CH_2$ end–group), 4.4 (OH)
Molecular Weight Series PMAA-DDT XXXg/mol		
pMAA–DDT 3640 g/mol	δ_6 DMSO	end–group: 0.9(b) CH_3, 1.4 & 2.3 (CH_2); backbone: 1.7–2.1 (CH_2), 1.2 (CH_3) 12.3(b) COOH
pMAA–DDT 7000 g/mol	δ_6 DMSO	end–group: 0.9(b) CH_3, 1.4 & 2.4 (CH_2); backbone: 1.7–2.1 (CH_2), 1.2 (CH_3) 12.3(b) COOH
pMAA–DDT 8610 g/mol	δ_6 DMSO	end–group: 0.8(b) CH_3, 1.5 & 2.3 (CH_2); backbone: 1.7–2.1 (CH_2), 1.2 (CH_3) 12.3(b) COOH
pMAA–DDT 13500 g/mol	δ_6 DMSO	0.9(b) end–group: 0.9(b) CH_3, 1.3 & 2.4 (CH_2); backbone: 1.7–2.1 (CH_2), 1.2 (CH_3) 12.3(b) COOH
End-Group Hydrophobicity Series PMAA-MAT		
pMAA–MAT	D_2O	end–group: 3.2 (CH_2), 10.5 (OH); backbone:,
pMAAA–PropT	D_2O	end–group: 0.8(b) (CH_3), 1.3&2.2 (CH_2); backbone: 1.7–2.1 (CH_2), 1.2 (CH_3) 12.3(b) COOH
pMAA–PentT	D_2O	end–group: 1.0(b) (CH_3), 1.3–2.2 (b) (CH_2); backbone: 1.7–2.1 (CH_2), 1.2 (CH_3) 12.3(b) COOH
pMAA–HT	δ_6 DMSO	end–group: 0.8(b) (CH_3), 1.2–2.4 (b) (CH_2); backbone: 1.7–2.1 (CH_2), 1.2 (CH_3) 12.3(b) COOH
pMAA–ODT	δ_6 DMSO	end–group: 0.9(b) (CH_3), 1.3–2.2.6 (b) (CH_2); backbone: 1.7–2.1 (CH_2), 1.2 (CH_3) 12.3(b) COOH
Multiple Thiols Containing End-Grouyp series		
pMAA–MES*	D_2O	end–group: 1.5 (SH), 2.9 (CH_2); backbone: 1.2 (CH_3), 2.1 & 2.6 (CH_2)
pMAA–EDT*	D_2O	end–group: 1.5 (SH), 2.9 & 2.6 (CH_2); backbone: 1.2 (CH_3), 2.0 & 3.6 (CH_2)
pMAA–NDT*	D_2O	end–group: 1.4 (SH), 2.9 & 2.6 (CH_2); backbone: 1.1 (CH_3), 2.1 & 3.6 (CH_2)
pMAA–PTMP*	δ_6 DMSO	end–group: 1.5 (SH), 2.6 & 4.1 (CH_2); backbone: 1.0 (CH_3), 1.8 & 2.3 (CH_2)

Table 2.1: ^{1}H NMR shifts for the polymeric stabilizers. (*) See Figures 2.9, 2.10, 2.11 and 2.12 for details).

(λ=337 nm). The instrument was operated in positive or negative ion reflectron mode. The accelerating voltage was 20 kV, while the grid voltage was maintained at 65.5%. The delay time was 150 ns, and laser fluence was attenuated to just above the threshold of ionization, which varied between matrices and preparations. The laser was fired at a frequency of 3 Hz, and spectra were accumulated in multiples of 25 laser shots, with 150 shots in total. Postacquisition processing of data were performed utilizing Data Explorer V4.0 software supplied by Applied Biosystems.

2.3 Results

All polymer ligands were synthesized by chain transfer methods using thiols (or diol / multithiols) as the chain transfer agent. A feature of this methodology is that it leads to a thioether and/or thiol functionalized polymeric chain of low molar mass oligomeric species with relatively narrow molecular weight distributions with a polydispersity index (PDI) typically below 1.5 (see Section 2.4.1 for details).

After each polymerization, any unreacted free thiol was removed by polymer re-precipitation in cold diethylether which was a good solvent for the thiol chain transfer agent. However, polymeric chains are slightly soluble in diethylether, this effect explaining the relatively low recovery yields.

2.3.1 DDT end–functionalized polymers with different main chains

A series of six water-soluble polymer ligands was synthesized using different monomer repeat units (Figure 2.2) in order to study the effect of the ligand chain structure on the average particle size and size distribution for the gold nanodispersions. The same thiol–containing chain transfer agent (dodecanethiol, DDT) was used in each case; as such, each ligand in the series was terminated with a dodecylthioether end group (see Figure 2.2). The number average molecular weight (M_n) for the six ligands was found to be in the range 1500–4500 g/mol (See Figures 2.2 and 2.3), the only exception being the polymeryzation of vinylpyrrolidone. The high M_n of pVP obtained under the same experimental conditions can be ascribed to the high VP chain transfer constant that can tend to reduce the chain transfer capacity of dodecanethiol.,[22,23] or to the fact that the termination process in the VP chain transfer polymerization tends to occur by
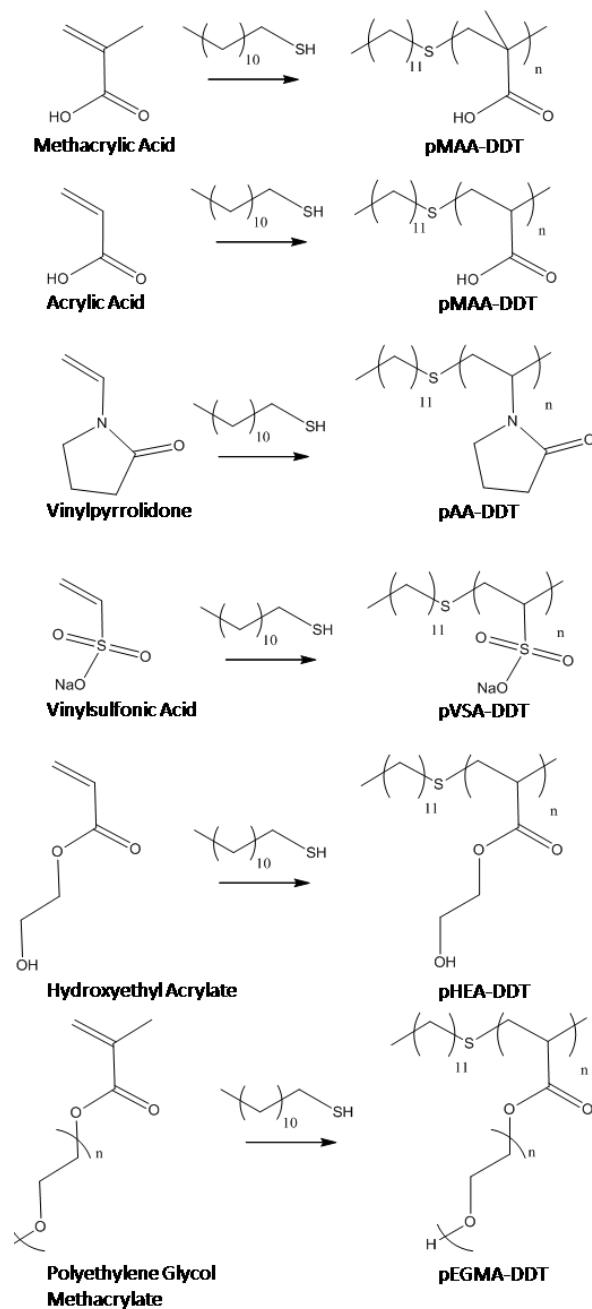
Figure 2.2: (Library of monomers used to produce the six dodecyl thioether containing polymers and chain transfer polymerization reaction scheme.

coupling rather than disproportionation (see Section 2.4.1).

A commercially available linear poly(methacrylic acid) (pMAA) sample (2000 g/mol) with no thioether end–group was also used as a control polymer to study the formation of gold nanoparticle in the absence of a dodecylthioether end–group (see Chapter 2
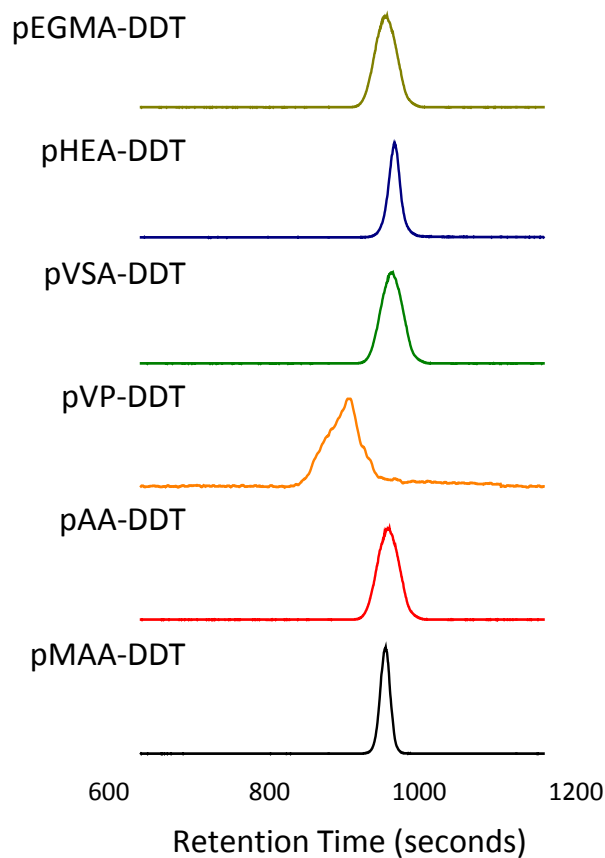
Figure 2.3: GPC elution curves of dodecyl thioether terminated polymer ligands prepared by chain transfer polymerization. (

Monomer	molecular weight (g/mol)		PDI	recovered yield
	M_n	M_w		
MAA	3220	3500	1.09	21%
AA	2560	3490	1.37	30%
VP	37320	77620	2.08	32%
VSA	2580	4850	1.88	27%
HEA	1816	2030	1.12	16%
EGMA	3470	4180	1.21	31%

Table 2.2: GPC elution data of dodecyl thioether terminated polymer ligands prepared by (chain transfer polymerization.

Section 3.3.1.1).

2.3.2 DDT end–functionalized pMAA of various molecular weights.

In order to study the influence of the polymeric stabilizer molecular weights on the gold nanoparticle sizes and size distributions, a series of pMAA–DDT of various molecular weight was synthesized. All polymers in this series were synthesized by chain transfer polymerization, in using DDT as the chain transfer agent, as described previously in Section 2.3.1. Polymers of different molecular weight were obtained by varying the DDT to MAA ratio from 10/20 to 10/0.63 whilst keeping the initiator and monomer concentrations constant (0.5 and 50 mmol/30ml respectively), a higher ratio leading to smaller polymer chains (see Section 2.4.2). The characteristics of those polymer chains are described in Table 2.3 and Figure 2.4.

The recovery yield tends to decrease whilst decreasing the polymers molecular weight. This trend can be ascribed to the purification process; low molecular weight polymers are more hydrophobic (mainly due to the presence of their hydrophybic end–groups) and fractions of those hydrophobic species may be lost during reprecipitation in diethylether.

2.3.3 pMAA chains with end–groups of different hydrophobicity

MAA/DDT (mol/mol)	molecular weight (g/mol)		PDI	recovered yield
	M_n	M_w		
100/10	3220	3500	1.09	21%
100/5	3640	4520	1.24	76%
100/2.5	7000	9540	1.36	86%
100/1.25	8610	11100	1.29	92%
100/0.63	13500	18600	1.40	89%

Table 2.3: GPC elution data of dodecyl thioether terminated polymer ligands of different molecular weights prepared by chain transfer polymerization.

The influence of the hydrophobic end–groups of the polymeric stabilizer on the formation of gold particles have also been studied. For this purpose, various pMAA were synthesized by chain transfer polymerization using different chain–transfer agents of increasing hydrophobicity (see Figure 2.5). This allowed the formation of various
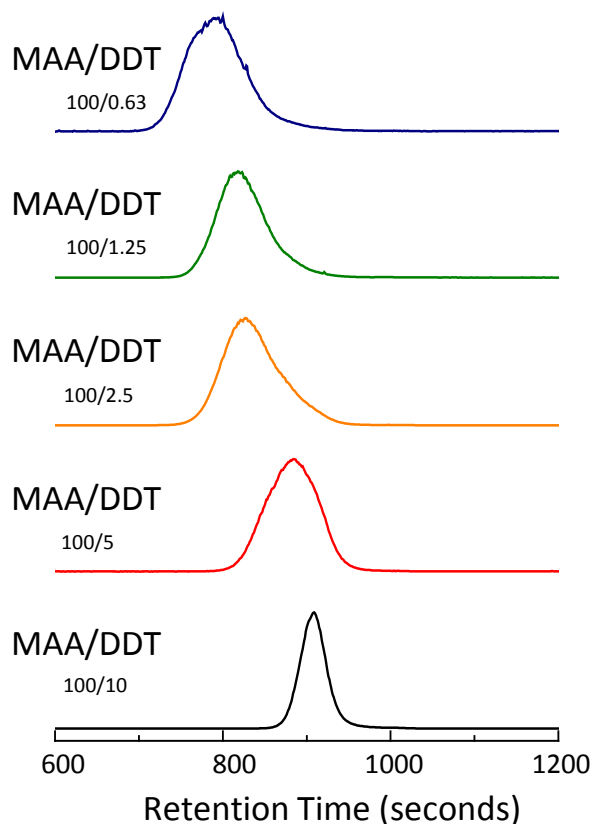
Figure 2.4: GPC elution curves of dodecyl thioether terminated polymer ligands of different molecular weights prepared by chain transfer polymerization using different ratios of MAA and DDT.

pMAA bearing different thioether containing end-groups of increasing hydrophobicity. The characteristics of the polymers produced using those chain–transfer agents are described in Figure 2.6 and Table 2.4.

The same molecular weight was targeted in each case (around 3000 g/mol) although it was not possible to achieve identical M_n for every sample using this chemistry (see Table 2.4), probably because the various thiols in the series have slightly different chain transfer constants (see Section 2.4.2).[24]

Once again, the recovered yield tends to decrease whilst increasing the "overall" hydrophobicity of the polymer chains (see Table 2.4).

43
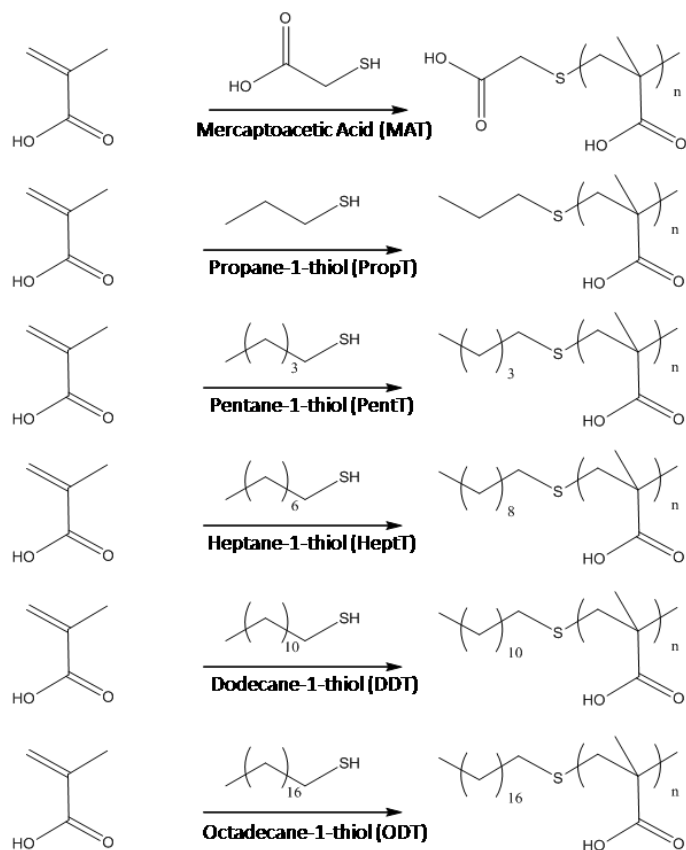
Figure 2.5: Library of chain–transfer agents of increasing hydrophobicity used to produce the six dodecyl thioether containing polymers and chain transfer polymerization reaction scheme.

Chain Transfer Agent	molecular weight (g/mol)		PDI	recovered yield
	M_n	M_w		
ODT	2980	3480	1.17	28%
DDT	3220	3550	1.09	21%
HT	2180	2550	1.17	39%
PentT	2300	2670	1.16	53%
PropT	1960	2340	1.19	59%
MAT	1780	2060	1.16	61%

Table 2.4: GPC elution data of pMAA polymer ligands bearing end-groups of increasing hydrophobicity prepared by chain transfer polymerization.

44
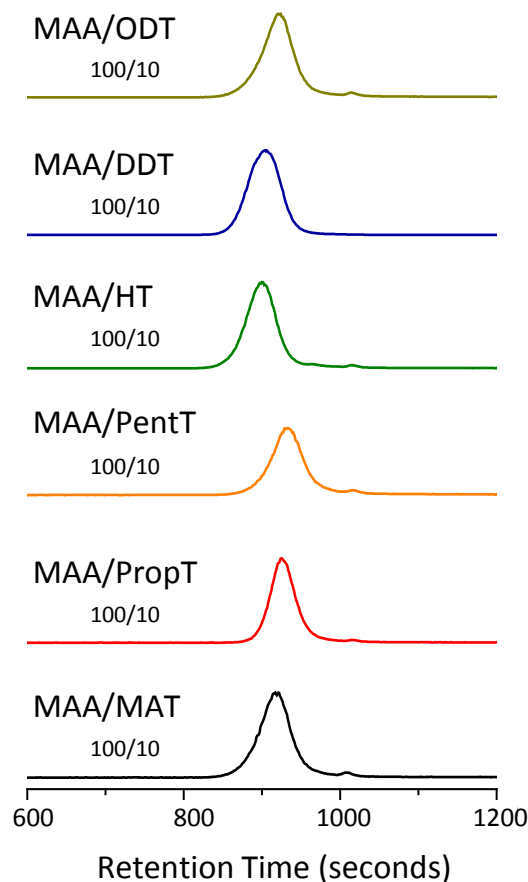
Figure 2.6: GPC elution data of pMAA polymer ligands bearing end-groups of increasing hydrophobicity prepared by chain transfer polymerization using constant MAA and CTA concentrations.

2.3.4 pMAA chains with multiple thiols/thioethers containing end-groups

The chain transfer methodology used to generate the thioether-terminated ligands discussed thus far can be readily adapted to produce ligands which contain both thioether and primary thiol functionalities — that is, polymer ligands with a multidentate binding capacity.

Herein, a series of pMAA ligands was synthesized using dithiols (2–ethanedithiol / EDT, 2,2–mercaptoethyl sulfide / MES, 1,9–nonanedithiol / NDT) or a tetrathiol (pentaerylthritiol tetra(3–mercaptopropionate, PTMP) as chain transfer agents (see Figure 2.7.

45
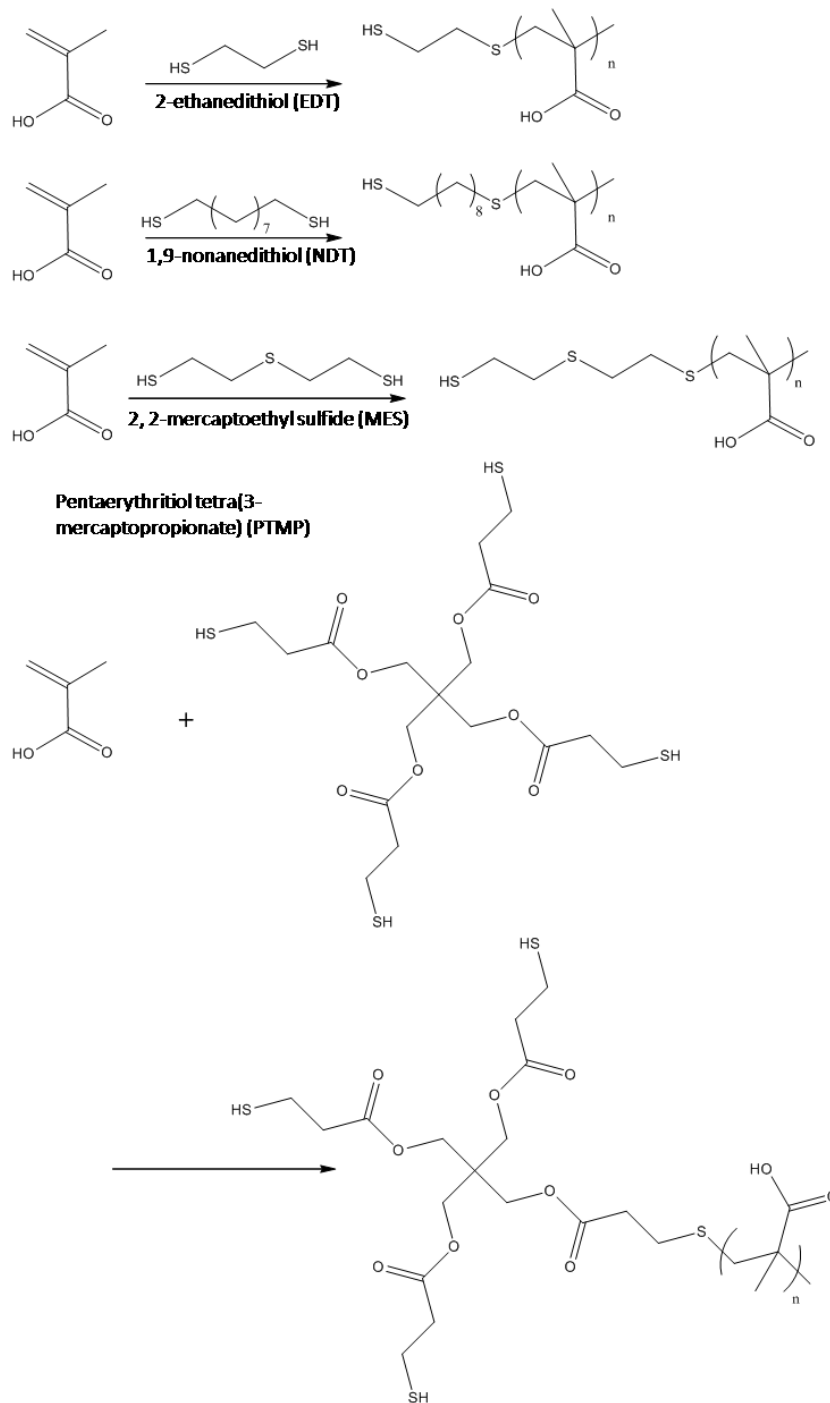
Figure 2.7: Library of chain–transfer agents containing multiple thiols and/or thioethers used to produce the six dodecyl thioether containing polymers and chain transfer polymerization reaction scheme.

Chain Transfer Agent	molecular weight (g/mol)		PDI	recovered yield
	M_n	M_w		
PTMP	1988	2239	1.13	70%
MES	1509	1861	1.23	50%
NDT	1745	1984	1.13	62%
EDT	1809	2125	1.17	40%

Table 2.5: GPC elution data of pMAA polymer ligands bearing end-groups containing multiple thiols and/or thioethers.

While it is not possible to entirely exclude the possibility of small amounts of product where two or more thiols are converted into pMAA thioethers, theoretical kinetic studies suggest strongly that the dominant average structure contains just one thioether–pMAA linkage per molecule (see Section 2.4.3). ^{1}H NMR spectra of polymer prepared using multiple thiols containing chain transfer agents show the presence of an SH chemical shift at 1.4 – 1.5 ppm, confirming this trend (see Figures 2.9, 2.10, 2.11.[25,26]

These structures all contain a mixture of thioether and thiol units and have sulphur denticities per chain ranging from two (pMAA–EDT and pMAA–NDT; one thioether and one thiol) to three (pMAA–MES; two thioethers and one thiol) up to four (pMAA–PTMP; one thioether and three thiols).

2.3.5   Protocols for MALDI–TOFMS analysis of pMAA–PTMP.

With one thioether and three free thiols containing end–group, pMAA–PTMP seems to be a particularly good candidate for the synthesis and stabilization of gold particles. Thus, extensive matrix–assisted laser desorption / ionization time–of–flight mass spectrometry (MALDI–TOF–MS) characterization of this polymer was carried out.

There has been considerable use of this technique for the characterization of synthetic polymers and the large body of work in this area has been the subject of several reviews.[27–30] However, only a few examples of the characterization of pMAA homopolymers by MALDI–TOF–MS can be found in the literature and the development of an aqueous based sample preparation and analytical protocol was needed to improve signal–to–noise ratios and resolution compared with existing methods. These protocols will subsequently be used for the characterization of the pMAA–PTMP coated gold
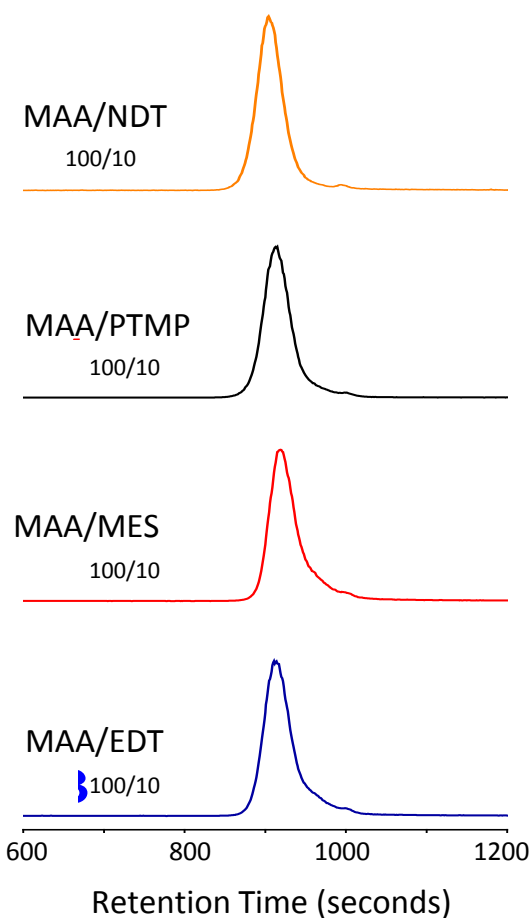
Figure 2.8: GPC elution curves for pMAA ligands synthesized using multiple thiol containing chain transfer agents at constant MAA and CTA concentrations.

nanoparticles (see Section 3.3.1.5).

Since the matrix assisted laser desorption process is still ambiguous (see Section, 2.4.4.1),[31–40] several sample preparation protocols were evaluated in order to improve the signal–to–noise ratio of the mass spectrographs and acquire structural data on the polymer. The various protocols that have been tested are detailed in Table 2.6. These strategies were based on existing methods that have proven useful for similar systems.[41]

Synthetic polymers are often ionized by cationization (positive ion mode). The doping of sample preparations with metal salts to achieve more homogeneous cationization, rather than relying on ubiquitous impurities, has become common practice.[42]

The THAP / DAC preparation (Figure 2.13f) is used for low molecular weight

48
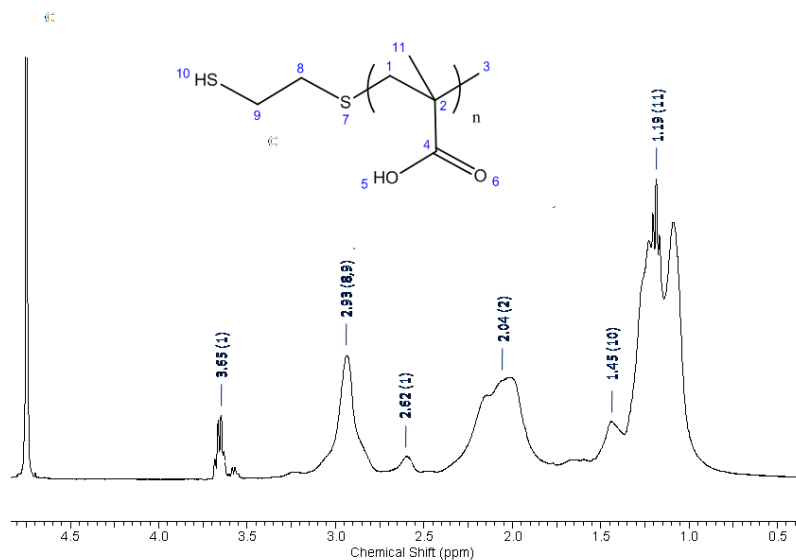
Figure 2.9: ^{1}H NMR spectra of MES terminated pMAA ligand (see Table 2.1).

Mode	Matrix	Solvent	Additive	Figure
Positive ion	DHB	MeOH		2.13a)
Positive ion	DHB	H$_2$O, MeCN		2.13b)
Positive ion	DHB	H$_2$O, MeCN	NaOAc	2.13c)
Positive ion	DHB	H$_2$O, MeCN	IXB	2.13d)
Positive ion	DHB	MeOH	TFA, IXB	2.13e)
Positive ion	THAP	H$_2$O, DAC		2.13f)
Positive ion	DHB DAC			
Negative ion	DHB	H$_2$O, MeCN		2.14a)
Negative ion	DHB	H$_2$O, MeCN	IXB	2.14b)
Negative ion	DHB TFA	MeOH	IXB	2.14c)
Negative ion	THAP	H$_2$O, DAC		2.14d)

Table 2.6: Strategies for the analysis of pMAA–PTMP by matrix–assisted laser desorption/ionization time–of–flight mass spectrometry.

oligonucleotides, with the NH4$^+$ ions acting as a buffer preventing replacement of acidic protons by metal ions.[43] IXB have been used previously for the characterization of polymeric acids by negative ion mode MALDI–TOF–MS.[44] TFA was also added to
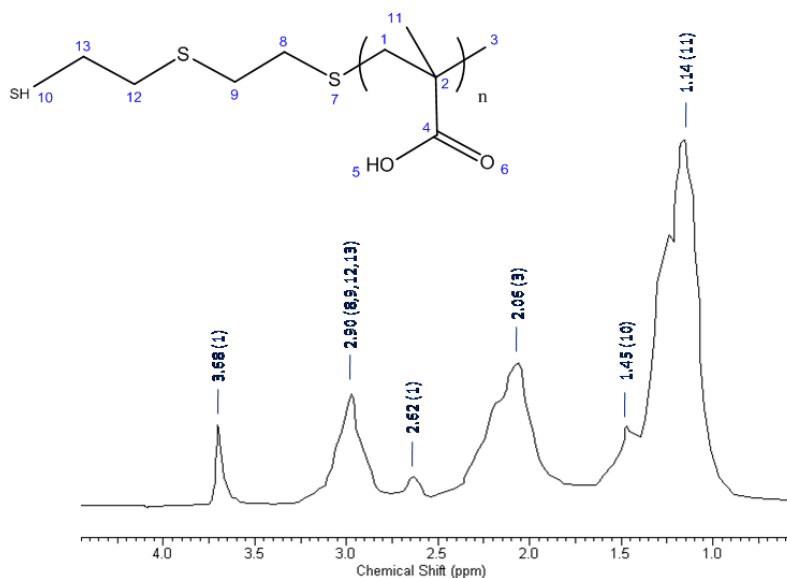
Figure 2.10: ^{1}H NMR spectra of EDT terminated pMAA ligand (see Table 2.1).

promote the acid form of the pendant groups, before ionization.

The observed distributions acquired in positive ion mode are very similar for all preparations (see Figure 2.13a,b,d,e and f), except when NaOAc was added (Figure 2.13c), and for DHB / DAC where no polymeric series were observed (not shown). In general, two polymeric series were clearly observed and both are isotopically resolved. Average molecular weight values obtained for the spectra are consistently slightly lower that those obtained by GPC (M_n 1500 g/mol). Such difference can be ascribed to the calibration process of the GPC, which uses polystyrene standards. Thus, the analysis of polymethacrylates (or other monomers) can be slightly over– or under–estimated due to variations of their polarity and/or shape compared to the standards. Furthermore, several MALDI studies of synthetic polymers show that this technique tends to under–estimate the size distribution and molecular weight of such species.[36,37,45–49]

The major series observed in Figure 2.13 corresponds to the $[M + Na]^+$ species, while the minor series is mass–shifted by +16 Daltons, which could correspond to either the $[M + K]^+$ species or the $[M + Na]^+$ species of an oxidation product. Accurate mass measurement would be required to differentiate between these isobaric species.

The data acquired in negative ion mode are presented in Figure 2.14. Again, no
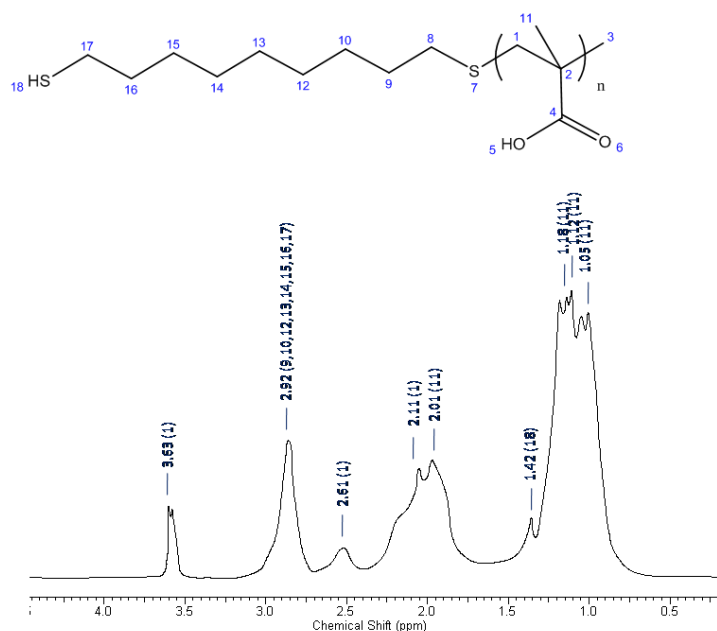
Figure 2.11: ^{1}H NMR spectra of NDT terminated pMAA ligand (see Table 2.1).

polymeric series were observed with DHB / DAC (not shown). No significant shifts of the polymer distribution or discrimination towards any mass region were observed between different sample preparations, and average molecular weight values were consistent with those obtained in positive ion mode (Figure 2.13). However, there were considerable differences in the relative intensities of the species observed. The major series in all the spectra were the [M - H]$^-$ species. There were at least four minor series observed; two series are mass-shifted by +22 and +38 Daltons from the major series and are likely to correspond to the [M - 2H + Na]$^-$ and [M - 2H + K]$^-$ species. Another series could correspond to the loss of H_2O. However, these species are not of sufficient intensity to confirm this assignment.

2.4 Discussion

2.4.1 Free–radical and chain–transfer polymerizations

The idealized process of free–radical polymerization, by comparison with other polymerization methods,[23] implies that the active center of a polymer chain (*i.e.* the radical) is retained by a single chain throughout the course of its growth. The growth of the
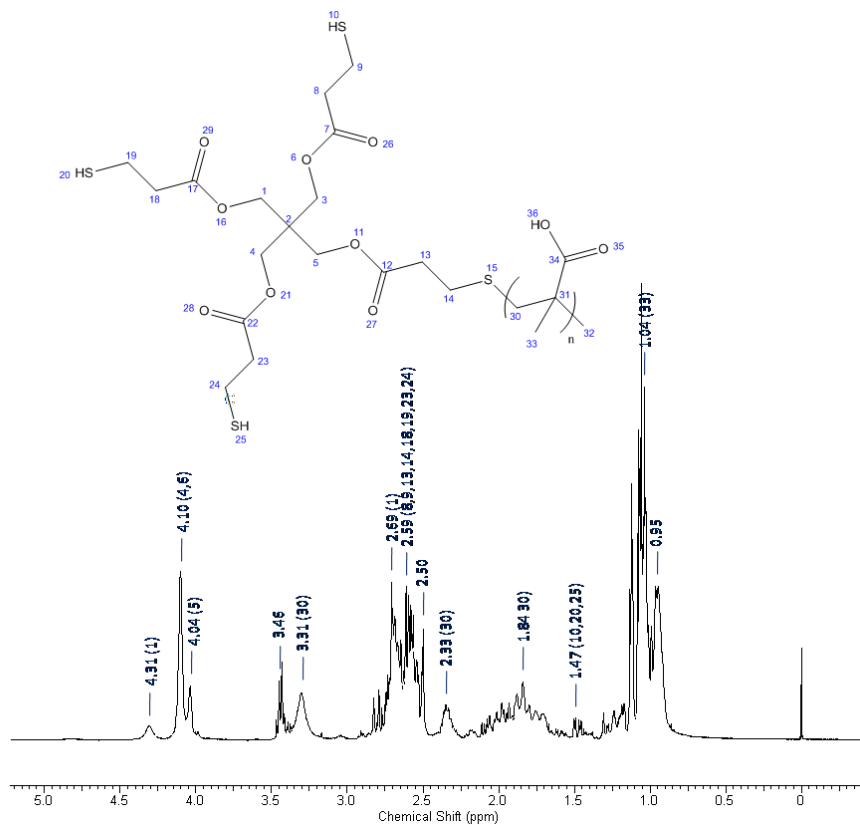
51

Figure 2.12: ^{1}H NMR spectra of PTMP terminated pMAA ligand (see Table 2.1).

chain occurs by sequential addition of monomer units.

The initiation process constitutes the first reaction step, leading to the formation of primary radicals. In this study, the formation of primary radicals is achieved by the thermal decomposition of AIBN (see Figure 2.15). The degree of dissociation is relatively low, but the so–formed radicals are sufficiently reactive to induce the polymerization, with an initiator efficiency close to the unity.[50,51]

The chain propagation process consists essentially of successive free radical attacks on one of the sp^2 carbon atoms of the monomer. One electron of the double bond pairs with the odd electron of the free radical and forms a bond between the free radical and this carbon atom. The remaining electron of the double bond shifts to the other carbon atom, which becomes a new free radical, as shown in Figure 2.16.

During the polymerization process, the propagating macroradical can react with other species in solution and transfer its active centre to this other species, stopping chain growth and forming a new active centre that can start a new growth. During

Figure 2.13: Positive ion MALDI–TOF–MS spectra for pMAA–PTMP. See Table 2.6 and Section 2.3.5 for detailed samples preparation protocols.

the free–radical polymerization process, such transfer can happen between the growing macroradical and the initiator, the monomers, or the solvents. The addition of a species of significantly higher transfer constant within the reaction, that is, a chain transfer agent can decrease and control the molecular weight, structure, and functionality of the so–formed polymeric chains. In this chain transfer polymerization process, thiol containing molecules have been used as chain–transfer agents. Mercaptans are widely used as CTA because of their readily abstractable hydrogen atom.[23]

A mechanism of chain–transfer of this nature consists of the removal by the chain radical of a hydrogen atom from the mercaptan. Thus, the chain molecule loses its
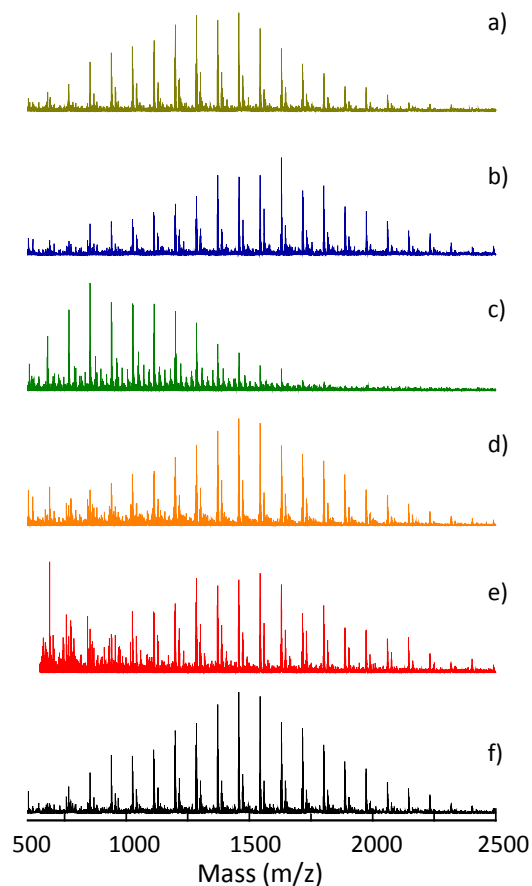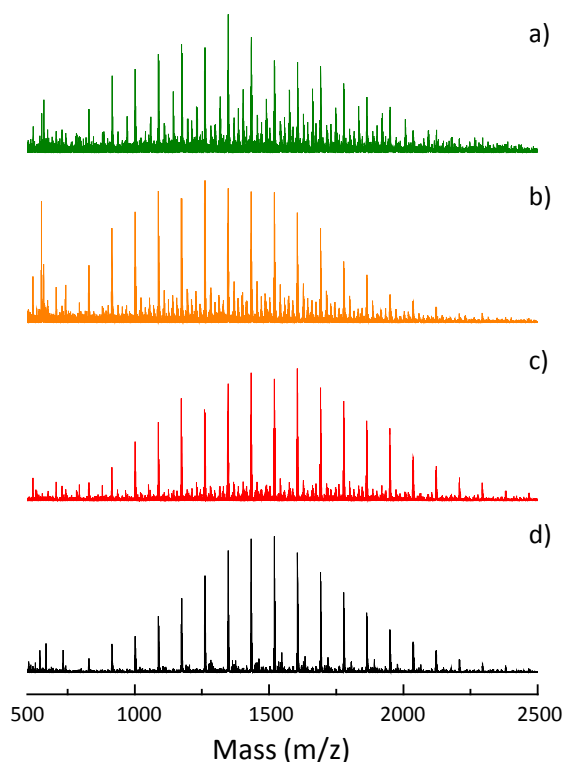
Figure 2.14: Negative ion MALDI–TOF–MS spectra for pMAA–PTMP. See Table 2.6 and Section 2.3.5 for detailed samples preparation protocols.

ability to grow, and the chain–transfer agent acquires the radical character as a consequence of the transfer process and can function as a new initiating species. Studies show that approximately one mole of mercaptan is consumed for each mole of polymer chain that is formed in the approximate ratio of one atom per molecule,[52,53] indicating that each polymer chain produced in using this method is functionalized by, on average, a single thioether (when using a single thiol containing chain–transfer agent). This chain–transfer process is shown in Figure 2.17.

Finally, the termination process is induced by bimolecular reaction between a pair of chain radicals that annihilates their active centers. This may occur by chain coupling, or by disproportionation, as depicted in Figure 2.18a) and b). However, studies show that, under the conditions used during this study, the disproportionation process is the dominant chain–terminating process, and that coupling occurs in a minor extent, again allowing the functionalization of the polymeric species by a single thioether.[54,55]
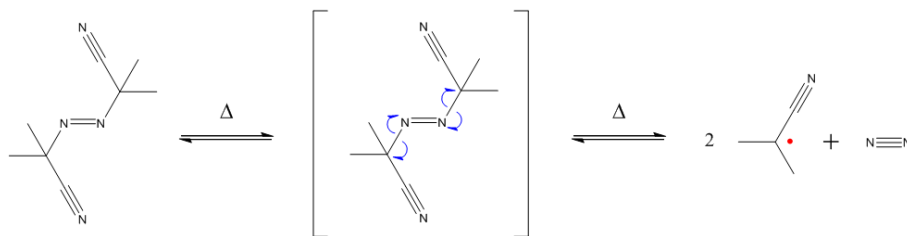
54

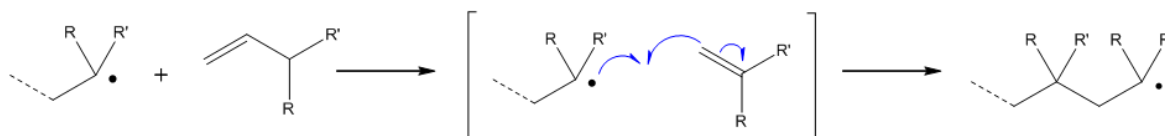Figure 2.15: Scheme of AIBN thermal dissociation.

Figure 2.16: Scheme of propagation steps in chain–transfer polymerization.

2.4.2 Polymer molecular weights and transfer constants.

In the case of a monofunctional chain transfer agent (*i.e.* containing a single thiol), the kinetic of the polymerization is mainly governed by the transfer reaction. Thereby, the relative rate of transfer agent to monomer is given by:

$$\frac{\partial [T]}{\partial [M]} = C_T \frac{[T]}{[M]} \tag{2.1}$$

where $[T]$ and $[M]$ are the transfer agent and monomer concentrations respectively, and C_T the transfer constant (with $C_T = \frac{K_T}{K_P}$, see Figure 2.19). Considering α the conversion, with respect to the monomer, the polymer concentration can be written $[M] = [M]_0 \times (1-\alpha)$. The degree of polymerization of instantaneously formed polymer is described by the Mayo equation and can be written as:

$$\frac{1}{\bar{D}_p} = \frac{1}{\bar{D}_{p0}} + C_T \frac{[T]}{M} \tag{2.2}$$

where $\bar{D}_p$ is the average degree of polymerization and $\bar{D}_{p0}$ is the average degree of polymerization in the absence of a transfer agent. Thus, the plot of the reciprocal of the average degree of polymerization $\frac{1}{\bar{D}_p}$ against the ratio of transfer agent to monomer concentration $\frac{[T]}{M}$ should be linear, the slope of the line representing the transfer constant to dodecanethiol in the present conditions.

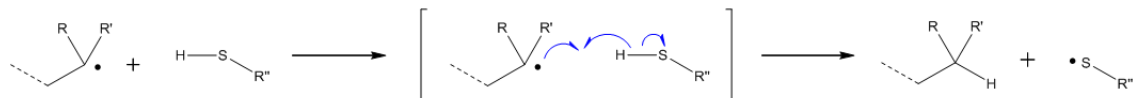Herein, the synthesis of pMAA–DDT polymer chains of various average number

Figure 2.17: Scheme of chain–transfer step in chain–transfer polymerization.
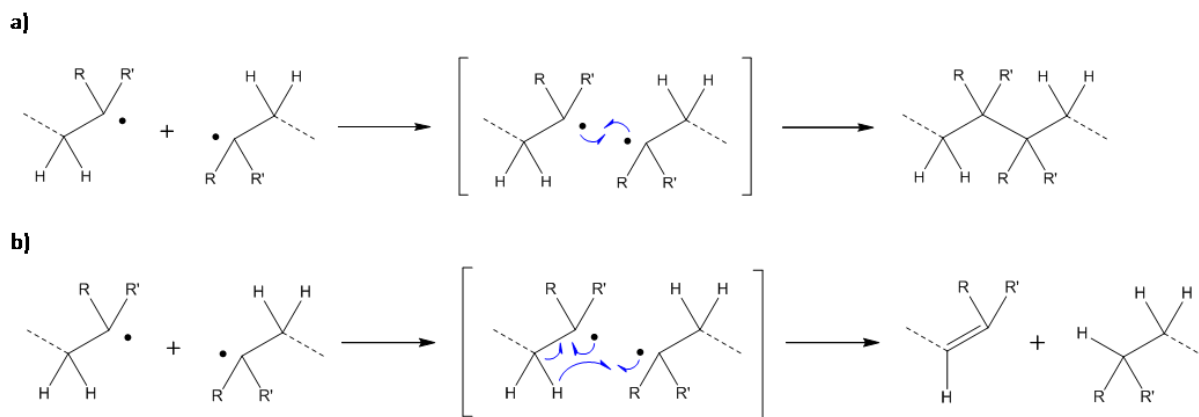
a)

b)

Figure 2.18: Scheme of termination step in chain–transfer polymerization; a) mechanism of termination by coupling, and b) mechanism of termination by disproportionation.

molecular weight was achieved by varying the ratio of chain transfer agent to monomer, a higher ratio leading to shorter chains of lower molecular weight (M_n). The Mayo plot of the pMAA–DDT polymerization under the experimental conditions used in this study (see Section 2.3.2) is presented in Figure 2.20

It shows a linear progression of $\frac{1}{D_p}$ relatively to $\frac{[T]}{[M]}$, as expected; the transfer constant to dodecanethiol C_T can be estimated as 0.22 and $\bar{D}_p$ as 166. Typical values of C_T found in the litterature for similar systems range between 0.1 and 0.6.[24,56,57]

2.4.3 Polymers with multiple thiol containing end–groups.

In the case of a chain transfer polymerization involving a dithiol (double transfer agent), the already–formed macrothiol can participate in subsequent chain transfer processes (see Figure 2.21). In this case, equation 2.2 is written as:

$$1/D_p = 1/D_{p_0} + C_T \frac{[SH]}{[M]} + C_T \frac{[PSH]}{[M]} \tag{2.3}$$

with $[SH]$ the concentration of thiols in solution ($= 2 \times [T]$, $[T]$ being the concentration of chain transfer agent), and $[PSH]$ the concentration of macrothiol. In this case, the concentration of PSH in the solution as a function of the concentration of monomers
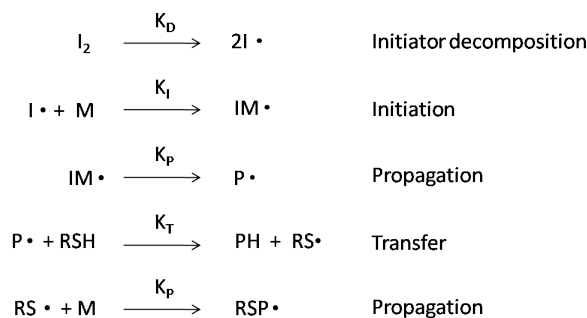
Figure 2.19: Overall mechanism of chain transfer polymerization in the presence of a single initiator.
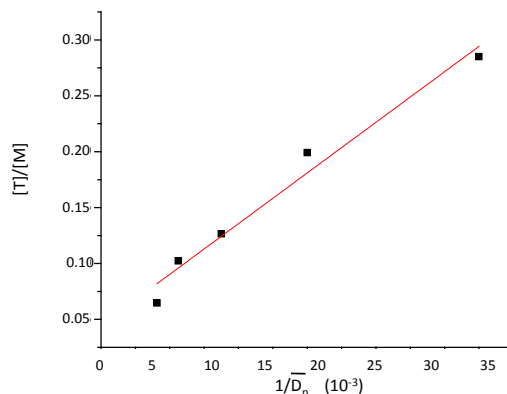
Figure 2.20: Mayo linear plot for pMAA–DDT of various M_n.

concentration is obtained from the relationship between the relative variations in concentration of dithiol containing transfer agent [T] and concentration of macrothiol [PSH] and can be written:

$$-\frac{\partial [PSH]]}{\partial [M]]} = \frac{\partial [T]}{\partial [M]} - C_T' \frac{[PSH]}{M} \tag{2.4}$$

The evolution of the primary chain transfer agent can be written as $\frac{\partial [T]}{\partial [M]} = 2C_T \frac{[T]}{[M]}$, the factor 2 representing the di–functional character of the initiator.

Considering α the conversion with respect to the monomer, the "instantaneous" monomer concentration can be described as $[M] = [M]_0 (1 - \alpha)$, with $[M]_0$ the initial monomer concentration, and the "instantaneous" chain transfer can be written as $[T] = [T]_0 (1 - \alpha)^{2C_T}$ where $[T]_0$ is the initial chain transfer agent concentration. Substituting $[M]$ and $[T]$ in equation 2.4 and integrating it over the conversion range up to α gives:

		K_D		
a)	I_2	$\xrightarrow{K_D}$	$2I\,\cdot$	Initiator decomposition
b)	$I\cdot + M$	$\xrightarrow{K_I}$	$IM\,\cdot$	Initiation
c)	$IM\cdot$	$\xrightarrow{K_P}$	$P\,\cdot$	Propagation
d)	$P\cdot + HSRSH$	$\xrightarrow{K_T}$	$PH + HSRS\cdot$	Transfer
e)	$HSRS\cdot + M$	$\xrightarrow{K_P}$	$HSRSP\cdot$	Propagation
f)	$HSRSP\cdot + HSRSH$	$\xrightarrow{K_T}$	$HSRSPH + HSRS\cdot$	Transfer
g)	$HSRSP\cdot$	$\xrightarrow{K_{Te}}$	$HSRSP$	termination =PSH
h)	$HSRSPH + P\cdot$	$\xrightarrow{K_T}$	$PH + \cdot SRSPH$	Transfer
i)	$M + \cdot SRSPH$	$\xrightarrow{K_P}$	$HPSRSP\cdot$	Propagation
j)	$HSRSH + HPSRSP\cdot$	$\xrightarrow{K_T}$	$HPSRSPH$	Transfer =PP

Figure 2.21: Overall mechanism of chain transfer polymerization in the presence of a double initiator. After formation of a "pri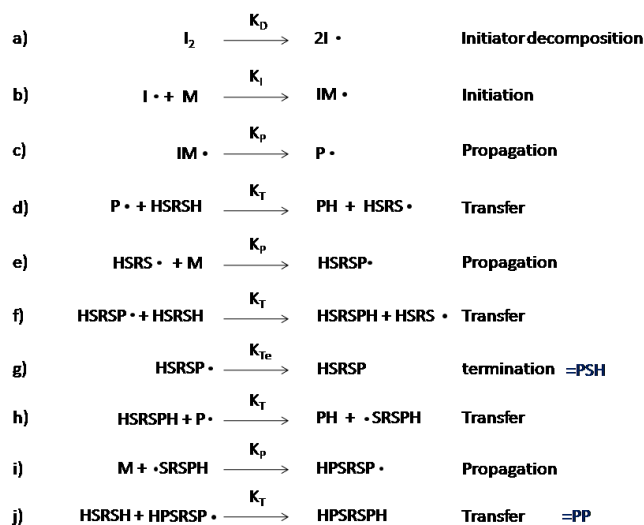mary" macrothiol and subsequent propagation along this reactive centre (steps d and e). If a second chain transfer with an unreacted chain transfer molecule occur, there is a rapid termination of the chain growth and formation of a new thiol radical (step f). However, in the case of a chain growth after stage e, "single" polymer chains are formed along a single thiol of the chain transfer agent and formation of PSH occurs (stage g). PSH might undergo a second chain transfer process and subsequent chain growth (stages i and j), leading to the formation of a "double" polymer along the two thiols of the chain transfer agent (PP).

$$-[PSH] = \left([HDT]_0\left((1-\alpha)^{2C_T} - 1\right)\right) - \int_0^\alpha C_T[PSH]d\left(ln(1-\alpha)\right) \qquad (2.5)$$

Thus, equation 2.5 gives the values of the concentration of macrothiols involved in a single chain growth $[PSH]$ at any conversion α

The instantaneous concentration of "double" polymer (*i.e.* polymer chains growing from both thiols of a chain transfer molecule at a conversion α can be written as:

$$[PP] = \int_0^\alpha]C_T[PSH]d\left(ln(1-\alpha)\right) \qquad (2.6)$$

Figure 2.22 show the relative variations in concentrations of both PSH and PP, calculated a typical case of polymerization in presence of dithiol double chain transfer agent (with arbitrary values of $C_[T]$). [PSH] is seen to increase faster than [PP], this effect being clearly marked at low conversion. As the chain transfer constant of the
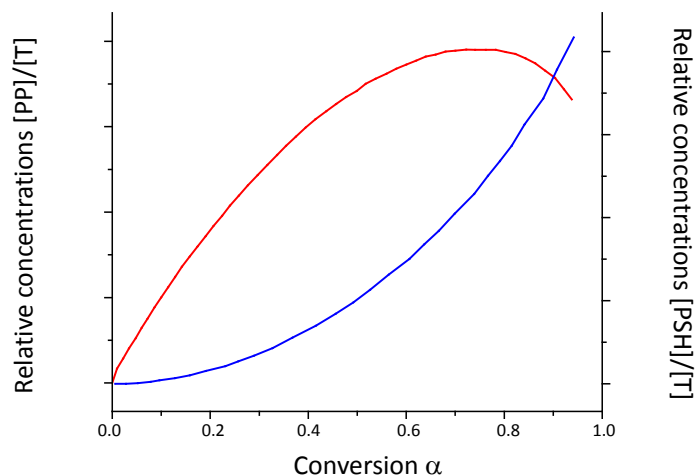
Figure 2.22: Theoretical variations in concentrations of PSH (red line) and PP (blue line) with conversion of polymerization in the presence of a dithiol containing chain transfer agent.

thiol groups in methacrylic acid polymerization is less than unity (dodecanethiol C_T was estimated as 0.22 in Section 2.4.2), their conversion can not reach completion during the polymerization process and is thus kept relatively low.[58] Thus, the reactions described in Section 2.3.4 can be described by the evolution of the curves depicted in Figure 2.22, where the theoretical concentration of $[PSH]$ is higher than the concentration of $[PP]$, meaning that most of the polymer chains are formed along a single thiol of the double initiator, leaving the other one free.

2.4.4   Protocols for MALDI-TOF–MS analysis of pMAA–PTMP.
2.4.4.1   MALDI–TOF–MS principle

The MALDI (matrix–assisted laser desorption ionization) process consists in dissolving the polymeric sample in a matrix, with a metallic ion salt when needed, and load the resulting mixture onto a target surface.[59] After evaporation of the solvent, the solid sample within the matrix is bombarded with a laser light (see Figure 2.23a). Here, a UV laser was used ($\lambda = 337$ nm). The matrices used (DHB, THAP) were chosen for their strong absorption at the laser wavelength.[60] Upon irradiation, the crystalline sample mixture is desorbed from the target surface for $\frac{m}{z}$ analysis.[59–62]

Analyte–analyte interactions, which would result in the formation of polymer clusters within the chamber, are minimized by high dilution of the sample within the matrix (typical dilutions of 1:1000).

a)

UV irradiation

Polymer analyte

Positive ions (Na⁺, H⁺)

Matrix

desorption

b)

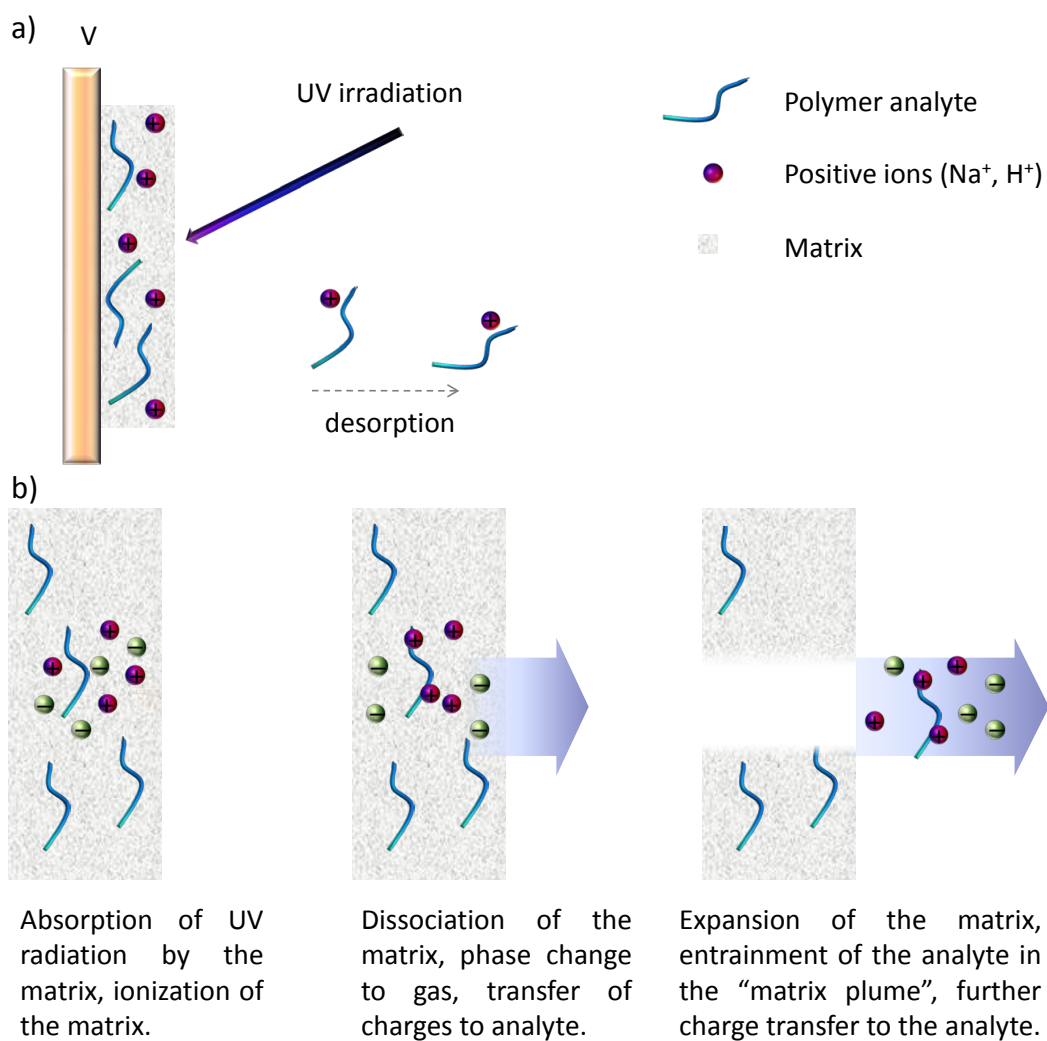| Absorption of UV radiation by the matrix, ionization of the matrix. | Dissociation of the matrix, phase change to gas, transfer of charges to analyte. | Expansion of the matrix, entrainment of the analyte in the "matrix plume", further charge transfer to the analyte. |

Figure 2.23: Schematic of a) the MALDI source and b) the detailed MALDI process.

Even though the desorption process is not yet completely understood, it seems that the laser irradiation leads to the breaking of the crystalline matrix structure, thus creating a pressured gas in which charge transfer between the matrix, the metal salt and the analyte can take place.[62] The so–formed gas transports the analyte, with further charge transfer reactions, as depicted in Figure 2.23b.

The use of a matrix that can absorb most of the laser energy allows analyte molecules

not to be broken, thus, making MALDI an interesting analytical methods for polymeric structures and to obtain an $\frac{m}{z}$ distribution with no (or few) chain breaks.

The selection of a suitable matrix is still a trial and error process and the search of useful matrix compounds has been an active area in MALDI research.[31–40] In general, the choice of matrix materials is achieved more or less empirically and can be completely unrelated to the analyte in terms of structure or physical properties. For the protocols tested herein, matrices were chosen for their low molecular weight and high UV absorbance (allowing vaporisation under laser excitation), the presence of carboxylic acid for cationization process,[39] and for their miscibility with the polymer structure in water or ethanol.

After acceleration of the ions produced through an applied potential, separation of species of different $\frac{m}{z}$ occurs. Thus, the ions cross ("fly") a distance d in a time t, with a velocity of $t = \frac{d}{v}$. Their "time of flight" is dependent on their velocity, or kinetic energy, which in turn, depends on their $\frac{m}{z}$ values (see equation 2.7.

$$v = \sqrt{2 \times z \times e \times v} \Rightarrow t = \sqrt{\frac{m}{z}} \times \sqrt{\frac{d}{2 \times e \times V}} \qquad (2.7)$$

The formed ions impact onto an ion–detector, and the time interval between the pulse of laser light and the impact of each ion on the detector is measured. This produces signals whose intensities are proportional to the number of ions arriving at the electron multiplier (molar response). The MALDI–TOF mass spectrum is then obtained by recording the detector signal as a function of time.

Here, the use of a "soft" ionization process allow the analysis of "unbroken" polymer structures; the distributions observed in Figures 2.13 and 2.14 are related, in some extent, to the size distribution of the polymer chains.

2.4.4.2 Evaluation of the different sample preparations

The observed isotope distributions of each species in both positive and negative ion mode extend 1 and 2 Daltons lower than the equivalent theoretical isotope distributions (Figure 2.14). The fractional masses of these additional ions are identical to the expected ions indicating two chemically similar species are overlapping, which differ by a single point of unsaturation. It has been shown previously that disulphide bonds may

form during the analysis of peptides that contain thiol groups.[63] The same changes may occur with the PTMP end–group in this case. The observed polymeric distributions are monomodal, and the relative intensities of the ^{12}C–isotope for the expected and additional species remain approximately constant across the distribution, which both signify possible disulphide bonds would be intramolecular.

The use of IXB appears to have some benefit in improving the signal–to–noise ratio, but it is interesting that the major series observed is still $[M + Na]^+$ when one would have expected the $[M + H]^+$ series to be increased. Good quality data were achieved with a significantly lower laser power compared with preparations without IXB. It should be noted that this improvement in the signal–to–noise ratio can be ascribed to the laser intensity as well as the use of IXB. Previous studies infer that analysis carried out using laser power close to the "threshold intensity", *i.e.* close to the minimum energy needed to break the matrix could benefit the quality of the spectra.[64] Little difference was observed between the spectra acquired with the DHB prepared in MeOH and in H$_2$O/MeCN.

The addition of TFA was intended to promote protonation, which succeeded for low mass matrix or impurity species, but resulted in a reduction of the signal-to-noise ratio of the cationized polymer species (Figure 2.13e). This result is contradictory to earlier studies of how pH affects the MALDI analysis of poly(methyl methacrylate).[65] The rationalization of this difference remains challenging since the desorption process is not yet clearly understood.[31–34]

The experiments realized in negative ion mode indicates that the use of IXB appear to enhance deprotonation and / or suppress replacement of acidic protons by metal ions, increasing the signal–to–noise ratio of the major series. Again, good quality data were achieved with a significantly lower laser power compared with preparations without IXB.[64] There is possibly a slight further enhancement and / or suppression when TFA is added (Figure 2.14c), but the most significant increase in signal–to–noise ratio was observed when the THAP / DAC method was used. This benefit must be balanced against the loss of potentially useful information of other species within the sample. The ions in each series were isotopically resolved and the additional ions observed 1 and 2 Daltons lower than the equivalent theoretical isotope distributions in positive ion

mode were also observed. There is increased confidence that these additional ions are not artifacts, even if they are a product of the MALDI–TOF–MS process.

2.5 Summary

Libraries of linear polymeric structures have been prepared by chain transfer polymerization, with the objective to use them as steric and/or electrosteric stabilizers for the formation and stabilization of gold nanoparticles. All polymers' backbones are hydrophilic, thus allowing the subsequent preparation of water soluble gold particles. They are all functionalized with a thioether (and/or thiol) containing end–group that can act as an "anchor" site and allow their adsorption onto gold surfaces. Some of those structures were prepared with end groups functionalities of various hydrophobicity in order to study the influence of this parameter during the particles formation and stabilization. The ability of those structures to stabilize gold particles is described in Chapter 3.

2.6 Bibliography

1. R.C. Mucic C.A. Mirkin R.L. Lestinger J.J. Storhoff, R. Elghanian. *J. Am. Chem. Soc.*, 120:1959, 1998.

2. A.W. Snow H. Wohltjen. *Anal. Chem.*, 70:2856, 1998.

3. C.M. Tsionsky A.J. Bard C. Demaille, M. Brust. *Anal. Chem.*, 69:2323, 1997.

4. D. Bethell D.J. Schiffrin R. Whyman M. Brust, M. Walker. *Chem. Commun.*, page 801, 1994.

5. R.W. Murray M.J. Hostetler, A.C. Templeton. *Langmuir*, 15:3782, 1999.

6. M. Sutton S.G.J. Mochrie M.B. Lurio A. Ruhm M.B. Lennox M.K. Corbierre, N.S. Cameron. *J. Am. Chem. Soc.*, 123:10411, 2001.

7. R.E. Morris A.B. Mayer, J.E. Mark. *Polym. J.*, 3:197, 1998.

8. R.E. Cohen Y.N.C. Chan, R.R. Schrock. *Chem. Mater*, 4:24, 1992.

9. T.K. Mandal R.R. Bhattacharjee. *J. Coll. & Int. Sc.*, 307:288, 2007.

10. J.R. Heine M.G. Bawendy K.F. Jensen J. Lee, V.C. Sundar. *Adv. Mater.*, 12:1102, 2002.

11. R.B. Lennox M.K. Corbierre, N.S. Cameron. *Langmuir*, 20:2867, 2004.

12. A.B.R. Mayer. *Mater. Sci. Eng.*, C6:155, 1998.

13. H.-A. Klok M. Moller S.T. Selvan, J.P. Spatz. *J. Chem. Mater.*, 10:132, 1998.

14. T.J. McCarthy J.J. Watkins. *Chem. Mater.*, 7:1991, 1995.

15. P. Alexendridis T. Sakai. *Langmuir*, 21:8019, 2005.

16. U.S. Schubert J.F. Gohy M. Filali, M.A.R. Meier. *Langmuir*, 21:7995, 2005.

17. D.T. Miles R.W. Murray W.P. Wuelfing, S.M. Gross. *J. Am. Chem. Soc.*, 120:12969, 1998.

18. P.V. Braun R.G. Schimmin, A.B. Schoch. *Langmuir*, 20:5613, 2004.

19. H. Jiang E. Kauppinen H. Tenhu J. Shan, M. Nuopponen. *Macromolecules*, 36:4526, 2003.

20. R. Haag J.D. Marty R. Thomann N. Lauth de Viguerie C. Mingotaud M. Kramer, N. Perignon. *Macromolecules*, 38:8308, 2005.

21. D.C. Sherrington S. Graham, P.A.G. Cormack. *Macromolecules*, 38:86, 2005.

22. F. Straub F. Haaf, A. Sanner. *Polym. J.*, 17:143, 1985.

23. T.P. Davis K. Matyjaszewski. *Handbook of Radical Polymerization.* Wiley Interscience, 2002.

24. E.H. Immergut E.A. Grulke, J. Brandrup. *Polymer Handbook.* Wiley–Interscience, 2004.

25. C. Draghici M. Teodorescu. *Polym. Bull.*, 56:359, 2006.

26. V.P. Balagangadharan C.P.R. Nair, P. Sivadasan. *J. Macromol. Sci., Pure Appl. Chem.*, A36:51, 1999.

27. B. Tan A.I. Cooper M.F. Wyatt, N. Schaeffer. *J. Am. Soc. Mass Spectrom.*, 18:1507, 2007.

28. M. W. F. Nielen. *Mass Spectrom. Rev.*, 18:309, 1999.

29. D.M. Hercules R. Murgasova. *Int. J. Mass Spectrom.*, 226:151, 2003.

30. M.S. Montaudo G. Montaudo, F. Samperi. *Science*, 31:277, 2006.

31. B.T. Chait R.C. Beavis, T. Chaudhary. *Org. Mass. Spectrom.*, 27:156, 1992.

32. R.C. Beavis. *Org. Mass Spectrom.*, 27:653, 1992.

33. K. Biemann P. Juhasz, C.E. Costello. *J. Am. Soc. Mass Spec.*, 4:399, 1993.

34. L.M. Smith M.C. Fitzgerald, R.G. Parr. *Anal. Chem.*, 65:3204, 1993.

35. C.K. Lim M.R. Russel, J.H. Lamb. *Rapid. Com. Mass. Spec.*, 9:968, 1995.

36. A. Vertes X. Tang, P.A. Dreifuss. *Rapid Commun. Mass Spec.*, 9:1141, 1995.

37. DeSimone R.W. Linton G.W. Lange R.M. Friedman A.M. Belu, J.M. *J. Am. Soc. Mass Spec.*, 7:11, 1996.

38. U.P. Sclunegger D.H.M. Liu. *Rapid Commun. Mass Spec.*, 10:483, 1996.

39. J.T. Watson D.A. Gage N. Xu, Z.H. Huang. *J. Am. Soc. Mass. Spec.*, 8:116, 1997.

40. P.J. Savickas S.F. Macha, P.A. Limbach. *J. Am. Soc. mass Spec.*, 11:731, 2000.

41. R.P. Lattimer G. Montaudo. *Mass Spectrometry of Polymers.* CRC Press, 2001.

42. M. Karas F. Hillenkamp U. Giessmann U. Bahr, A. Deppe. *Anal. chem.*, 64:2866, 1992.

43. M. Schar H.E. Moser U. Pieles, W. Zurcher. *Nucleic Acid Res.*, 21:3191, 1993.

44. D.E. Karr P.O. Danis. *Macromolecules*, 28:8548, 1995.

45. H.J. Rader K. Mullen H. Schlaad A.H.E. Muller R.-P. Kruger J. Spickermann, K. Martin. *Eur. Mass. Spec.*, 2:161, 1996.

46. D.M. Haddleton P.J. Derrik J. Axelsson, E. Scrivener. *Macromolecules*, 29:8875, 1996.

47. J.E. Varney E. Scrivener P.J. Derrick D.M. Haddleton P.M. Lloyd, K.G. Suddaby. *Eur. Mass. Spec.*, 1:293, 1995.

48. C. McEwen C. Jackson, B. Larsen. *Anal. Chem.*, 68:1303, 1996.

49. L. Li D.C. Schriemer. *Anal. Chem.*, 69:4169, 1997.

50. G. Wittig G.V. Schultz. *Naturwissenschaften*, 27:387, 1939.

51. G. V. Schultz. *Z. Electrochem.*, 47:265, 1941.

52. R.E. Allen R.J. Dearborn R.H. Snyder, J.M. Stewart. *J. Am. Chem. Soc.*, 68:1422, 1946.

53. G.D. Sands F.T. Wall, F.W. Banes. *J. Am. Chem. Soc.*, 68:1429, 1946.

54. D Whittle C.H Bamford, G.C Eastmond. *Polymer*, 10:771, 1969.

55. D.M. Haddleton K.G. Suddaby M.D. Zammit, T.P. Davis. *Macromolecules*, 30:1915, 1997.

56. J. Sreedhar V.R. Gouariker, N.V. Viswanathan. *Polymer Science.* 1986.

57. V.P. Balagangadharan C.P. Reghunadhan Nair, P. Sivadasan. *J. Macromol. Sci. A*, 36:51, 1999.

58. T. Corner. *Polym. Sci.*, 62:95, 1984.

59. G. Siuzdak. *Mass Spectrometry for Biotechnology.* Academic Press, San Diego, CA, 1996.

60. W. H.J. Rader, W. Schrepp. *Acta Pol.*, 49:272, 1998.

61. R.C. Beavis B.T. Chait F. Hillenkamp, M. Karas. *Anal. Chem.,*, 63:1193A, 1991.

62. R.J. Cotter. *Time–of–flight Mass spectrometry.* ACS Professional Reference Books,, 1997.

63. L.D.S. Yadav. *Organic Spectroscopy*. Kluwer Academic, 2005.

64. F. Mayer G. Standing W. Ens, Y. Mao. *Rapid Commun. Mass Spec.*, 5:117, 1991.

65. P. Williams D. Dogruel, R.W. Nelson. *Rapid Commun. Mass Spectrom.*, 10:801, 1996.

Chapter 3

Size–Controlled Synthesis of Near–Monodisperse Polymer Coated Gold Nanoparticles

3.1 Introduction

IN MODERN NANOSCALE science, it is important to understand and control the physical and chemical properties of gold nanoparticles, which are generally size dependent.[1,2] Gold nanoparticles are commercially available in many forms, and numerous preparative methods for particles from about 1 nm to several micrometers diameter are documented in the literature.[3–7] Nevertheless, only a handful of standard procedures are employed routinely to prepare gold particles for a multitude of applications. These methods are reliable, simple to carry out, and lead to uniform particles with a narrow size distribution in the desired range. The most widely applied procedures to obtain gold hydrosols are variations of the classic Turkevich–Frens citrate reduction route.[8,9] Most hydrophobic (and some hydrophilic) particles are prepared by borohydride reduction in an organic solvent in the presence of thiol capping ligands using either a two-phase liquid/liquid system or a suitable single-phase solvent.[10–19] The latter approach is usually employed for particles in the 1 to *ca.* 8 nm range.

Gold nanoparticles are useful in a broad range of applications,[20–22] but practical limitations are apparent when monodispersity is required, for example, in electrochemical quantized capacitance charging,[21–23] single-electron transistor assembly,[24] and ap-
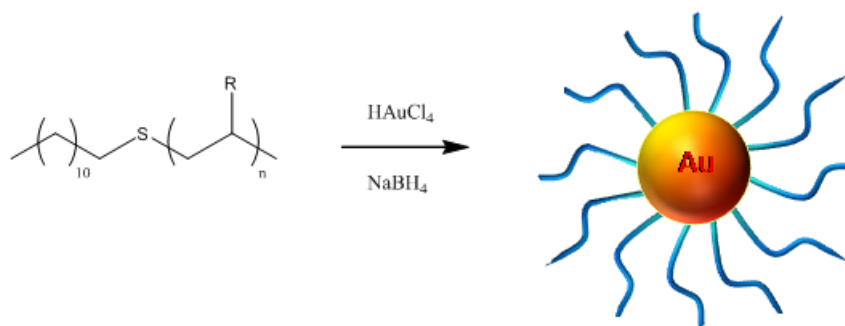
Figure 3.1: Scheme representing the polymer stabilized gold nanoparticle preparation (bottom).

plications such as thermal gradient optical imaging.[25] In many cases, monodisperse fractions of particles must be prepared, usually in low yield following cumbersome size separation procedures, such as size exclusion chromatography, centrifugation or serial filtration procedures.[26,27] Moreover, such fractionation methods do not necessarily lead to monodisperse samples.[28] The availability of a simple, robust protocol for the gram–scale preparation of water–soluble uniform gold nanoparticles below 5 nm is thus of great practical value for numerous applications.

Furthermore, there is a real need to introduce complementary characterization methods to assess the degree of control over particle size for the bulk sample; many studies rely exclusively on TEM measurements, often using a relatively small sampling area. It is easy to significantly overestimate the monodispersity of a sample using TEM analysis in isolation.[29,30]

In this Chapter, a methodology for the preparation of near monodisperse gold nanoparticles using series of water-soluble polymeric ligands described in Chapter 2 is presented (see Figure 3.1). The size of the so–formed particles can be adjusted between one and five nanometres by varying the polymer/gold ratio.[31] The near monodispersity of the particles, their water solubility and the one pot synthesis all make this method an attractive and versatile synthetic route when most other methods for producing monodisperse particles use fractionation, adding a costly and time consuming step to the synthesis.

All gold suspensions have been characterized by different analytical methods (*i.e.* transmission electron microscopy, UV–visible absorption spectroscopy and dynamic

light scattering) to ensure the observed sizes and dispersions are representative of the whole samples.

3.2 Experimental

3.2.1 Materials

Hydrogen tetrachloroaurato trihydrate ($HAuCl_4.3H_20$) and sodium borohydride ($NaBH_4$) were purchased from Aldrich and used as received, unless otherwise described. For all experiments, Milli-Q water (18.2 MΩ) was used, purified using an ultrapure system MilliQ Plus 185 (Millipore purification pack). $0.45\mu m$ pore size Millex–HA microfilter were purchased from Millipore. Dialysis membranes (7000 daltons cut–off) were purchased from Pierce Chemicals.

3.2.2 Methods

3.2.2.1 Gold nanoparticle synthesis

indexGold nanoparticles!SynthesisA general procedure for the preparation of polymer–stabilized gold nanoparticles in water is described as follows. An aqueous solution of $HAuCl_4$ (10 ml, 0.5 mM) was added to an aqueous polymer solution under vigorous stirring to give a final concentration of $HAuCl_4$ of 0.5 mM. Each particle preparation was repeated at four different polymer concentrations (0.006, 0.06, 0.6 and 6 mM) — that is, four different particle preparations were produced for each polymer ligand. Freshly prepared $NaBH_4$ solution (1 mL, 50 mM) was added after mixing the gold / polymer solutions for one hour. The reducing agent was added rapidly in two aliquots (2 × 0.5 mL). The reaction was allowed to continue overnight under uniform and vigorous stirring. The gold nanoparticles were separated from excess unreacted polymer ligand by filtration through 450 um pore size filters three times and then, concentrated with a Vivaspin centrifugal filter (Vivascience, Hannover, Germany; 10000 g/mol cut–off). Lastly, the particles were dialyzed against water overnight using a 7000 Da cut–off dialysis membrane in order to remove any last traces of unreacted polymer ligand.

3.2.2.2 Gold nanoparticle characterization.

UV–visible spectroscopy UV–visible spectra were carried out using a microplate reader (Quant, Bio–Tek Instruments). The aqueous gold nanoparticle solutions (200 μl) were analyzed in 96–well microplate at 25°C.

Dynamic light scattering Dynamic light scattering (DLS) measurements were carried out with Zetasizer Nano ZS (Malvern, UK) instrument equipped with a 1 cm optical path cell. Each sample was analyzed three times.

Transmission electron microscopy Transmission electron microscopy (TEM) micrographs of the colloidal dispersions were obtained using a JEM–2000EX/FX instrument operated at an accelerating voltage of 200 kV. A high-resolution carbon–supported copper mesh was used to support the colloidal dispersions. Specimens for inspection by TEM were prepared by evaporating a droplet of the filtered and dialyzed gold nanoparticle solutions onto a carbon–coated copper mesh grid directly from water. The diameter of each particle was quantified using ImagesJ software (1.34s, NIH, USA) to analyze the digitized photographic images for each sample in the magnification range 200,000 – 500,000 times. A histogram of the particle size distribution and the average particle diameter were obtained by measuring about 200 particles in arbitrarily chosen areas in the photograph.

Mass spectrometry of gold nanoparticles. Ion exchange resin was loaded with NH_4^+ ions. HPLC–grade acetonitrile (MeCN) and Milli–Q water were used where appropriate. The DHB matrix solution was made to a concentration of 10 mg/mL in 1:1 (v/v) H_2O/MeCN. A solution of pMAA–PTMP was prepared (10 mg/mL in H_2O), and 200 μL was placed into a plastic, snap–top vial. Roughly 0.5 mg of NNH_4^+ loaded resin was added, and the solution was agitated via vortex mixer at slow speed for 20 s. Sample and matrix solutions were mixed in a 1:10 ratio in a separate plastic vial. A 0.5 μL amount of the final mixture was spotted onto a stainless steel sample plate and dried in a stream of cool air. MALDI–TOF–MS data were acquired using an Applied Biosystems Voyager DE–STR spectrometer (Framingham,MA), which was equipped with a nitrogen laser ($\lambda = 337$ nm). The instrument was operated in negative–ion, linear mode. The accelerating voltage was 25 kV, while the grid voltage was maintained
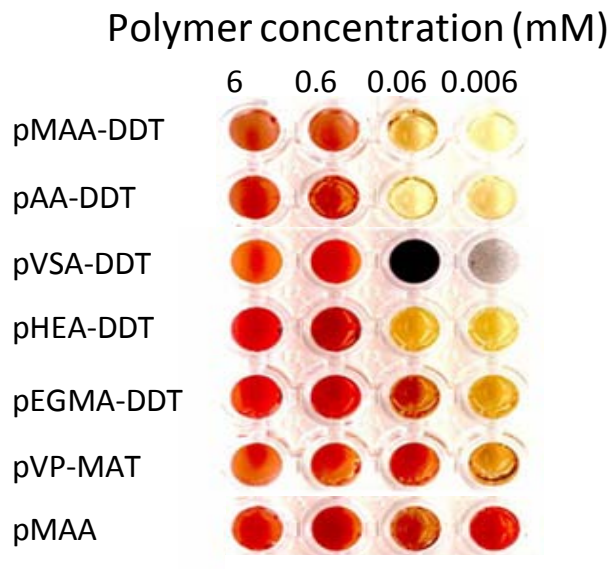
71

Figure 3.2: Color images of gold suspensions stabilized with various DDT terminated polymers at different polymers concentrations.

at 91%. The delay time was 450 ns, and laser fluence was attenuated to just above the threshold of ionization. The laser was fired at a frequency of 3 Hz, and spectra were accumulated in multiples of 25 laser shots with 150 shots in total. Postacquisition processing of data was performed utilizing Data Explorer V4.0 software supplied by Applied Biosystems

3.3 Results

3.3.1 Gold nanoparticle synthesis

3.3.1.1 Influence of the polymer main chain

All six thioether-terminated polymer ligands (pMAA–DDT, pAA–DDT, pVP–DDT, pVSA–DDT, pHEA–DDT and pEGMA–DDT described previously in Chapter 2 Section 2.3.1 gave rise to stable red-colored gold nanodispersions at a polymer concentration of 0.006 mM. At higher polymer concentrations, the relative performance of the ligands varied markedly. Color images of the as-produced polymer-stabilized gold nanodispersions are shown in Figure 3.2. In general, the color of nanodispersions changed from red to yellow when the polymer concentration was varied from 0.006 to 6.0 mM, indicating that particles of different average sizes were prepared in each case.
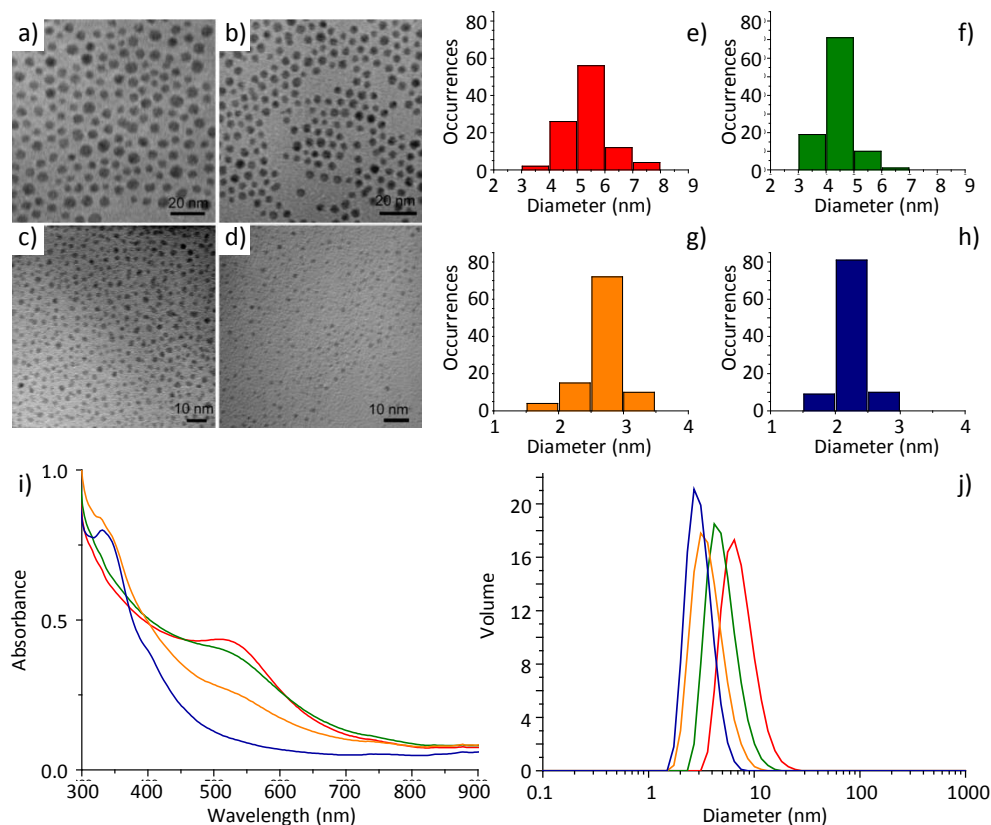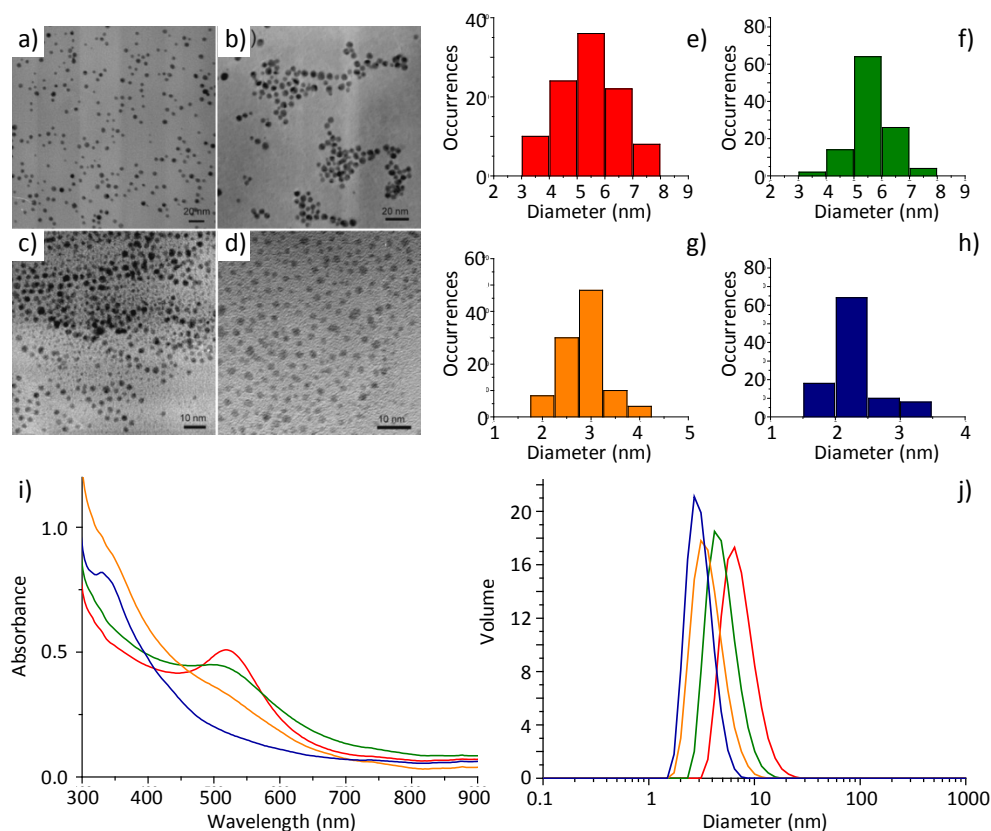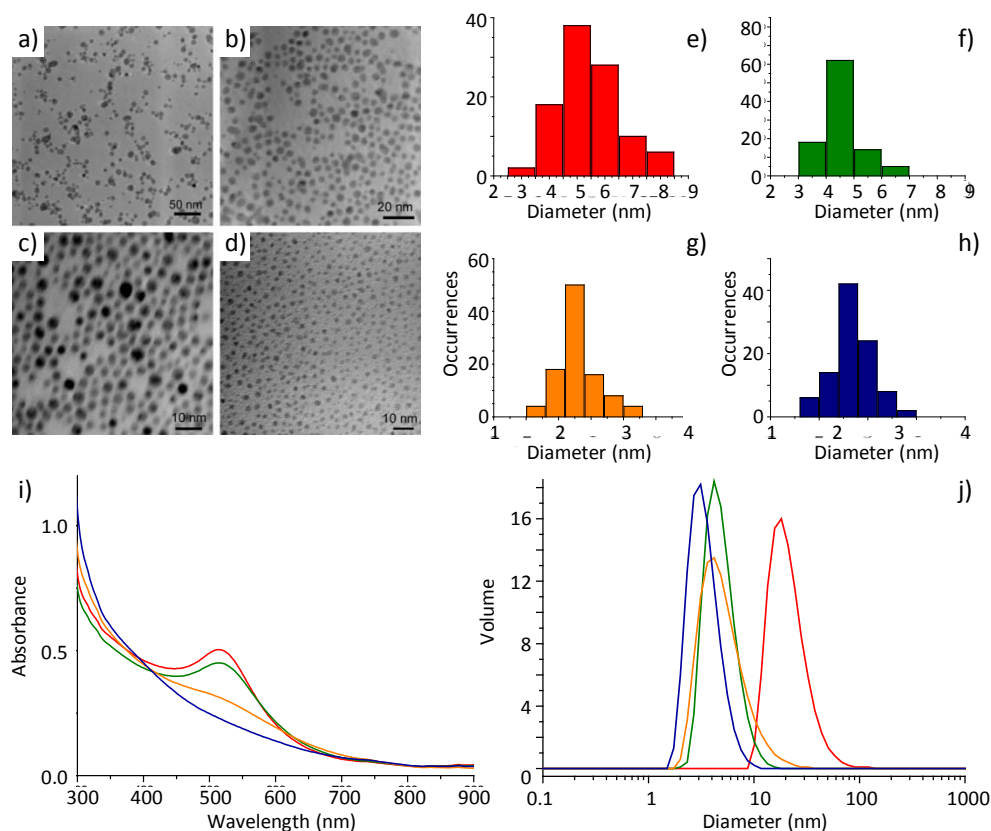
Figure 3.3: TEM images of pMAA–DDT stabilized gold nanoparticles obtained from polymer concentration at a) 0.006, b) 0.06, c) 0.6 and d) 6 mM; e), f), g) and h) histograms of the corresponding distribution of particle sizes of a), b), c) and d), respectively. (i) UV–visible spectra of pMAA–DDT stabilized gold nanoparticles obtained from polymer concentration at 0.006 (red line), 0.06 (green line), 0.6 (orange line) and 6.0 mM (blue line), respectively. (j) DLS graphs of pMAA–DDT stabilized gold nanoparticles obtained from polymer concentration at 0.006 (red line), 0.06 (green line), 0.6 (orange line) and 6.0 mM (blue line), respectively.

The polymer ligand pVSA–DDT was an exception to this trend; at higher concentrations of pVSA–DDT (0.6 mM and 6.0 mM), the gold nanodispersion turned dark blue / black and precipitation was observed (Figure 3.2) indicating that the particles are not stable against aggregation with this ligand. The reasons of this effect are difficult to explain, however, one can arguably ascribe it to the presence of sulphurs along the polymer backbone that might interfere during the gold particles growing process and/or act as a "cross–coupling" agent after partial hydrolysis of the polymer, leading to particles aggregation along the polymer chains.[32,33]
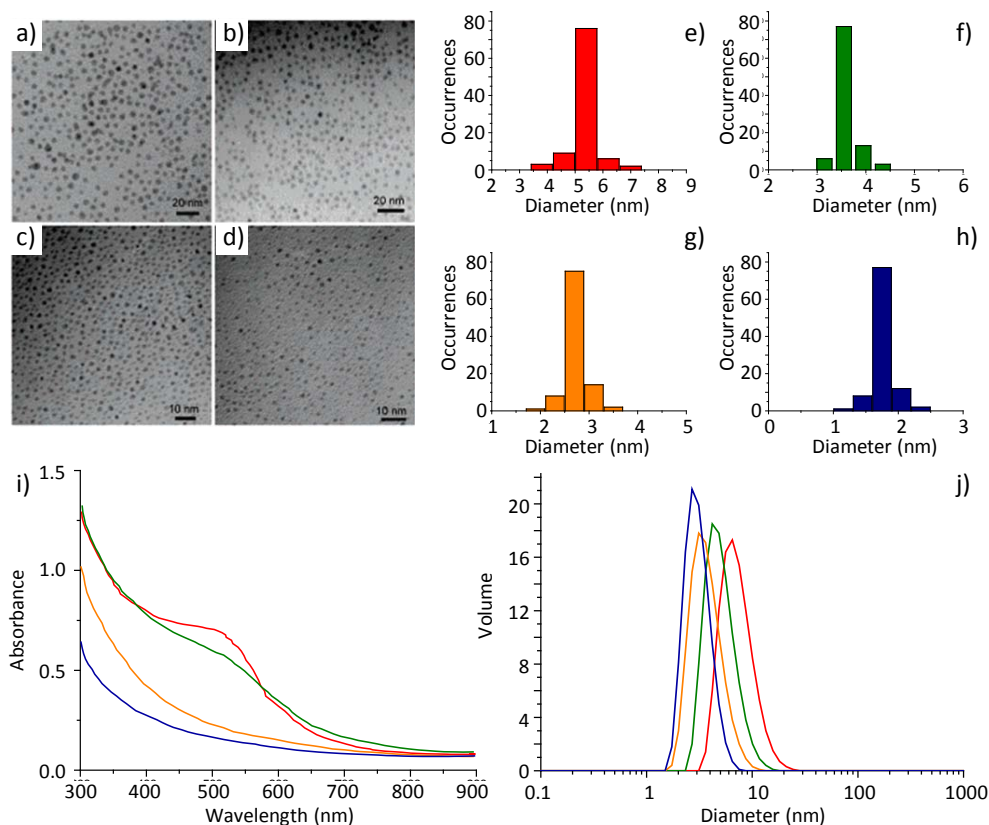
73

Figure 3.4: TEM images of pHEA–DDT stabilized gold nanoparticles obtained from polymer concentration at a) 0.006, b) 0.06, c) 0.6 and d) 6 mM; e), f), g) and h) histograms of the corresponding distribution of particle sizes of a), b), c) and d), respectively. (i) UV–visible spectra of pHEA–DDT stabilized gold nanoparticles obtained from polymer concentration at 0.006 (red line), 0.06 (green line), 0.6 (orange line) and 6.0 mM (blue line), respectively. (j) DLS graphs of pHEA–DDT stabilized gold nanoparticles obtained from polymer concentration at 0.006 (red line), 0.06 (green line), 0.6 (orange line) and 6.0 mM (blue line), respectively.

All of the stable nanodispersions were characterized by transmission electron microscopy (TEM), UV–visible absorption spectroscopy and dynamic light scattering, the results are depicted in Figures 3.3, 3.4, 3.5, 3.6, 3.7 and 3.8.

Overall, ligands pMAA-DDT (M_n = 3220 g/mol) and pAA-DDT (M_n = 2550 g/mol) gave rise to gold nanoparticles with the most narrow size distribution over the polymer concentration range 0.006-6.0 mM. The UV–visible absorption spectra vary strongly as the concentration of the polymer ligands are changed and suggest that the average particle size is below 5 nm for all samples since larger particles would exhibit
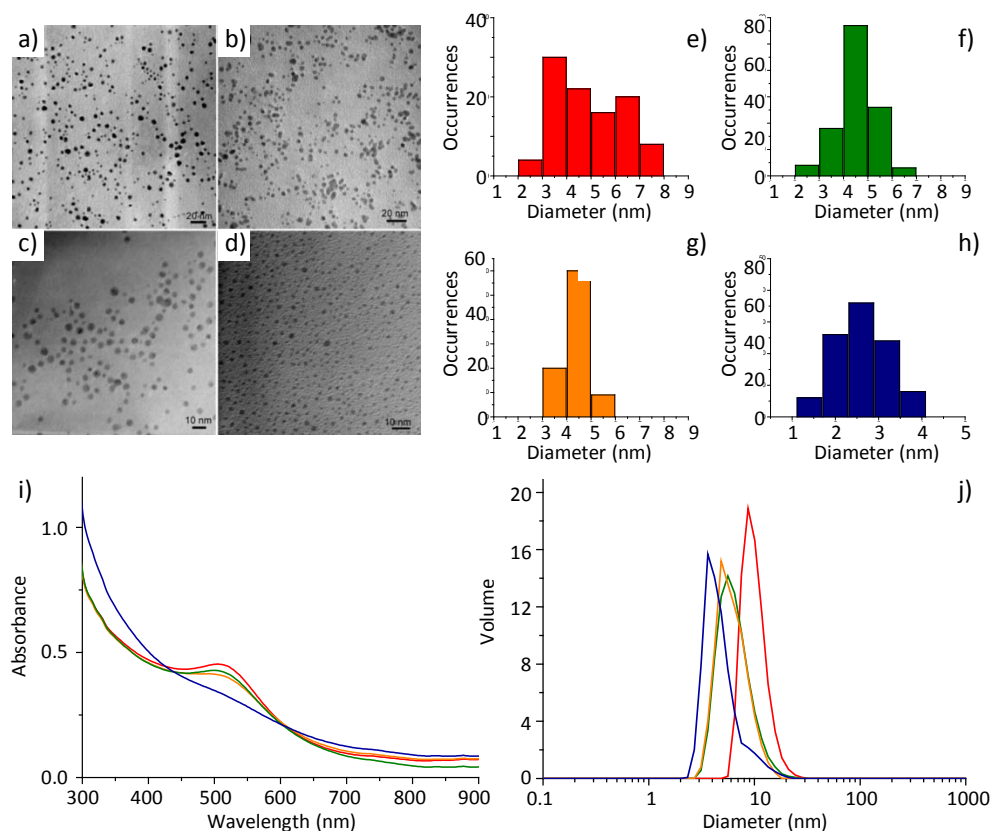
Figure 3.5: TEM images of pEGMA–DDT stabilized gold nanoparticles obtained from polymer concentration at a) 0.006, b) 0.06, c) 0.6 and d) 6 mM; e), f), g) and h) histograms of the corresponding distribution of particle sizes of a), b), c) and d), respectively. (i) UV–visible spectra of pEGMA–DDT stabilized gold nanoparticles obtained from polymer concentration at 0.006 (red line), 0.06 (green line), 0.6 (orange line) and 6.0 mM (blue line), respectively. (j) DLS graphs of pEGMA–DDT stabilized gold nanoparticles obtained from polymer concentration at 0.006 (red line), 0.06 (green line), 0.6 (orange line) and 6.0 mM (blue line), respectively.

a sharper and more intense plasmon absorption band close to 525 nm.[11,16]

Some of the spectra for particles produced at higher polymer concentrations (6.0 mM) do not show a plasmon band at all, indicating that most particles are below *ca.* 3 nm in size.[34] The series of spectra obtained is well–known for size-separated (fractionated) particles in the range below 5 nm but unprecedented for as–prepared samples.[13,31] The ability to prepare spectroscopically–distinct samples with diameters below 5 nm suggests a narrow particle size distribution for each sample. To confirm this by TEM, it was convenient to first isolate the particles from excess polymer by
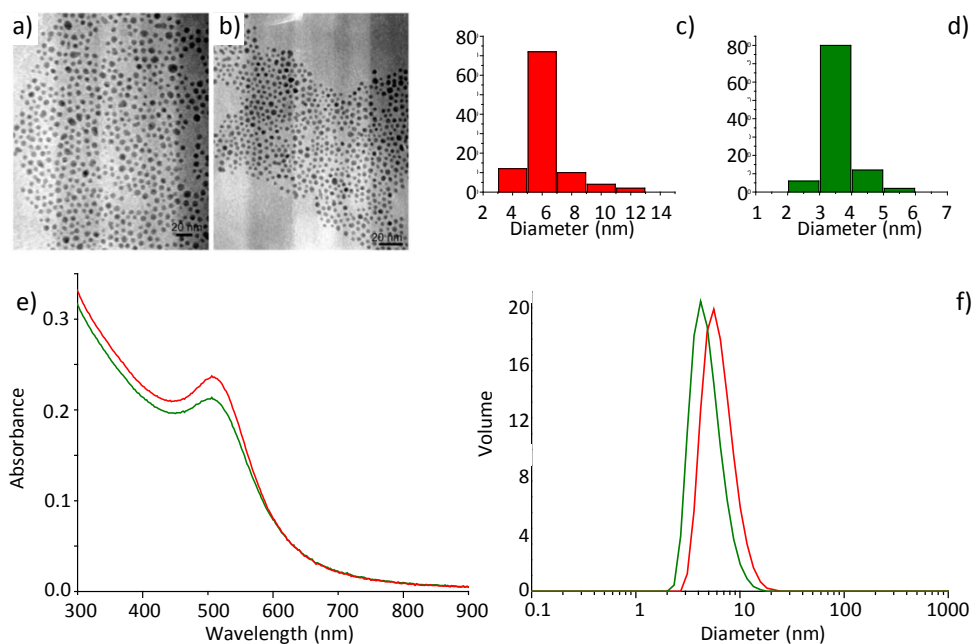
Figure 3.6: TEM images of pAA–DDT stabilized gold nanoparticles obtained from polymer concentration at a) 0.006, b) 0.06, c) 0.6 and d) 6 mM; e), f), g) and h) histograms of the corresponding distribution of particle sizes of a), b), c) and d), respectively. (i) UV-visible spectra of pAA–DDT stabilized gold nanoparticles obtained from polymer concentration at 0.006 (red line), 0.06 (green line), 0.6 (orange line) and 6.0 mM (blue line), respectively. (j) DLS graphs of pAA–DDT stabilized gold nanoparticles obtained from polymer concentration at 0.006 (red line), 0.06 (green line), 0.6 (orange line) and 6.0 mM (blue line), respectively.

filtration and dialysis (dialysis membrane molecular weight cut-off = 7000 g/mol). This procedure avoids the need to phase-transfer the particles into an organic solvent prior to TEM analysis.[13]

Characterization by TEM confirms that the particles produced using ligands pMAA–DDT and pAA–DDT have very narrow size distribution (see Figures 3.3 and 3.6). Since size non–uniformities can be easily underestimated by TEM due to size segregation phenomena during sample preparation, large and representative areas were imaged in order to support the claim of near–monodispersity.

Figure 3.7: TEM images of pVP–DDT stabilized gold nanoparticles obtained from polymer concentration at a) 0.006, b) 0.06, c) 0.6 and d) 6 mM; e), f), g) and h) histograms of the corresponding distribution of particle sizes of a), b), c) and d), respectively. (i) UV–visible spectra of pVP–DDT stabilized gold nanoparticles obtained from polymer concentration at 0.006 (red line), 0.06 (green line), 0.6 (orange line) and 6.0 mM (blue line), respectively. (j) DLS graphs of pVP–DDT stabilized gold nanoparticles obtained from polymer concentration at 0.006 (red line), 0.06 (green line), 0.6 (orange line) and 6.0 mM (blue line), respectively.

The average particle sizes and particle size distribution for all samples as estimated from TEM are summarized in Table 3.1 (the error estimates were deduced from the standard deviation to the gaussian distribution of particles size histograms built on TEM observations).

By contrast, gold nanoparticles produced using a commercially–available PMAA ligand with no thioether end–group were found to be larger (between 3 and 12 nm), even at higher polymer concentrations (6.0 mM), and exhibited a much broader particle size distribution (See Figure 3.9).
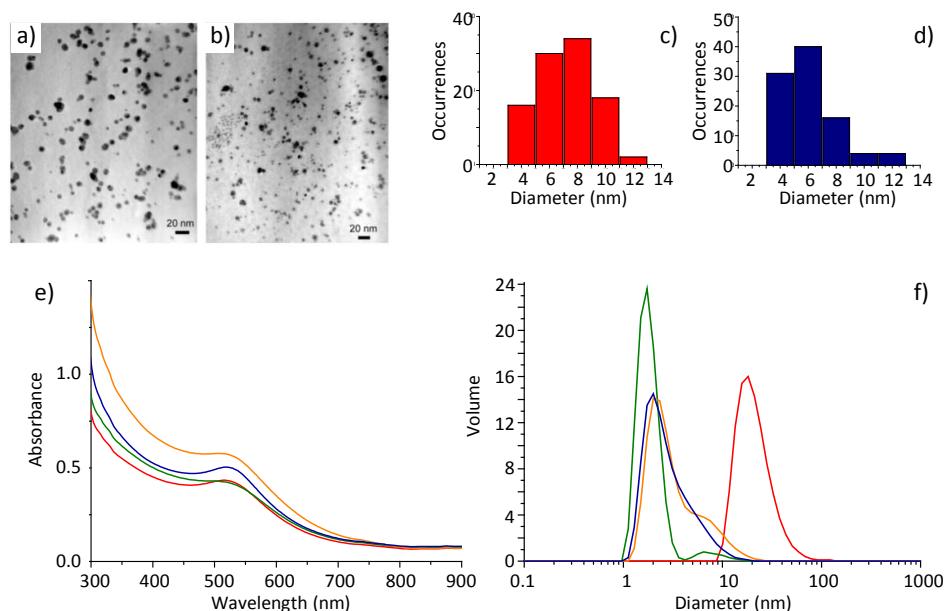
77

Figure 3.8: TEM images of pVSA–DDT stabilized gold nanoparticles obtained from polymer concentration at a) 0.006, b) 0.06; c) and d), histograms of the corresponding distribution of particle sizes of a) and b) respectively. (e) UV–visible spectra of pVSA–DDT stabilized gold nanoparticles obtained from polymer concentration at 0.006 (red line) and 0.06 (green line), respectively. (f) DLS graphs of pVSA–DDT stabilized gold nanoparticles obtained from polymer concentration at 0.006 (red line) and 0.06 (green line), respectively.

Polymer Ligand	Particles Diameter							
	0.006 mM		0.06mM		0.6mM		6mM	
	TEM	DLS	TEM	DLS	TEM	DLS	TEM	DLS
pAA-DDT	5.3±0.4	6.5	3.7±0.3	4.9	2.7±0.2	3.8	11.8±0.2	1.4
pMAA-DDT	5.3±0.7	5.0	4.0±0.4	3.6	2.8±0.3	2.8	1.7±0.3	1.5
pVSA-DDT	6.0±1.5	5.5	3.6±0.5	4.2				
pHEA-DDT	5.2±1.0	6.4	4.6±0.8	4.3	2.7±0.5	3.2	2.0±0.3	2.8
pEGMA-DDT	7.7±1.9	7.5	4.6±0.7	4.2	3.6±0.7	3.9	2.7±0.4	3.0
pVP-DDT	5.0±1.4	8.5	4.7±0.9	5.6	4.2±0.7	4.9	2.6±0.6	3.6

Table 3.1: Effect of monomer main chain on gold nanoparticles produced using DDT thioether–capped vinyl polymers (size distributions were calculated using the TEM pictures).

78

Figure 3.9: TEM images of pMAA stabilized gold nanoparticles obtained from polymer concentration at a) 0.006 and b) 6 mM; c) and d),histograms of the corresponding distribution of particle sizes of a) and b) respectively. e) UV–visible spectra of pMAA stabilized gold nanoparticles obtained from polymer concentration at 0.006 (red line), 0.06 (green line), 0.6 (orange line) and 6.0 mM (blue line), respectively. f) DLS graphs of pMAA stabilized gold nanoparticles obtained from polymer concentration at 0.006 (red line), 0.06 (green line), 0.6 (orange line) and 6.0 mM (blue line), respectively.

To further corroborate the near–monodispersity and sample uniformity in these materials, bulk samples were also studied using dynamic light scattering. Like TEM, this technique also has inherent limitations (*e.g.*, limited measurement range) and should not in any case be expected to give particle diameters which are similar to the TEM observations since DLS gives an average measurement of the hydrodynamic radius of the particles when TEM gives images of the gold core (see Section 3.4.2) Nonetheless, a major advantage of DLS is that it gives a bulk measurement — that is, providing that there is no settling or precipitation. The method avoids selective sampling as can occur in TEM. As such, DLS can serve as a very useful corroboratory technique in combination with TEM and UV–visible measurements. Figures 3.3, 3.4, 3.5, 3.6, 3.7 and 3.8. show series of DLS measurements for the different gold nanoparticles stabilized by DDT containing capping agents, as produced at the four different polymer concentrations. DLS data of the particles are summarized in Table 3.1 These measurements

pMAA-DDT			Polymer concentration (mM)			
M_n	M_w	(g/mol)	6	0.6	0.06	0.006
3220	3600					
3640	4520					
7000	9540					
8610	11100					
13500	18800					

Figure 3.10: Color images of gold suspensions stabilized with pMAA–DDT of various molecular weight at different polymers concentrations.

confirm that each sample exhibits a relatively monodisperse and unimodal distribution of particle sizes. Moreover, using DLS it is possible to distinguish clearly between the four samples and to gain a rapid estimate (typical measurement time below 5 minutes) of the average particle size and the breadth of the particle size distribution.

3.3.1.2 Influence of the polymer molecular weight

Having established that the carboxylic acid–based monomers (acrylic acid and methacrylic acid) gave rise to the most promising ligands, the influence of ligand number average molecular weight (M_n) was investigated. The series of five different molecular weight pMAA–DDT ligands described in Section 2.3.2 (referred to hereafter as pMAA–DDT$_{3220}$, pMAA–DDT$_{3640}$, pMAA–DDT$_{7000}$, pMAA–DDT$_{8610}$ and pMAA–DDT$_{13500}$ from lowest to highent M_n) were used as stabilizing agents. Colour pictures of the produced particles are shown in Section 2.3.2 Figure 3.10.

The pMAA–DDT ligand system was chosen since this polymer gave rise to relatively narrow particle size distribution and because it proved easier to achieve good molecular weight control with the methacrylate monomer in comparison with the pAA–DDT system (which also produced comparably monodisperse particles), as shown in Figure 2.3. As before, the gold particle size was found to decrease with increasing polymer concentration for all of the five ligands synthesized (pMAA-DDT$_{3220}$ to pMAA–DDT$_{13500}$, as shown in Figures 3.3, 3.11, 3.12, 3.13, 3.14 and Table 3.2).
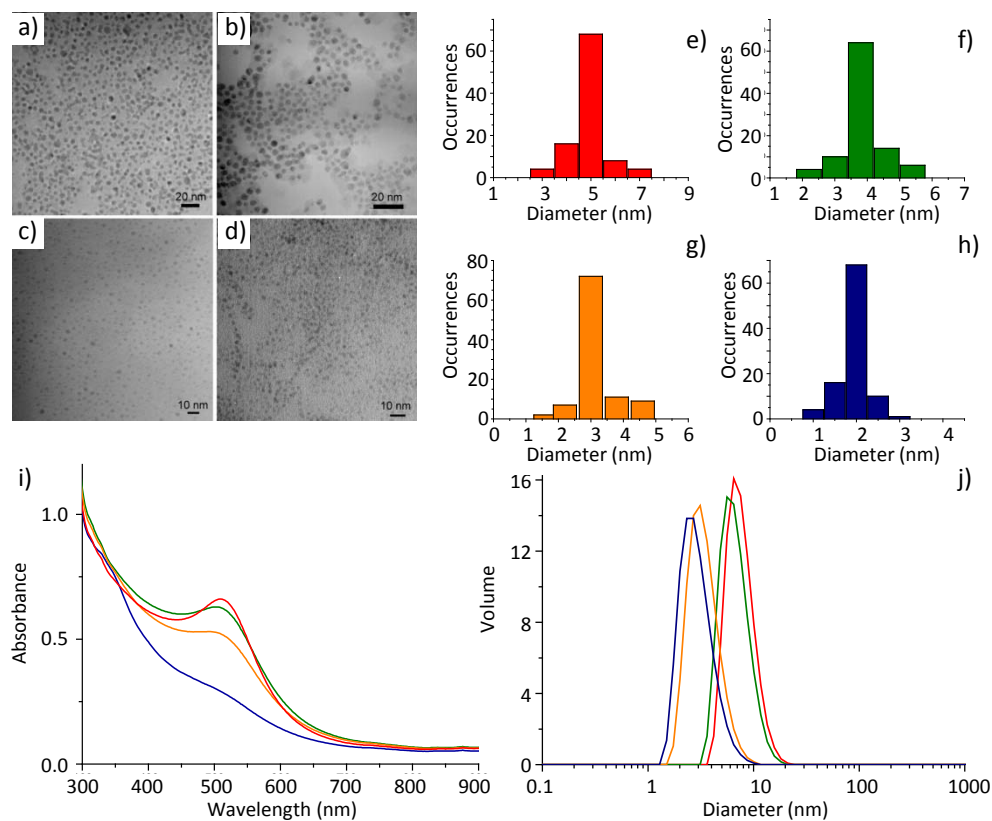
Figure 3.11: TEM images of 3640g/mol pMAA-DDT stabilized gold nanoparticles obtained from polymer concentration at a) 0.006, b) 0.06, c) 0.6 and d) 6 mM; e), f), g) and h) histograms of the corresponding distribution of particle sizes of a), b), c) and d), respectively. (i) UV–visible spectra of pMAA–DDT stabilized gold nanoparticles obtained from polymer concentration at 0.006 (red line), 0.06 (green line), 0.6 (orange line) and 6.0 mM (blue line), respectively. (j) DLS graphs of pMAA-DDT stabilized gold nanoparticles obtained from polymer concentration at 0.006 (red line), 0.06 (green line), 0.6 (orange line) and 6.0 mM (blue line), respectively.

Characterization by TEM, UV–visible spectroscopy, and DLS indicated that all of the polymer molecular weights studied gave rise to size–controlled gold nanoparticles with relatively narrow particle size distributions. It was apparent, however, from the combined characterization data that the lowest molecular weight polymer ligand (pMAA–DDT$_{3220}$, Section 2.3.2 Figure 2.4) gave the best overall control of the gold particle size distribution (see Figure 3.3). It is important to note that the gold particles were synthesized using a constant molar concentration of the ligands – that is, the amount of ligand was adjusted to take account of the number–average molecular
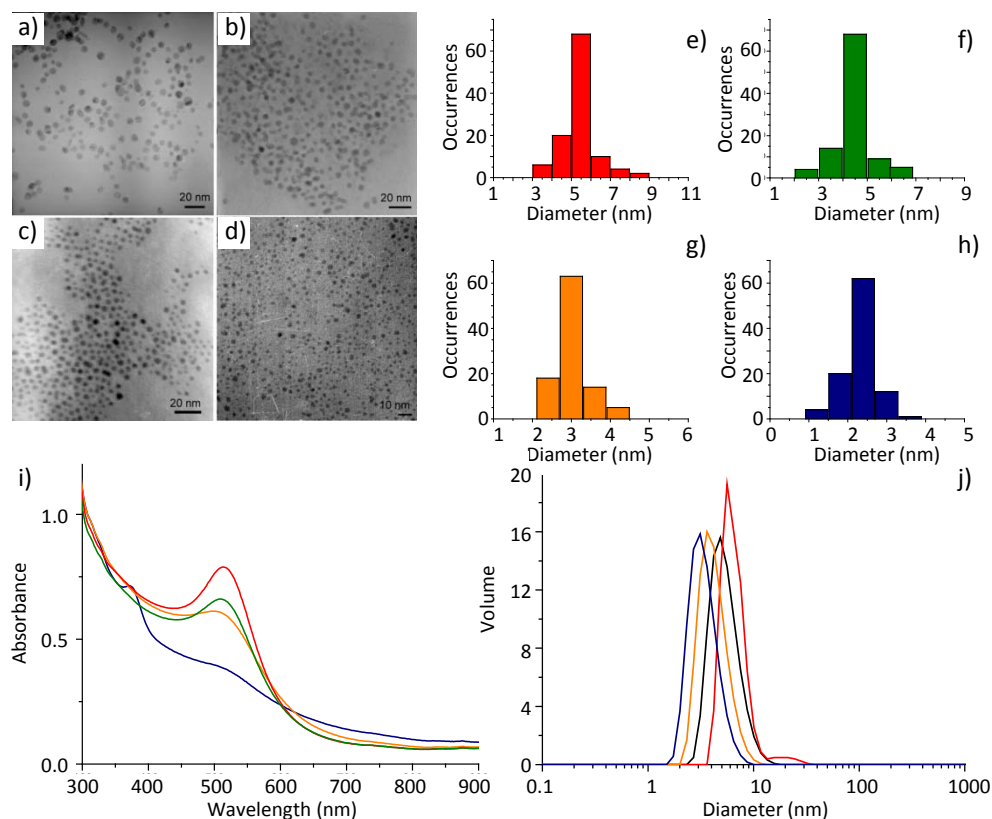
81

Figure 3.12: TEM images of 7000g/mol pMAA-DDT stabilized gold nanoparticles obtained from polymer concentration at a) 0.006, b) 0.06, c) 0.6 and d) 6 mM; e), f), g) and h) histograms of the corresponding distribution of particle sizes of a), b), c) and d), respectively. (i) UV–visible spectra of pMAA–DDT stabilized gold nanoparticles obtained from polymer concentration at 0.006 (red line), 0.06 (green line), 0.6 (orange line) and 6.0 mM (blue line), respectively. (j) DLS graphs of pMAA-DDT stabilized gold nanoparticles obtained from polymer concentration at 0.006 (red line), 0.06 (green line), 0.6 (orange line) and 6.0 mM (blue line), respectively.

weight, M_n. As such, the series of samples was prepared with (approximately) the same molar ratio of polymer ligand chains to gold in each case. The average size of the as produced particles (determined by TEM) seem to increase slightly when the polymeric stabilizer molecular weight increases, as shown in Table 3.2 and Figure 3.15.

3.3.1.3 Influence of the polymer end–group hydrophobicity

Attention was then turned to the influence of the hydrophobicty of the thioether end–group on the particle synthesis. The series of six low molar mass pMAA polymers with

pMAA-DDT Mn	Particles Diameter							
	0.006 mM		0.06mM		0.6mM		6mM	
	TEM	DLS	TEM	DLS	TEM	DLS	TEM	DLS
13500 g/mol	7.6±2.3	17.9	5.2±1.0	7.0	4.2±0.9	5.4	2.8±0.6	2.4
8610 g/mol	5.2±1.5	9.1	5.0±1.2	6.6	4.0±0.8	5.4	2.7±0.5	3.2
7000 g/mol	5.5±0.9	5.6	4.3±0.7	4.9	3.1±0.4	3.6	2.4±0.4	3.0
3640 g/mol	4.9±0.8	6.5	3.8±0.6	5.7	2.9±0.4	3.1	2.1±0.4	2.5
3220 g/mol	5.3±0.7	5.0	4.0±0.4	3.6	2.8±0.3	2.8	1.7±0.3	1.5

Table 3.2: Effect of polymer molecular weight on gold nanoparticles produced using pMAA–DDT ligands (size distributions were calculated using the TEM pictures).

increasingly hydrophobic end–groups described in Chapter 2 Section 2.3.3 (that is, C_2 to C_{18}) was used to stabilize gold particles (pMAA–MAT, pMAA–PropT, pMAA–PentT, pMAA–HT, PMAA–DDT, and pMAA–ODT)

Again, a constant molar concentration of ligand was used in each particle preparation, adjusting for M_n in each case. The first ligand in this series (pMAA–MAT) has a carboxylic acid end-group which mimics the polymer repeat unit structure and can be considered to be essentially hydrophilic. By contrast, pMAA–ODT has a C_{18} end group which is comparable in length with the polymeric chain itself (total M_n for pMAA–ODT = 2980 g/mol); that is, approximately 31 repeat units of acrylic acid and 9 repeat units of "ethylene" in the end group.

As such, one might expect that the end-group in pMAA–ODT could play a significant mechanistic role and this structure is perhaps best considered as a low molar mass thioether-linked diblock copolymer. As for all the polymer ligands reported here thus far, the average gold particle size was found to have a strong dependence on polymer concentration for the six ligands in this end–group series (see Table 3.3). Overall, the combined results from TEM, UV–visible spectroscopy and DLS indicate clearly that increasing the hydrophobicity of the thioether end–group leads to a greater degree of control over the resulting gold particle size distribution. This is evident from examination of the TEM images and DLS data for the particles (see Figures 3.17, 3.18, 3.19, 3.20, 3.3, 3.21 and Table 3.3).

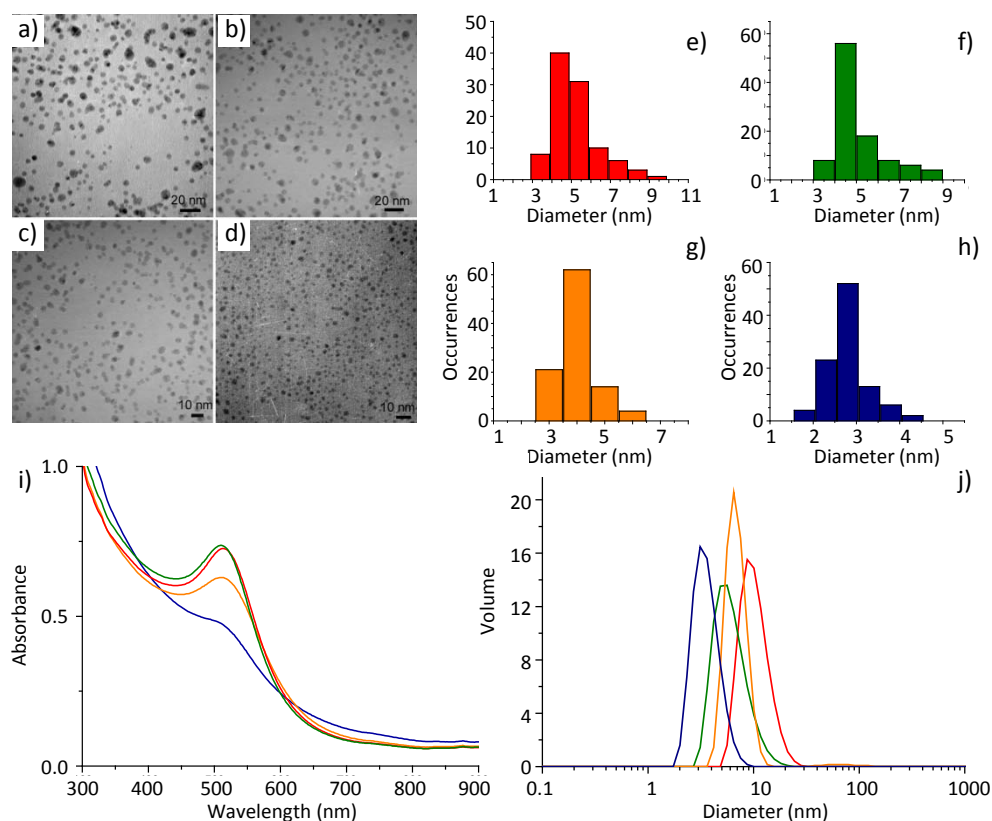The polymer with the most hydrophilic end–group, 2–mecapto acetic acid (pMAA–

Figure 3.13: TEM images of 8610g/mol pMAA-DDT stabilized gold nanoparticles obtained from polymer concentration at a) 0.006, b) 0.06, c) 0.6 and d) 6 mM; e), f), g) and h) histograms of the corresponding distribution of particle sizes of a), b), c) and d), respectively. (i) UV–visible spectra of pMAA–DDT stabilized gold nanoparticles obtained from polymer concentration at 0.006 (red line), 0.06 (green line), 0.6 (orange line) and 6.0 mM (blue line), respectively. (j) DLS graphs of pMAA-DDT stabilized gold nanoparticles obtained from polymer concentration at 0.006 (red line), 0.06 (green line), 0.6 (orange line) and 6.0 mM (blue line), respectively.

MAT), gave rise to particles with a broad size distribution (see Figure 3.17).

The particle size distribution for samples prepared at all four polymer concentrations was observed to decrease significantly as the length and hydrophobicity of the end–group was increased from propyl– (pMAA–PropT, Figure 3.18) to pentyl– (pMAA–PentT, Figure 3.19) to heptyl– (pMAA–HT, Figure 3.20) and dodecyl–thioether (pMAA–DDT, Figure 3.3). This effect is apparent from both TEM images and DLS data for the samples; the sizes and size distribution of the as–prepared particles are summarized in Table 3.3.
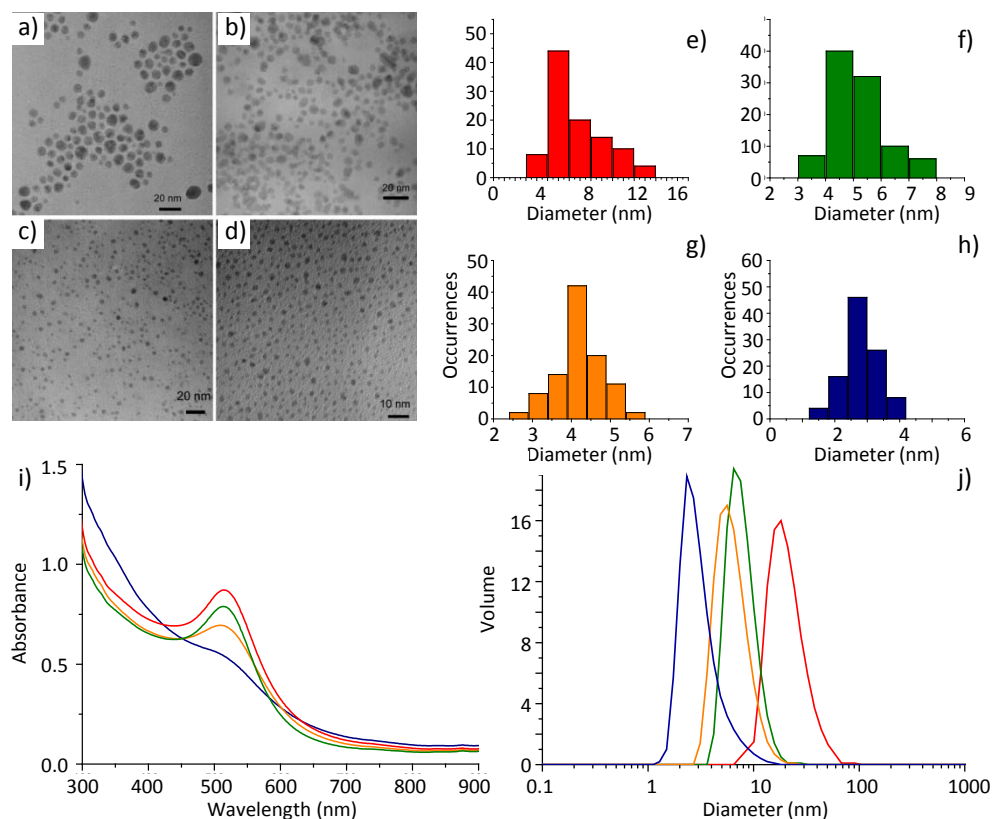
Figure 3.14: TEM images of 13500g/mol pMAA-DDT stabilized gold nanoparticles obtained from polymer concentration at a) 0.006, b) 0.06, c) 0.6 and d) 6 mM; e), f), g) and h) histograms of the corresponding distribution of particle sizes of a), b), c) and d), respectively. (i) UV–visible spectra of pMAA–DDT stabilized gold nanoparticles obtained from polymer concentration at 0.006 (red line), 0.06 (green line), 0.6 (orange line) and 6.0 mM (blue line), respectively. (j) DLS graphs of pMAA-DDT stabilized gold nanoparticles obtained from polymer concentration at 0.006 (red line), 0.06 (green line), 0.6 (orange line) and 6.0 mM (blue line), respectively.

The influence of end–group structure appears to be somewhat greater than the influence of ligand molecular weight over the range 1500 – 3000 g/mol (see Figure 3.15) and these changes in particle size were therefore ascribed primarily to an end–group effect. Moreover, the most monodisperse particles were observed with the most hydrophobic thiols (DDT, ODT) which gave rise to the highest molar mass ligands in the series; that is, the trend is in opposition to the molecular weight variation described in Section 3.3.1.2, confirming a more important influence of the polymers end–groups hydrophobicity compared to their average molecular weight on the size distribution of
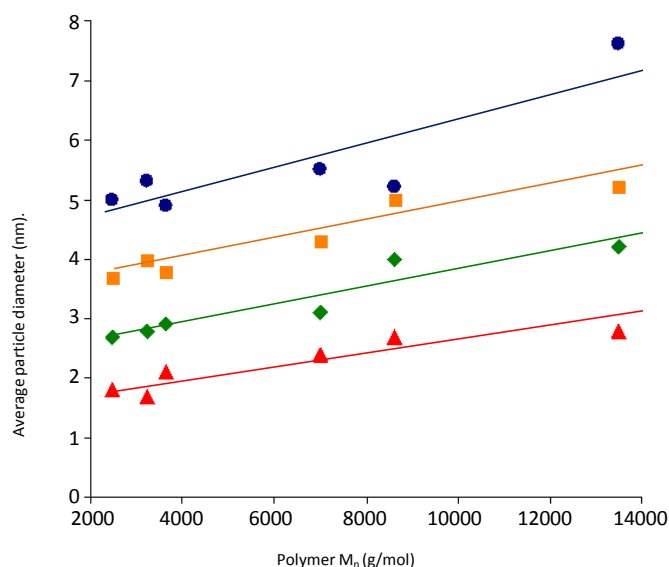
Figure 3.15: Average gold particle size plotted against molecular weight of the capping agent for particles synthesised using 6 mM (red), 0.6 mM (green), 0.06 mM (orange) and 0.006 mM (blue) concentrations respectively.
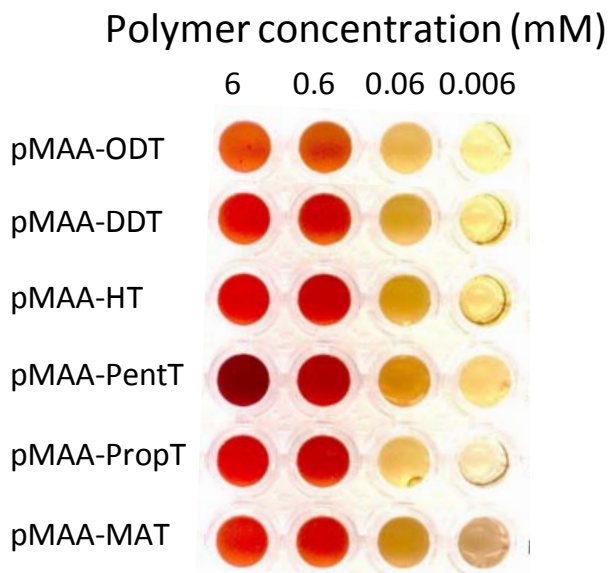

Figure 3.16: Color images of gold suspensions stabilized with pMAA bearing end–groups of increasing hydrophobicity at different polymers concentrations.

the particles.

Interestingly, particles prepared using the polymer with the most hydrophobic en–group, pMAA–ODT, at a concentration of 0.06 mM formed large aggregated supra–
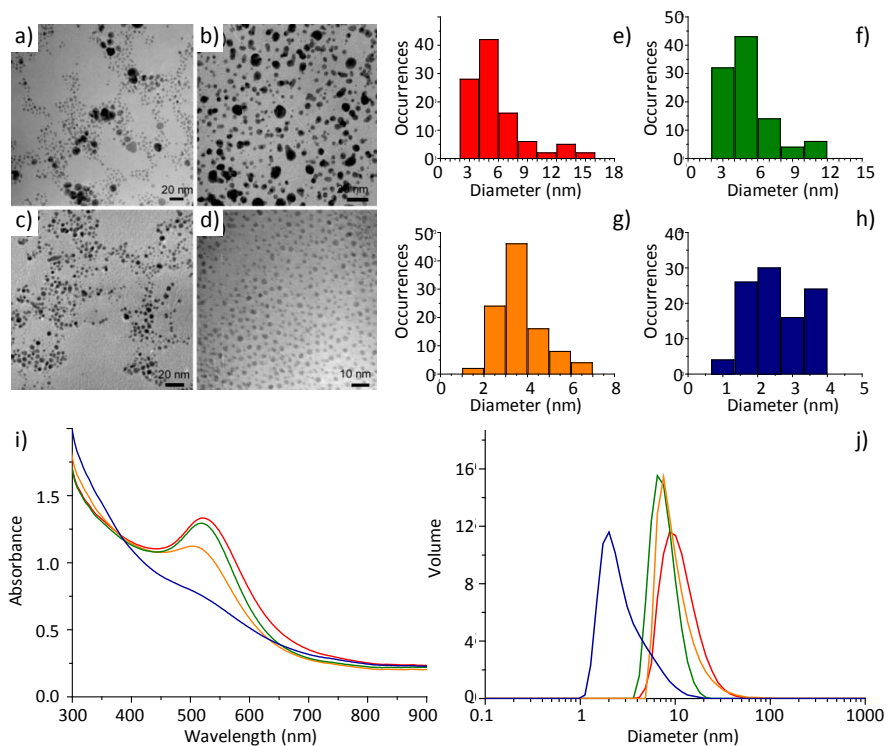
Figure 3.17: TEM images of pMAA–MAT stabilized gold nanoparticles obtained from polymer concentration at a) 0.006, b) 0.06, c) 0.6 and d) 6 mM; e), f), g) and h) histograms of the corresponding distribution of particle sizes of a), b), c) and d), respectively. (i) UV–visible spectra of pMAA–MAT stabilized gold nanoparticles obtained from polymer concentration at 0.006 (red line), 0.06 (green line), 0.6 (orange line) and 6.0 mM (blue line), respectively. (j) DLS graphs of pMAA–MAT stabilized gold nanoparticles obtained from polymer concentration at 0.006 (red line), 0.06 (green line), 0.6 (orange line) and 6.0 mM (blue line), respectively.

particles when imaged by TEM but not at the other polymer concentrations which were used (*i.e.*, 0.006, 0.6, 6.0 mM). These large spheres are believed to be formed as a result of the drying process involved in the sample preparation since they were only observed by TEM and there was absolutely no evidence for such aggregates in either DLS or UV-visible measurements for this sample. Indeed, DLS, UV–visible spectroscopy and TEM images (Figure 3.21) suggest that ligand pMAA–ODT gives rise to gold nanodispersions with comparably narrow size distribution to those observed with ligand pMAA–DDT. This further highlights the advantage of using a range of complementary characterization methods to analyze these materials.
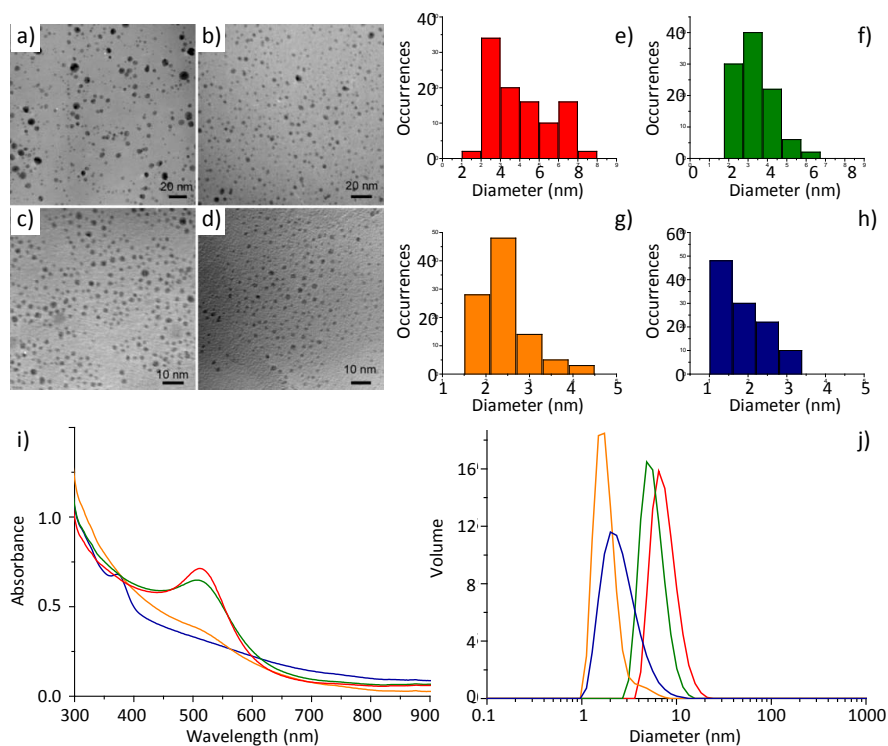
Figure 3.18: TEM images of pMAA-PropT stabilized gold nanoparticles obtained from polymer concentration at a) 0.006, b) 0.06, c) 0.6 and d) 6 mM; e), f), g) and h) histograms of the corresponding distribution of particle sizes of a), b), c) and d), respectively. (i) UV–visible spectra of DDT-PMAA stabilized gold nanoparticles obtained from polymer concentration at 0.006 (red line), 0.06 (green line), 0.6 (orange line) and 6.0 mM (blue line), respectively. (j) DLS graphs of pMAA–propT stabilized gold nanoparticles obtained from polymer concentration at 0.006 (red line), 0.06 (green line), 0.6 (orange line) and 6.0 mM (blue line), respectively.

In summary, it is evident that control over particle size distribution is enhanced when the length of the hydrophobic end–group is increased for pMAA ligands of M_n ranging from 1800 to 3000 g/mol, at least up to C_{18} hydrophobic chain lengths.

3.3.1.4 Influence of polymer with multiple thiol/thioether containing end–groups

As before, the range of multidentate ligands was evaluated for the synthesis of gold nanoparticles at four different polymer concentrations in the range 0.006–6.0 mM, using the polymer structures described in Chapter 2 Section 2.3.4. As for all other ligands studied, the average particle size decreased significantly as the polymer concentration
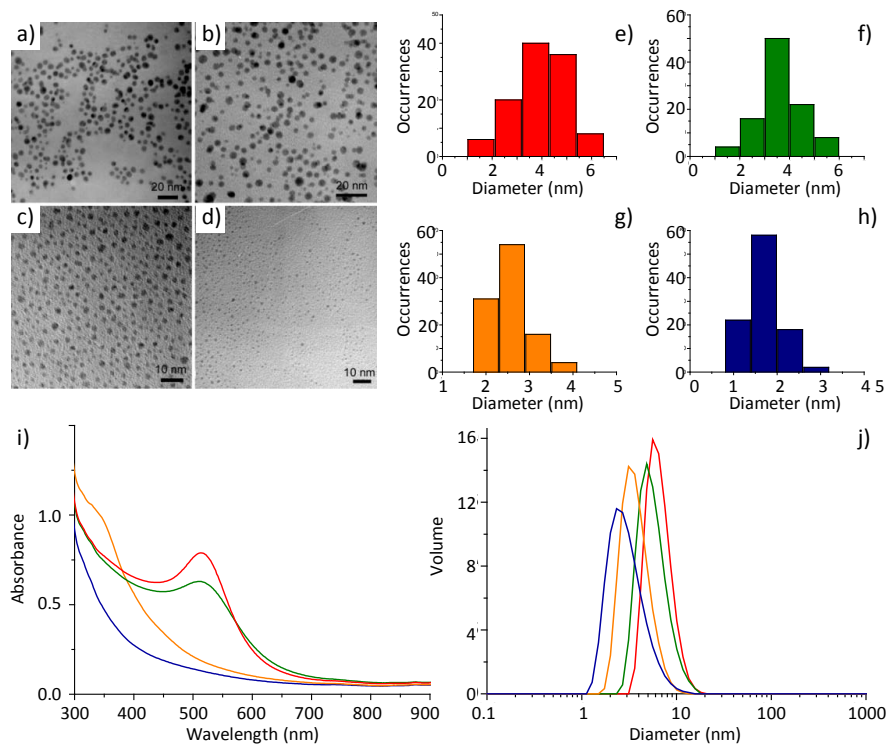
Figure 3.19: TEM images of pMAA–PentT stabilized gold nanoparticles obtained from polymer concentration at a) 0.006, b) 0.06, c) 0.6 and d) 6 mM; e), f), g) and h) histograms of the corresponding distribution of particle sizes of a), b), c) and d), respectively. (i) UV–visible spectra of pMAA–pentT stabilized gold nanoparticles obtained from polymer concentration at 0.006 (red line), 0.06 (green line), 0.6 (orange line) and 6.0 mM (blue line), respectively. (j) DLS graphs of pMAA–PentT stabilized gold nanoparticles obtained from polymer concentration at 0.006 (red line), 0.06 (green line), 0.6 (orange line) and 6.0 mM (blue line), respectively.

was increased and a colour shift from red to yellow can be observed for the so–formed suspensions, as depicted in Figure 3.22.

In general, characterization by TEM, UV–visible and DLS indicated that these multidentate ligands gave good (and in one case unprecedented) control over the gold particle size distribution (see Table 3.4).

The broadest particle size distribution in this series were obtained with ligand pMAA–EDT (Figure 3.23); the particle size distribution for this ligand were comparable to (though slightly narrower than) those obtained for ligand pMAA–PropT (Table 3.4 and Figure 3.23) which also contains a C_3 end–group structure but just one sulphur
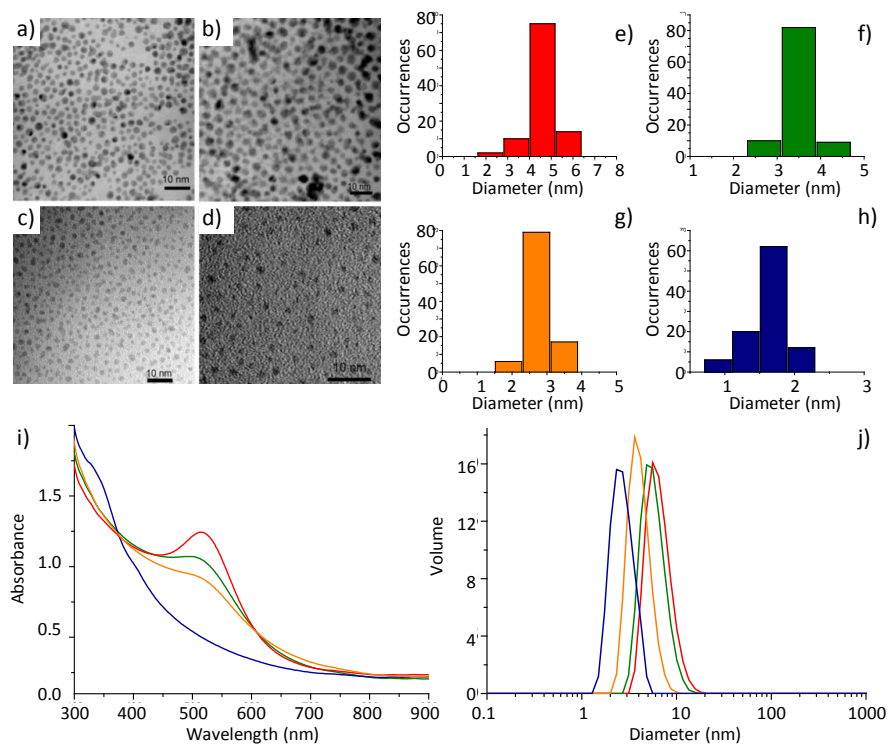
Figure 3.20: TEM images of pMAA–HT stabilized gold nanoparticles obtained from polymer concentration at a) 0.006, b) 0.06, c) 0.6 and d) 6 mM; e), f), g) and h) histograms of the corresponding distribution of particle sizes of a), b), c) and d), respectively. (i) UV–visible spectra of pMAA–HT stabilized gold nanoparticles obtained from polymer concentration at 0.006 (red line), 0.06 (green line), 0.6 (orange line) and 6.0 mM (blue line), respectively. (j) DLS graphs of pMAA–HT stabilized gold nanoparticles obtained from polymer concentration at 0.006 (red line), 0.06 (green line), 0.6 (orange line) and 6.0 mM (blue line), respectively.

functionality per chain. This further supports the hypothesis that a significant hydrophobic end–group is beneficial in these ligands, as noted in Section 3.3.1.3. Indeed, the particles obtained using ligand pMAA–NDT (which also contains one thioether and one thiol) appeared to be more monodisperse than those prepared with pMAA–EDT at all four polymer concentrations (see Figures 3.23, 3.24 and Table 3.4).

By contrast, the tetradentate ligand, pMAA–PTMP, behaved quite differently, both in terms of phase behaviour during reaction and in terms of the nanoparticles that were produced. First, an opaque white solution was observed immediately upon addition of the polymer ligand to the AuHCl$_4$ solution and prior to the addition of the reducing
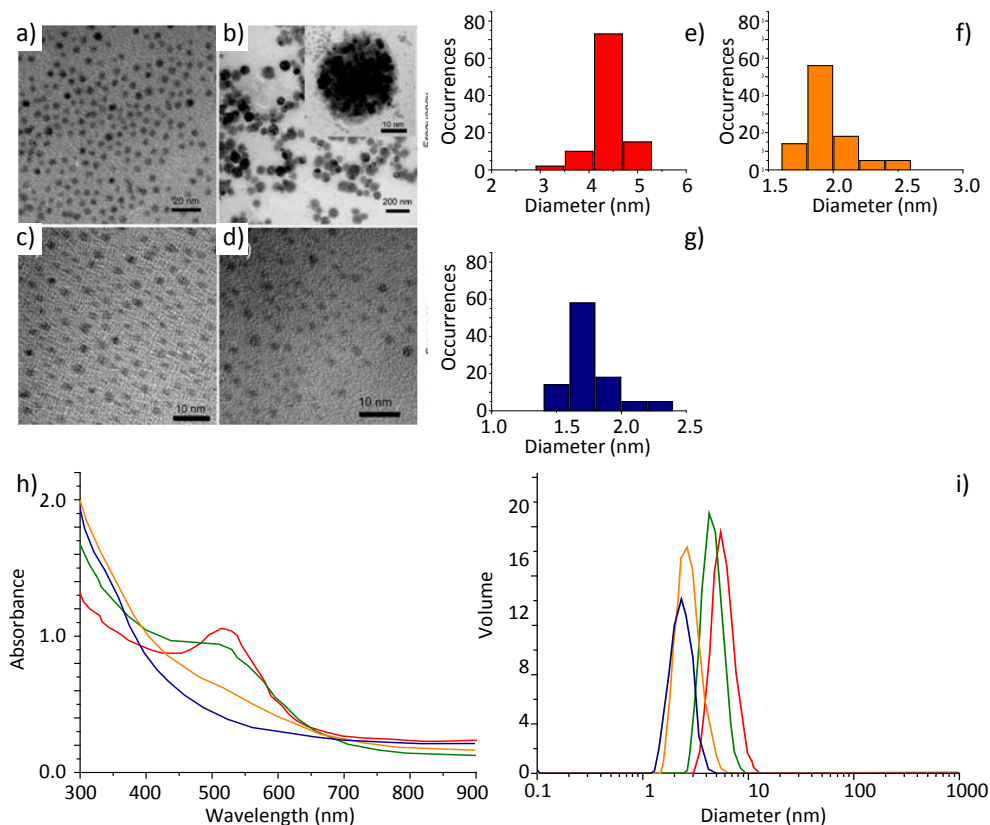
Figure 3.21: TEM images of pMAA–ODT stabilized gold nanoparticles obtained from polymer concentration at a) 0.006, b) 0.06, c) 0.6 and d) 6 mM; e), f), g) and h) histograms of the corresponding distribution of particle sizes of a), b), c) and d), respectively. (i) UV–visible spectra of pMAA–ODT stabilized gold nanoparticles obtained from polymer concentration at 0.006 (red line), 0.06 (green line), 0.6 (orange line) and 6.0 mM (blue line), respectively. (j) DLS graphs of pMAA–ODT stabilized gold nanoparticles obtained from polymer concentration at 0.006 (red line), 0.06 (green line), 0.6 (orange line) and 6.0 mM (blue line), respectively.

agent. This effect was observed at all polymer concentrations (from 0.06 to 6.0 mM) and suggests that the Au^{III} species was reduced to a Au^{I} thiolate salt by the thiol–containing pMAA–PTMP ligand, as suggested previously for ligands such as p–HS–CH$_2$–(C$_6$H$_4$)C(CH$_3$)$_3$.[35] This behavior was not observed with any of the other thiol containing monomers (pMAA–EDT, pMAA–NDT, pMAA–MES), even at the highest polymer concentrations studied (6.0 mM).

The fact that pMAA–PTMP gives rise to this effect even at the lowest polymer concentration (0.006 mM) may suggest that phase separation occurs as a result of the

pMAA-DDT Mn	Particles Diameter							
	0.006 mM		0.06mM		0.6mM		6mM	
	TEM	DLS	TEM	DLS	TEM	DLS	TEM	DLS
pMAA-MAT	5.2±2.8	9.3	5.0±2.2	7.5	3.6±1.0	6.5	2.2±0.7	2.0
pMAA-PropT	4.1±1.7	6.6	3.2±0.9	5.0	2.4±0.6	2.1	1.9±0.6	1.6
pMAA-PentT	4.9±1.1	5.8	3.5±0.8	4.9	2.6±0.5	3.3	1.7±0.4	2.4
pMAA-HT	4.6±0.7	5.8	3.5±0.4	5.1	2.8±0.4	3.6	1.7±0.3	2.6
pMAA-DDT	5.3±0.7	5.0	4.0±0.4	3.6	2.8±0.3	2.8	1.7±0.3	1.5
pMAA-ODT	4.5±0.3	5.6		4.2	1.9±0.2	2.6	1.7±0.2	2.3

Table 3.3: Effect of end–group hydrophobicity on the formation old nanoparticles produced using thioether–capped pMAA ligands (size distributions were calculated using the TEM pictures).
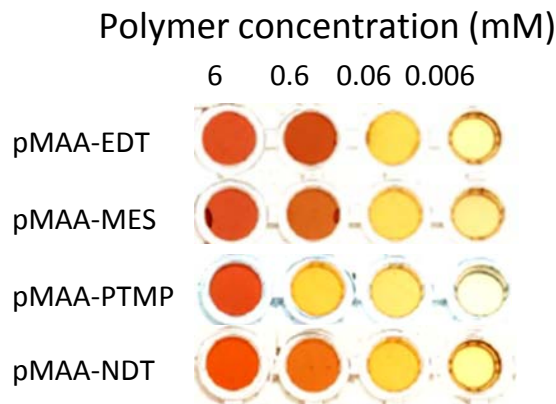

Figure 3.22: Color images of gold suspensions stabilized with bearing end–groups containing multiple thiols and/or thioethers at different polymers concentrations.

multidentate nature of the pMAA–PTMP ligand which can, unlike the other three thiol–containing ligands, react with more than one gold species. Upon addition of the reducing agent, NaBH$_4$, the opaque milky solutions became quite rapidly transparent and assumed the yellow / orange / red colors observed for other ligands at these polymer concentrations. However, inspection of the UV–visible spectra for the pMAA–PTMP preparations reveals significant differences in comparison to the other PMAA ligand structures studied (Figure 3.26). At equivalent polymer concentrations, the pMAA– PTMP ligand leads to particles which exhibit UV–spectra with a much less pronounced plasmon band at 515 nm (see Figures 3.3 and 3.26 for comparison). At the higher poly-

pMAA-DDT Mn	Particles Diameter							
	0.006 mM		0.06mM		0.6mM		6mM	
	TEM	DLS	TEM	DLS	TEM	DLS	TEM	DLS
pMAA-EDT	4.5±0.5.	6.1	3.3±0.5	4.2	2.8±0.3	3.9	1.8±0.3	2.0
pMAA-NDT	4.7±0.6	5.6	3.5±0.5	4.9	2.5±0.5	3.0	1.7±0.3	2.1
pMAA-MES	4.0±0.3	5.0	3.4±0.3	4.1	2.7±0.2	3.2	1.8±0.2	2.3
pMAA-PTMP	3.7±0.2	4.7	2.8±0.2	3.1	1.9±0.1	1.8		

Table 3.4: Effect of end–group denticity on gold nanoparticles produced using thioether–apped pMAA ligands (size distributions were calculated using the TEM pictures).

mer concentrations in particular (0.6 mM and 6.0 mM), the plasmon band has entirely disappeared. In general, the UV–spectra are consistent with this multidentate ligand giving rise to significantly smaller particles at a given polymer concentration. This was confirmed by both TEM and DLS analysis. Figure 3.26 shows the TEM analysis for particles produced using pMAA–PTMP at 0.006, 0.06, and 0.6 mM, respectively. These particles are both smaller and more monodisperse than any of the samples prepared using other ligands at these concentrations (see Tables 3.1 and 3.4).

For example, the particles prepared using pMAA–PTMP at 0.006 mM had an average diameter as estimated by TEM of 3.7 ± 0.2 nm compared with 5.3 ± 0.7 nm for particles produced using pMAA–DDT at the same concentration (Tables 3.1 and 3.4). Spreads on the particle size distributions are estimated from the full width at half maximum of the gaussian fits of the particles size distribution histograms determined by TEM.

Similarly, smaller and more monodisperse particles were observed at 0.06 mM and 0.6 mM (Figure 3.26 and Table 3.4). At a pMAA–PTMP concentration of 6.0 mM, however, it was not possible to observe the particles by TEM suggesting an average cluster size below 1 nm which is consistent with the UV–visible spectrum for particles produced at this concentration (Figure 3.26h). DLS analysis corroborates all of these observations. By DLS, the particles produced at 0.006, 0.06, and 0.6 mM pMAA–PTMP concentrations have narrow size distribution (Figure 3.26i) and average diameters of 4.0 nm, 2.5 nm, and 1.8 nm, respectively. The DLS measurement for the
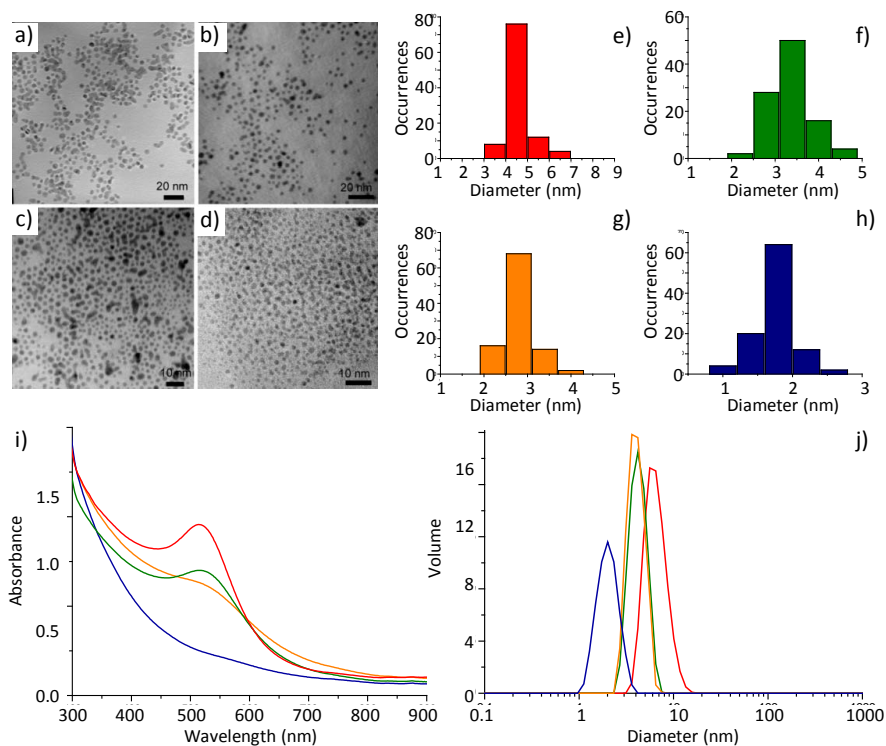
Figure 3.23: TEM images of pMAA–EDT stabilized gold nanoparticles obtained from polymer concentration at a) 0.006, b) 0.06, c) 0.6 and d) 6 mM; e), f), g) and h) histograms of the corresponding distribution of particle sizes of a), b), c) and d), respectively. (i) UV–visible spectra of pMAA–EDT stabilized gold nanoparticles obtained from polymer concentration at 0.006 (red line), 0.06 (green line), 0.6 (orange line) and 6.0 mM (blue line), respectively. (j) DLS graphs of p-MAA-EDT stabilized gold nanoparticles obtained from polymer concentration at 0.006 (red line), 0.06 (green line), 0.6 (orange line) and 6.0 mM (blue line), respectively.

particles produced at 6.0 mM pMAA–PTMP is suggestive of an average particle size below 1 nm, although it must be noted that the DLS instrument used to calculate these size distribution is not suitable for sizing particles with diameter that small and the precise shape of the distribution shown in 3.26i) for this sample (particularly sub–1 nm) should not be over–interpreted. Nonetheless, all three characterization methods (UV–visible spectroscopy, TEM and DLS) are consistent with a sample where the bulk of the size distribution in the 1 nm range.

In general, the size distribution for the particles produced using pMAA–PTMP were narrower than those observed using other ligands in this study. This was most evident
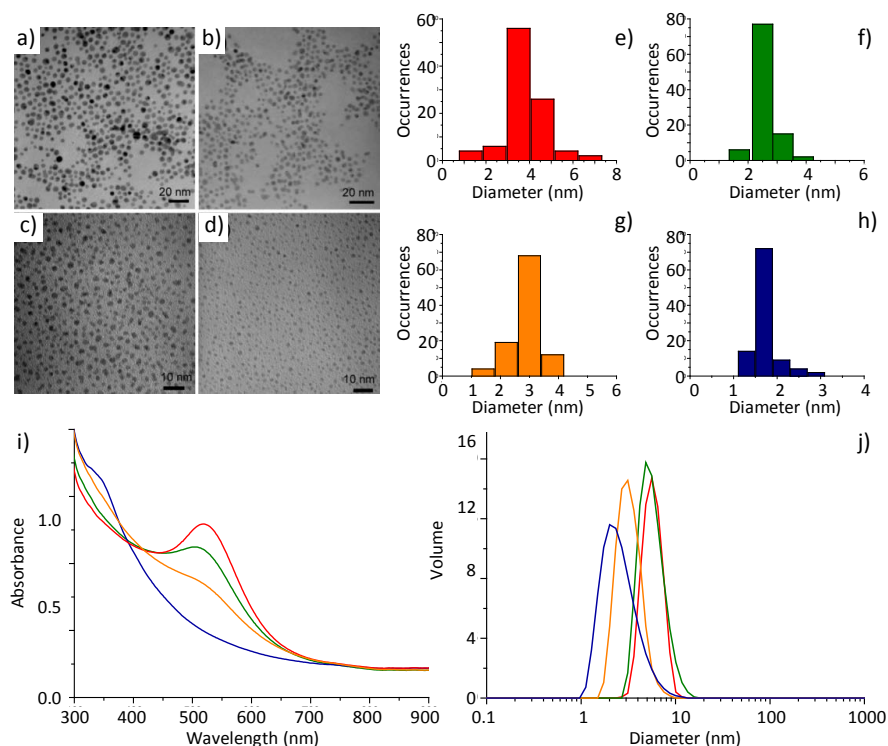
Figure 3.24: TEM images of pMAA–NDT stabilized gold nanoparticles obtained from polymer concentration at a) 0.006, b) 0.06, c) 0.6 and d) 6 mM; e), f), g) and h) histograms of the corresponding distribution of particle sizes of a), b), c) and d), respectively. (i) UV–visible spectra of pMAA–NDT stabilized gold nanoparticles obtained from polymer concentration at 0.006 (red line), 0.06 (green line), 0.6 (orange line) and 6.0 mM (blue line), respectively. (j) DLS graphs of pMAA–NDT stabilized gold nanoparticles obtained from polymer concentration at 0.006 (red line), 0.06 (green line), 0.6 (orange line) and 6.0 mM (blue line), respectively.

for the particles synthesized at a 0.006 mM pMAA–PTMP concentration where a very monodisperse sample was observed which formed ordered hexagonal arrays on the TEM grid, as shown in Figure 3.27a). A lower magnification TEM image presented in Figure 3.27b) confirmed that this monodispersity was a feature of the bulk sample and the very narrow size distribution observed by DLS (black line, Figure 3.26i) further supports this interpretation. The characteristics of those particles will be further developed in Chapter 4.
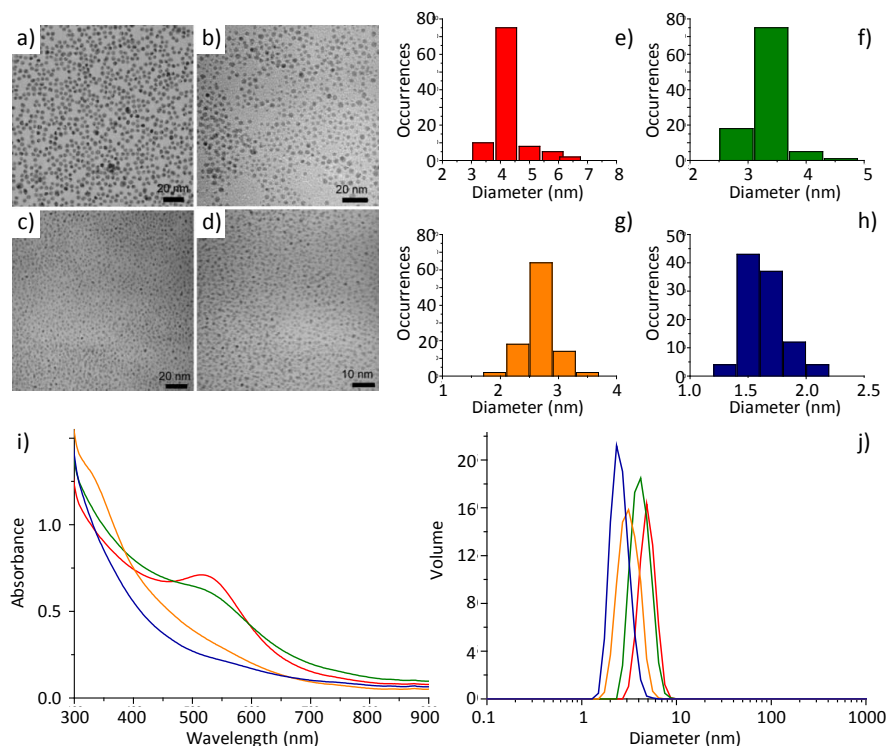
Figure 3.25: TEM images of pMAA–MES stabilized gold nanoparticles obtained from polymer concentration at a) 0.006, b) 0.06, c) 0.6 and d) 6 mM; e), f), g) and h) histograms of the corresponding distribution of particle sizes of a), b), c) and d), respectively. (i) UV–visible spectra of pMAA–MES stabilized gold nanoparticles obtained from polymer concentration at 0.006 (red line), 0.06 (green line), 0.6 (orange line) and 6.0 mM (blue line), respectively. (j) DLS graphs of pMAA–MES stabilized gold nanoparticles obtained from polymer concentration at 0.006 (red line), 0.06 (green line), 0.6 (orange line) and 6.0 mM (blue line), respectively.

3.3.1.5 MALDI–TOF–MS analysis of pMAA–PTMP stabilized gold nanoparticles.

Gold particles prepared using a 6 mM pMAA–PTMP concentration could not be imaged by TEM, and DLS measurements cannot be completely interpreted (Section 3.3.1.4, Figure 3.26). Thus, in an attempt to determine their size and mass, the gold suspension was investigated by MALDI–TOF–MS according to the protocol determined previously for pMAA–PTMP polymeric chains (see Chapter 2 Section 2.3.4).

Several preparations of different concentration were tested with a DHB matrix in positive ion mode, but no clear result could be obtained. Thus, the sample was analyzed
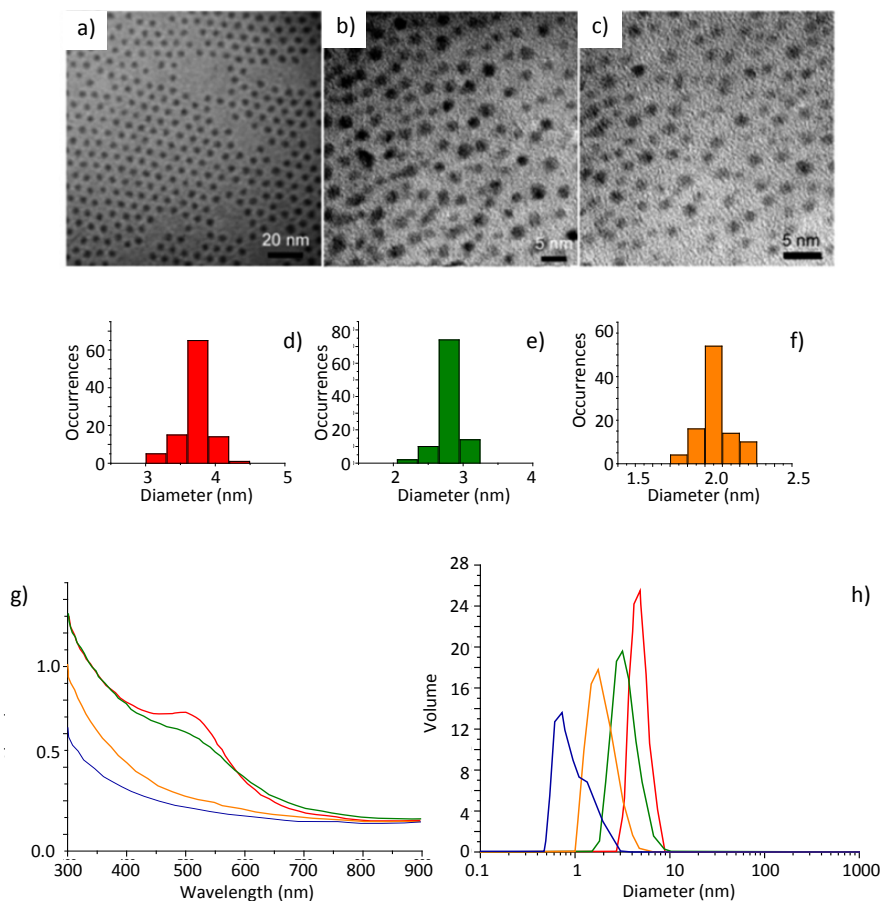
Figure 3.26: TEM images of pMAA–PTMP stabilized gold nanoparticles obtained from polymer concentration at a) 0.006, b) 0.06, c) 0.6 and d) 6 mM; e), f), g) and h) histograms of the corresponding distribution of particle sizes of a), b), c) and d), respectively. (i) UV–visible spectra of pMAA–PTMP stabilized gold nanoparticles obtained from polymer concentration at 0.006 (red line), 0.06 (green line), 0.6 (orange line) and 6.0 mM (blue line), respectively. (j) DLS graphs of pMAA–PTMP stabilized gold nanoparticles obtained from polymer concentration at 0.006 (red line), 0.06 (green line), 0.6 (orange line) and 6.0 mM (blue line), respectively.

in negative ion mode, in a 3–MTA / DAC matrix (3–MTA was used instead of THAP because it is more suitable for analysis of high molecular weight species[36]), in using H_2O/MeCN as a solvent.

The spectrum shows a broad multimodal mass distribution ranging from m/z values between about 5 and 17 kDa. This is broadly consistent with LDI mass spectrometry data reported for thiolate monolayer protected Au_{75} clusters,[37] although the high molar mass "tail" for the produced pMAA–PTMP stabilized nanoparticles sample extends to
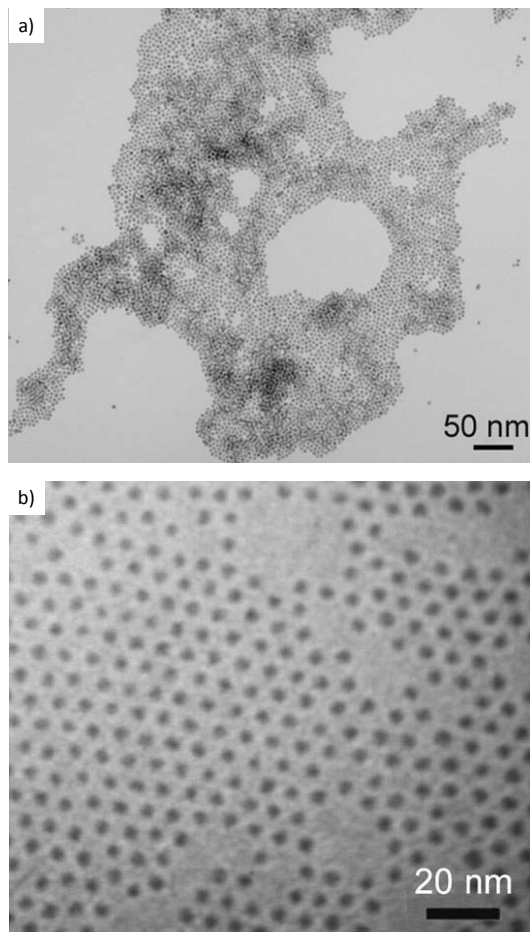
Figure 3.27: Low magnification TEM images of pMAA–PTMP stabilized gold nanoparticles obtained at a polymer concentration of 0.006 mM.

lower mass values. This may suggest that the clusters are somewhat smaller or may be a function of the analysis conditions.

The data are consistent, however, with the absence of particles containing more than 100 gold atoms and confirms the nanometer cluster size suggested by UV–visible spectroscopy and DLS.

The fine structure of the MALDI–TOF–MS distribution shown in Figure 3.28 shows a multitude of peaks separated by $\frac{m}{z}$ values of 32 Daltons, which may suggest loss of Au / Au–S moieties from the main fragment ion.[37,38]
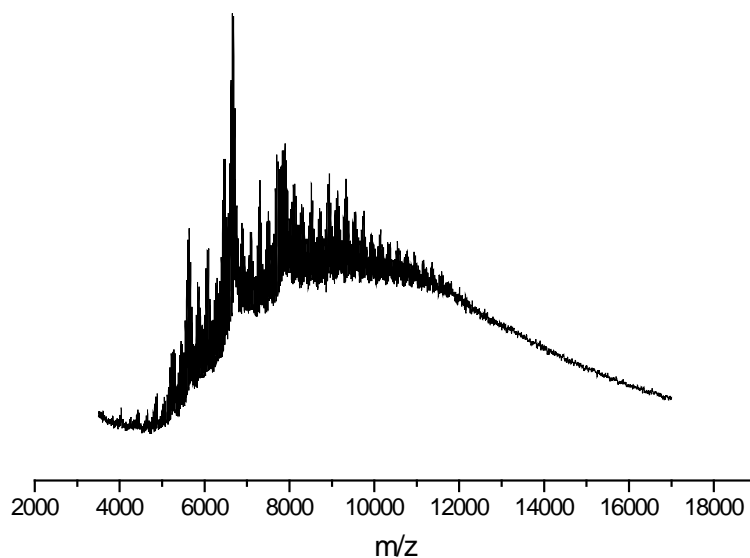
Figure 3.28: Positive ion mode MALDI–TOF–MS spectrum for pMAA–PTMP protected gold clusters.

3.4 Discussion

3.4.1 Synthesis process rules.

The synthetic procedure described above does not differ from other methods reported elsewhere [16,39] in a sense that it involves the reduction of Au^{III} into Au^{I} by the thiol / thioether–containing stabilizer in the reaction vessel, and then, the complete reduction of Au^{I} to Au^{0} by addition of a strong reducing agent ($NaBH_4$).

The mechanism of gold particles formation and the causes of their dispersion in size using different methods are not completely understood. [17] Therefore, the rationalization for the formation of highly monodisperse nanoparticles using the procedure described in this Chapter remains challenging.

However, from the various data described above, a number of basic design rules can be formulated for the effect of the polymeric ligands nature on the formation of gold nanoparticles.

Polymeric main chain. For the DDT–capped ligands, pMAA and pAA were found to be the most effective polymers with the pVSA–DDT ligand in particular showing incompatibility with this synthetic route (Figure 3.8). pAA–DDT ligands (Figures 3.6) gave somewhat narrower particle size distributions (7 – 9% standard deviation by TEM) than the pMAA–DDT ligand series (10 – 14% standard deviation) at all concentrations studied (Figure 3.3) possibly because of its higher water solubility. Both of these carboxylic-acid-containing polymers gave rise to much narrower particle size distributions than ligands pHEA–DDT, pEGMA–DDT and pVP–DDT, which led to standard deviations in the range 15 – 28% (Table 3.1 and Figures 3.4,3.5 and 3.7). pAA and pMAA are polyfunctional molecules bearing a carboxylic acid group on each monomer and, as such, have the potential to stabilize these particles by a combination of both steric and electrostatic mechanisms (see Chapter 1 Section 1.4). Both pAA [40,41] and pMAA [42] (without thioether end groups) have been used previously as stabilizers for the preparation of stable nanodispersions of materials such as cerium oxide, [40] nickel ferrite, [41] and zinc oxide. [42]

Polymers concentrations. The resulting particle size is strongly dependent on the polymer concentration over the range 0.006 – 6.0 mM, with higher polymer concentrations leading to smaller particles. It is quite common to produce small particles when using a high polymer concentration and can be explained by seeding and growth mechanistic considerations (see Chapter 1 Section 1.6). [2,8,9,43,44]

Polymer molecular weight. A consistent but relatively modest molecular weight trend was observed for the pMAA–DDT ligands, and at a given molar concentration, lower molar mass pMAA–DDT chains give rise to smaller and more monodisperse particles (Figure 3.15). It should be stressed however that the four "standard" polymer concentrations (0.006, 0.06, 0.6 and 0.6 mM) were defined on the basis of the molar mass of the polymer repeat unit and not on the polymer molecular weight; as such, the number of polymer chains (and hence the number of available reactive thioether end groups) depended on the total M_n for each sample. This effect was weak but reproducible at all ligand concentrations. It has been predicted that, in the small particle limit, a weak increase in particle size will be observed for larger (*i.e.*, higher

M_w) passivant molecules because they require more time to diffuse and passivate the growing nanoparticle.[45] This prediction was not supported by data for Me–PEG–SH ligands of various molecular weights,[45] but our observations are broadly consistent with this hypothesis. An alternative hypothesis, put forward by the same research,[45] is that heteroatom–containing polymers such as Me–PEG–SH (and by analogy pMAA and pAA) act as a net which assists in particle nucleation by more rapidly supplying gold atoms to small, unstable gold clusters. In this case, larger polymers might enhance the effect by being larger nets.[45] Our data for pMAA–DDT ligands do not suggest that this is the main effect, although it is possible that both gold atom sequestration and ligand diffusion play opposing roles in the system with ligand diffusivity (for lower M_n species) dominating in this case.

End–group hydrophobicity. An increased particle monodispersity was observed for the pMAA ligands with more hydrophobic ends groups (C_{12} and C_{18} containing thioethers, Figures 3.21 and 3.3). It is known, that alkanethiols physisorb onto $Au^{(111)}$ surfaces through van der Waals interactions and that this physisorption enthalpy depends on the alkyl chain length.[46] The physisorption enthalpy per CH_2 group was found to be of the order of 6.1 kJ/mol, which implies that for alkanethiols longer than about 14 carbon atoms the physisorption enthalpy may exceed the chemisorption enthalpy.[46] The pMAA ligands produced using monofunctional alkanethiol chain–transfer agents contain thioether,[47] not thiol end–groups. Dialkyl sulfides bind less strongly to Au, having bond strengths near 60 kJ/mol as compared with the 130 kJ/mol value typical of chemisorbed alkanethiol–Au bonds.[46,48] Unlike alkanethiols, where both physisorbed (approximately 60 kJ/mol) and chemisorbed (approximately 120 kJ/mol) forms have been observed, dialkyl sulfides do not readily chemisorb to $Au^{(111)}$ and only physisorption (60 kJ/mol) occurs.[46,48] On the basis of these previous observations, it is conceivable that the pMAA ligands with longer hydrophobic alkyl end–groups physisorb more strongly to the growing Au particles and that this causes the enhanced control over particle size distribution.

End–group denticity. End–group!Multiple thiol containingThe multidentate ligand pMAA–PTMP gave rise to gold particles which were quite distinct from those obtained

with the other ligands studied here. In particular, the particles were much smaller at a given ligand concentration and more monodisperse. Remarkably narrow size distributions were observed at a ligand concentration of 0.006 mM (Figure 3.26 and 3.27). At this stage, this effect could not be fully rationalized, but it is clear that the structure of the pMAA–PTMP ligand differs in a number of respects. First, one might expect the tetradentate end group to have a larger footprint[19] and hence for each pMAA–PTMP ligand to passivate an increased area on the gold particle surface at a given molar coverage. Second, it is possible that the sticking probability for this ligand is enhanced and that this affects the kinetics of passivation. Third, the end–group, if multiply bound to the gold surface, may help to stabilize very small clusters, which is consistent with the marked decrease in particle size that was observed with this ligand at a given polymer concentration. These particles are also very stable toward the presence of salt, or pH variations.[31] The characteristics of those pMAA–PTMP gold particles are further investigated in Chapter 4.

In combination, these "rules" have allowed the production of ligands that are significantly more effective than those reported previously.[13] The precise physical explanation of these various effects is more complex, although some trends may be rationalized quite readily.[31]

3.4.2   Combined characterizations and correlations

All the gold suspensions produced in this study have been analyzed by TEM and DLS, so as not to overestimate sizes and distributions. The DLS average particle size measurements are quite close to those measured by TEM over the different samples analyzed, and a correlation between the sizes measured by both DLS and TEM is presented in Figure 3.29. It should be noted that the sizes observed by DLS are slightly bigger than the ones determined by TEM. The reason for this difference is that the DLS gives a measure of the particles hydrodynamic radius (*i.e.* the gold core, the polymer layer, and a layer of solvent around the particles, see Chapter 1 Section 1.8.3) when the TEM gives images of the electron dense core. In this study, DLS results were presented in volume, rather than in scattered light intensity. The scattered light intensity increases by 10^6 with the square of the particles molecular weight, thus, small
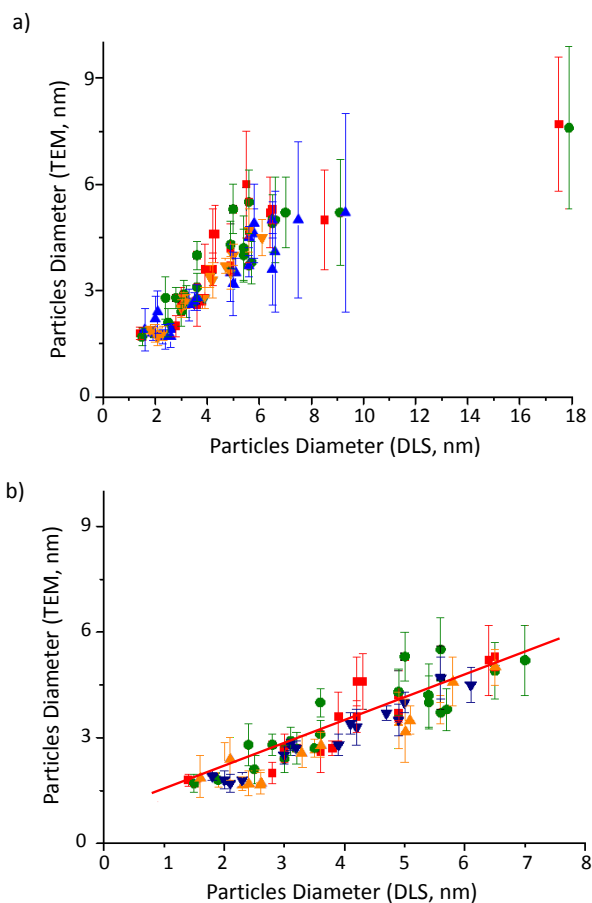
Figure 3.29: a) Correlation between particle diameters measured by TEM and measured by DLS for nanoparticles produced using capping agent of different main chains (red), capping agents of different molecular weight (green), capping agent with end-groups of different hydrophobicity (orange) and capping agents containing multiple thiols and/or thioether (blue). (b) Correlation between TEM and DLS measurements excluding samples with broad particle size distribution (more than 1 nm by TEM).

amount of impurities in the micrometer range would show a large peak on the spectra. Presentation of DLS data in volume is herein used to correct this difference in intensities and make the results easier to read.[49]

3.5 Summary

In conclusion, a simple protocol for the preparation of near monodisperse gold hydrosols in the small size regime below 5 nm has been developed. The particle size is controlled by varying the concentration of the stabilizing polymer. Polymer structures have been

optimized to control the growth of gold nanoparticles (polymer main-chain, molecular weight and end-group), leading to an unprecedented narrow size distribution in the 1 - 5 nm size range. This simple, one pot protocol is a particularly good alternative to replace previous methods whenever precise size control and monodispersity are required.

3.6 Bibliography

1. L.M. Liz-Marzan. *Langmuir*, 22:32, 2006.

2. D. Astruc M.C. Daniel. *Chem. Rev.*, 104:293, 2004.

3. E. Matijevic D.V. Goia. *Colloids Surf. A: Phys. Eng. Asp.*, 146:139, 1999.

4. A.J. Papworth A.I. Cooper I. Hussain, M. Brust. *Langmuir*, 19:4831, 2003.

5. C.J. Murphy N.R. Jana, L. Gearheart. *Langmuir*, 17:6782, 2001.

6. P.P. Provencio J.P. Wilkoxon. *J. Am. Chem. Soc.*, 126:6402, 2004.

7. R. Boese F. Bamdermann S. Meyer G.H.M. Calis W.A. Vandervelden G. Schmid, R. Pfeil. *Chem. Ber. Recl.*, 14:3634, 1981.

8. G. Frens. *Nat. Phys. Sci.*, 241:20, 1973.

9. J. Hillier J. Turkevich, P.C. Stevenson. *Disc. Faraday Soc.*, 11:55, 1951.

10. L. Demers L. Cuccia G.R. Brown R.B.Lennox A. Badia, S. Singh. *Chem. Eur. J.*, 2:359, 1996.

11. G. Nelles N. Weber R. Seshadri W. Tremel M. Bartz, J. Kuther. *J. Mater. Chem.*, 9:1121, 1999.

12. L. Armelao R.L. Donkers F. Polo C. Toniolo F. Maran L. Fabris, S. Antonello. *J. Am. Chem. Soc.*, 128:326, 2006.

13. Z.X. Wang B. Tan D.C. Sherrington S.P. Rannard A.I. Cooper M. Brust I. Hussain, S. Graham. *J. Am. Chem. Soc.*, 127:16398, 2005.

14. K. Schaumburg C.J. Kiely. M. Brust A.G. Kanaras, F.S. Kamounah. *Chem. Commun.*, page 2294, 2002.

15. J.T. Khoury T.G. Schaaff I. Vezmar M.M. Alvarez R.L. Whetten, M.N. Shafigulin. *Acc. Chem. Res.*, 32:397, 1999.

16. D. Bethell D.J. Schiffrin R. Whyman M. Brust, M. Walker. *Chem. Commun.*, page 801, 1994.

17. C.J. Zhong J.E. Harris R.W. Vachet M.R. Clak J.D. Londono S.J. Green J.J. Stokes G.D. Wignall G.L. Glish M.D. Porter N.D. Evans R.W. Murray M.J. Hostetler, J.E. Wingate. *Langmuir*, 14:17, 1998.

18. R.W. Murray A.C. Tempelton, M.P. Wuelfing. *Acc. Chem. Res.*, 33:27, 2000.

19. D.T. Miles R.W. Murray W.P. Wuelfing, S.M. Gross. *J. Am. Chem. Soc.*, 120:12969, 1998.

20. C.J. Kiely M. Brust. *J. Coll. Surf.. A: Phys. Eng. Asp.*, 202:175, 2002.

21. T. Pellegrino D. Zanchet C. Micheel S.C. Williams R. Boudreau M.A. Le Gros C.A. Larabell P.A. Alivisatos W.J. Parak, D. Gerion. *Nanotechnology*, 14:R15, 2003.

22. T. Liedl A.M. Javier L. Manna W.J. Parak T. Pellegrino, S. Kudera. *Small*, 1:48, 2005.

23. M.J. Hostetler J.J. Pietron R.W. Murray T.G. Schaaff J.T. Khoury M.M. Alvarez R.L. Whetten S.W. Chen, R.S. Ingram. *Science*, 280:2098, 1998.

24. P. Moriarty. *Rep. Prog Phys.*, 64:297, 2001.

25. A. Maali B. Lounis M. Orrit P. Boyer, P. Tamarat. *Science*, 297:1160, 2007.

26. J.E. Hutchinson S.F. Sweeney, G.H. Woehrle. *J. Am. Chem. Soc.*, 128:3190, 2008.

27. P. Provencio J.P. Wilkoxon, J.E. Martin. *Langmuir*, 16:9912, 2000.

28. F. Stellacci A.M. Mayes A. Akthakul, A.I. Hochbaum. *Adv. Matter.*, 17:532, 2005.

29. D.J. Buttrey W.D. Pyrz. *Langmuir*, 24:11350, 2008.

30. M. Hoppert. *Microscopic Techniques in Biotechnology*. Wiley VCH, 2003.

31. I. Hussain N. Schaeffer M.F. Wyatt M. Brust A.I. Cooper Z. Wang, B. Tan. *Langmuir*, 23:885, 2007.

32. J. Zhao J.X. Wang S.C. Wang Y. Zhang, Z. Wang. *Ch. Chem. Lett.*, 17:277, 2006.

33. S.P. Armes X. Bories-Azeau. *Macromolecules*, 35:10241, 2002.

34. A. Henglein. *Chem. Rev.*, 89:1861, 1989.

35. R.W. Murray T. Huang. *J. Phys. Chem. B*, 107:7434, 2003.

36. R.J. Cotter. *Time–of–flight Mass spectrometry.* ACS Professional Reference Books,, 1997.

37. A.J. Mills R.W. Murray R. Balasubramanian, R. Guo. *J. Am. Chem. Soc.*, 127:8126, 2005.

38. T.G. Schaaff. *Anal. Chem.*, 76:6187, 2004.

39. J. Hillier J. Turkevich, P.P.C. Stevenson. *Disc. Faraday Soc.*, 11:55, 1951.

40. J.F. Berrett M. Morvan A. Sehgal, Y. Lalatonne. *Langmuir*, 21:9359, 2005.

41. X.R. He D.H. Chen. *Mater. Res. Bull.*, 36:1369, 2001.

42. .X.L. Ma X.S. Pang Q..Zhao E.J. Tang, G.X. Cheng. *Appl. Surf. Sc.*, 252:5227, 2006.

43. J. Turkevich. *Gold Bull.*, 18:125, 1985.

44. J. Turkevich. *Gold Bull.*, 18:86, 1985.

45. P.V. Braun R.G. Schimmin, A.B. Schoch. *Langmuir*, 20:5613, 2004.

46. S.L. Bernasek G. Scoles D.J. Lavrich, S.M. Wetterer. *J. Phys. Chem. B*, 102:3456, 1998.

47. K. Inoue S. Shinkai J. Huskens D.N. Reinhoudt X.-M. Li, M.R. de Jong. *J. Mater. Chem.*, 11:1919, 2001.

48. S.J. Duncan D.B. Pedersen. *J. Phys. chem. A*, 109:11172, 2005.

49. R. Pecora B.J. Berne. *Dynamic Light Scattering with Applications to Chemistry, Biology and Physics.* Dover publications Inc., 1999.

Chapter 4

Size–Dependent Fluorescence Switching of Polymer–Stabilized Gold Clusters

4.1 Introduction

I N THE LAST DECADES, nanoparticles, and particularly noble metal nanoparticles, have been intensively studied because of their size–dependent physical and chemical properties.[1–4] Since nanoparticle's dimensions are comparable to biomolecules, they can be used as probes for sensitive biosensors and as building blocks for biologically driven self-assembly of nanostructures.[5–10] Therefore, the design and preparation of nanoparticles linked to biological molecules, such as peptides,[2,11] proteins[8,12,13] or DNA strands[14,15] has been a focus of research. Semi–conductor nanoparticles have been commonly used as biolabels, because they exhibit a strong visible fluorescence upon UV–visible excitation when their size is smaller than the Böhr radius (a tenth of nanometer for spherical CdSe particles).[16–19] Such an effect is not present in the case of noble metal nanoparticles, because metals do not have a band gap (see Chapter 1 Section 1.7). However these particles strongly affect the properties of organic dyes in their vicinity, inducing fluorescence quenching or, in the contrary, fluorescence enhancement, in a distance–dependant manner.[20–26]

In the past few years, new synthetic routes have allowed the manufacture of small metal nanoparticles, some of them exhibiting a strong fluorescence (compared to the bulk[27]) in the visible or near–infrared region when excited upon UV–visible light. Although the photophysical mechanism leading to such optical properties is not yet com-
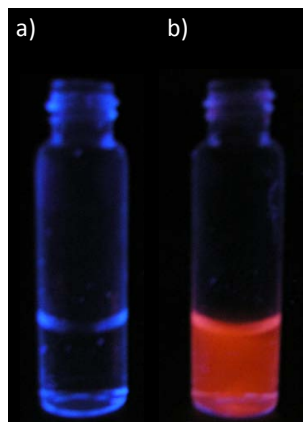
Figure 4.1: Colour picture of a) 1.7 nm and b) 1.1 nm pMAA–PTMP gold nanoparticles suspension under UV–visible irradiation ($\lambda = 345$ nm).

pletely understood, it is thought to be induced by the electronic transitions that occur upon excitation between the occupied d bands and the sp bands above the Fermi level.[28,29] This effect is dependent on the size of the particles, typically occurring only for diameters smaller than *ca.* 2 nm.[30–32] It is also, in some extent, dependent on the nature of the protective capping monolayer.[33,34] Most methods reported for the synthesis of fluorescent metal nanoparticles involve multiple-steps preparations, *e.g.* etching the surface of a larger particle,[35–37] or the use of organic solvents,[38,39] with the exception of tiopronin and glutathione protected nanocrystals.[30–32] Zheng *et al.* reported the formation of gold clusters with an intense blue fluorescence and a 41 ± 5% efficiency using polyamidoamine (pAMAM) dendrimers as stabilizers.[40] However, other studies suggest that the fluorescence can be attributed to the dendrimers rather than to the dendrimer–nanoparticle conjugates.[41,42] This highlight the importance of cautious characterization when dealing with fluorescent metalic clusters of this kind.

In Chapter 3, the one–step synthesis of highly monodisperse gold nanoparticles has been described, the particles size could be tuned between 1.7 nm and 6 nm by changing the polymer backbone structure, the nature of the polymer end–group and the relative amount of gold precursor to polymer.[43,44]

In this Chapter, using a higher molecular weight pMAA–PTMP polymeric stabilizer, the size–range tunability of the so–formed gold particles has been extended to the sub 2 nm range and a transition from non–fluorescent to fluorescent nanoparticles be-

tween 1.1 nm and 1.7 nm has been demonstrated (see Figure 4.1. The most fluorescent nanomaterial has a 3% quantum yield, and is made of a 1.1 nm gold core and a 6.9 nm hydrodynamic radius. Extensive characterizations and control experiments demonstrate that the fluorescence originates from the polymer–capped gold nanoparticle and is strongly dependent on the nanoparticle size and capping agent nature. A model of the core / shell nanoparticle structure, based on different characterization methods, is proposed.

4.2 Experimental

4.2.1 Materials

Hydrogen tetrachloroaurate^{III} trihydrate, pentaerythritol tetrakis (3–mercaptopropionate), 2,2–Azobis(2–methylpropionitrile, methacrylic acid, and sodium borohydride (NaBH4$_4$) were purchased from Aldrich, sodium perchlorate (NaClO$_3$from AnalR, tris(2,2–bipyridyl) ruthenium^{II} chloride hexahydrate from Acros Organics. All chemicals were used as received. For all experiments, Milli–Q water (18.2 M$|Omega$) was used, purified using an ultrapure system MilliQ Plus 185 (Millipore purification pack). 0.45μm pore size Millex–HA microfilter were purchased from Millipore.

4.2.2 Methods

4.2.2.1 Polymeric stabilizer synthesis

The methacrylic acid monomer (50 mmol), chain transfer agent (PTMP, 1 mmol) and Azobismethylpropionitrile (0.080 g, 0.50 mmol) were heated in ethanol (30 mL) under nitrogen at 75°C in a round-bottomed flask fitted with a reflux condenser (Radleys Carousel Reactor). The reaction was carried out for 5 hours under agitation. The resulting product was precipitated into cold diethyl ether (100 mL), filtered using a Buchner funnel, and dried in vacuo at 45°C for 24 h.

4.2.2.2 Polymeric stabilizer characterization

^{1}**H NMR** ^{1}H NMR spectrum was recorded on a 400 MHz Bruker DPX–400 spectrometer using δ6 DMSO as a solvent in a 5 mm quartz NMR tube. ^{1}H NMR of pMAA–PTMP (δ6 DMSO) chemical shifts (ppm): end–group: 1.5 (SH), 2.6 & 4.1

(CH_2); backbone: 1.0 (CH_3), 1.8 & 2.3 (CH_2)

Gel permeation chromatography   Gel permeation chromatography (GPC) was performed using a Polymer Laboratories system equipped with a PL–ELS 1000 evaporative light scattering detector and a series of PC mix gel columns 5 μm MIXED C and D. THF was used as the eluent at a flow rate of 1.0 ml/min at 40°C. Calibration was carried out using EasiCal polystyrene standards (Polymer Laboratories). The polymer was first converted to the methyl ester using TMS-diazomethane reagent to render it soluble in THF.

Elemental analysis   An inductively coupled plasma atomic emission spectroscopy (ICP–AES) (Spectro Ciros CCD) was used to measure the composition of the gold suspensions. The signal intensity to concentration was calibrated on a six points plot determined using standard commercial solutions of gold and sulphur.

4.2.2.3   Gold nanoparticles synthesis

In a typical experiment, 25 μL of a 20 mM $HAuCl_4$ solution was added to a 1 mL aqueous polymer solution and left for two hours. The final reduction step was achieved by adding 100 μL of a freshly prepared 5 mM $NaBH_4$ aqueous solution. The nanoparticles were allowed to form and after 24 hours, the unreacted polymer was removed by dialysis against water and / or by size exclusion chromatography.

4.2.2.4   Gold nanoparticles characterization

UV–visible absorption spectroscopy   UV–visible spectra were carried out on a spectromax plus 384. The aqueous gold nanoparticles solutions (300 μL) were analyzed in a 1 cm path length quartz cuvette at room temperature.

Fluorescence emission and excitation spectroscopy   Fluorescence spectra were carried out using an Aminco–Bowman Series 2 luminescence spectrometer. The aqueous gold nanoparticles solutions (200 μL) were analyzed in quartz cuvette at room temperature.

Quantum yield calculations   The quantum yield of the most fluorescent gold nanoparticles suspension (prepared using 4 mM pMAA–PTMPA and 0.5 mM HAuCl$_4$ concentrations, see Section 4.3.2 for details) was calculated in using tris(2,2–bipyridyl) ruthenium hexahydrate[II] as a standard. five aqueous solutions of different concentrations were prepared for both the standard and the nanoparticles suspensions. The quantum yield was calculated by comparing the plots of the integrated emission spectra against the UV–visible extinction spectra for the standard and the gold suspension (at $\lambda = 436$ and 450 nm respectively).

High resolution transmission electron microscopy   The specimens were examined by high resolution transmission electron microscopy (HR–TEM) on a Jeol JEM–2011 electron microscope operated at 200 kV and FEI TITAN 80 / 300 microscope operated at 300 kV. Gold suspensions were deposited on a copper specimen grid supported by a holey carbon film and left for drying. The diameter of each particle was quantified using ImagesJ software (1.34s, NIH, USA) to analyze the digitized photographic images for each sample in the magnification range 200,000 – 500,000 times. A histogram of the particle size distribution and the average particle diameter were obtained by measuring about 200 particles in arbitrarily chosen areas in the photograph.

Size exclusion chromatography   Size exclusion chromatography was carried out on a 50 cm length Sephadex G25 at a flow rate of 0.680 mL/min at room temperature. 15ml of gold nanoparticles suspension prepared in using an Au/S ratio of 1/8 (that is, 4 mM pMAA–PTMP and 0.5 mM HAuCl$_4$ concentratiions) were freeze–dried, redispersed in 1 mL of water and eluted through the column. The output was detected by UV–Visible absorption (detection at $\lambda = 206$ nm) and the chemical composition of the fractions (gold and sulphur) was analysed by ICP–AES.

Multiphoton confocal microscopy   Multiphoton confocal microscopy was carried out on a Zeiss microscope. A drop of gold suspension was allowed to dry onto a glass layer and examined under laser excitation ($\lambda = 458$ nm, $P = 0.94$ W) at a magnification of 65×.

Fluorescence recovery after photobleaching FRAP measurements were carried out in a capillary (1 mm diameter) loaded with a gold nanoparticles suspension (4 mM pMAA–PTMP and 0.5 mM HAuCl$_4$). Photobleaching was induced by illuminating the capillary (Section: 1mm) by using an argon laser ($\lambda = 488$ nm, $P = 1$ W) during 500 to 1000 ms. After photobleaching, the beam was attenuated by using a OG515 filter, 90% of the fluorescence intensity was recovered after approximately 180 s. The evolution of the fluorescence was monitored by a CCD camera.

Photothermal microscopy A non–resonant probe laser beam (HeNe, $\lambda = 633$ nm) and an heating beam (Nd:YAG laser, $\lambda = 532$ nm) were overlaid and focused on the sample by means of a high NA microscope objective ($\times$ 100, NA=1.4). The intensity of the heating beam was modulated by an acousto–optic modulator. The sample consists on a dried film of pMAA–PTMP stabilized nanoparticles prepared in using a 4 mM ligand concentration diluted in a PVP matrix (1/1000) on a glass slide. It was mounted on a piezoelectic scanner (see Section 4.3.6.1 for details). The size of the observed particles was deduced by comparaison with a commercial colloidal gold suspension (dodecanethiol stabilized AuNPs, 3 nm) analysed using the same experimental conditions.

X–ray photoelectron spectroscopy (XPS) Samples were prepared for XPS by pipetting solutions of the polymer capped gold nanoparticles onto adhesive carbon discs. Solvent was allowed to evaporate off under ambient conditions to leave a waxy film. A gold foil (Au^0) foil, Au$_2$O$_3$ and AuCl(PPh$_3$) were mounted directly on the adhesive carbon discs. X–ray photoelectron spectra were collected on a Kratos Axis Ultra X–ray photoelectron spectrometer with monochromatic Al–$k\alpha$ radiation and charge neutralization. Survey scans were ired in one sweep in 250 meV steps with a dwell time of 200 ms / step and pass energy of 80 electronvolts. High resolution scans of the C^{1s} region were acquired in 1 sweep in 100 meV steps with a dwell time of 200 ms/step and pass energy of 20 eV. The Au^{4f} X–ray photoelectron spectra for all samples (except those prepared from 0.4 mM pMAA–PTMP and 0.5 mM HAuCl$_4$ were acquired in 5 sweeps in 100 meV steps with a pass energy of 20 eV and a dwell time of 200 ms / step. Au^{4f} X–ray photoelectron spectra of the sample prepared from 0.5 mM pMAA–PTMP

M_n=6359g/mol
M_w=7524g/mol
PDI=1.2
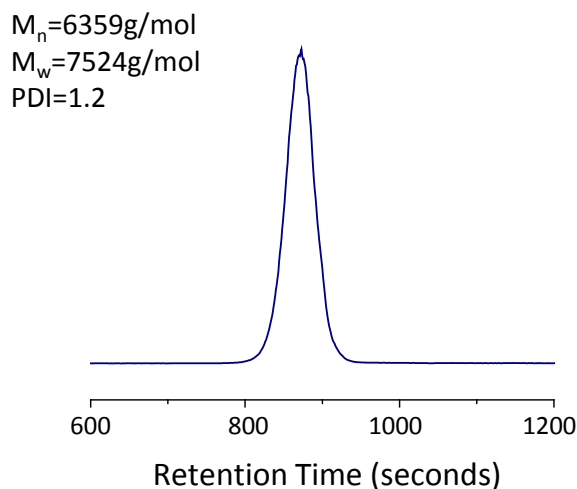
Figure 4.2: GPC elution curve of pMAA–PTMP stabilizer.

and 0.5 mM $HAuCl_4$ were acquired in 10 sweeps with a dwell time of 500 ms and pass energy of 20 eV. For analysis, six of these scans were averaged after calibration to the to the C^{1s} carbonyl peak of acrylic acid units at 289.33 electronvolts.

Extended X–Ray absorption fine structure (EXAFS)   X–ray absorption spectra of the (Au in the polymer films) at the Au–L3 absorption edge were collected at beamline 12–BM–B of the Advanced Photon Source (APS) in Chicago, USA. The bending magnet beamline uses a water–cooled, double-crystal, fixed-exit monochromator with Si(111) crystals capable of operations between 4.5 and 30 keV. A double mirror system (flat plus torroid) with a cutoff energy of 22 keV focuses the beam in the experimental station to 0.8 mm x 1 mm. Data were collected on polymer films mounted on adhesive backed carbon tabs in fluorescence-yield mode with a Canberra 13–element Ge detector. Eight spectra collected sequentially on each sample were averaged for further analysis of the EXAFS.

4.3   Results

4.3.1   Polymer stabilizer synthesis

In Chapter 3, the one–step synthesis of various water–soluble, polymer–stabilized monodisperse gold nanoparticles has been reported.[43,44] It was shown that their sizes and dis-

persions are governed by he polymer stabilizer structure (main chain and thiol and/or thioether containing end-group), the molecular weight (M_n) of the polymeric stabilizer, and more importantly, the relative amount of gold and stabilizer ligand used during the synthesis; a higher gold / polymeric ligand ratio leading to the formation of larger particles.

It was also found that, amongst all the different polymeric stabilizers that were used, pMAA–PTMP (pentaerythritol tetrakis(3–mercaptopropionate) terminated polymethacrylic acid) produced the most promising results, since it allows making small and monodisperse nanoparticles, that are also chemically and physically stable (to the presence of salt, or pH variations for example).[43] This polymeric stabilizer is made up of a linear chain of water–soluble methacrylic acid units and of an hydrophobic end–group that contains, on average, three thiols and one thioether (see Section 2.3.4 Figure 2.7). This ligand is believed to be an efficient capping agent probably because of the presence of the three sulphurs that can form quasi–covalent bonds with gold.

In the study presented in Chapter 3 Section 3.3.1.4, the highest polymeric ligand concentration used for the synthesis of gold particles was 6 mM. This is the higher polymer concentration that could be reached in aqueous conditions, due to limited solubility of the polymers containing an end–group of relatively high hydrophobicity, like PTMP.

In this Chapter, a pMAA–PTMP with a higher molecular weight than in the previous study was targeted in order to counterbalance the hydrophobicity of the end–group, thus obtaining a better solubility in water up to approximately 30 mM. Increasing the solubility of the polymer allows a lower gold / ligand ratio to be used. Since the size of the so–formed gold particles is directly dependent on the relative concentration of gold initiator and polymeric ligand, the use of this polymer should therefore lead to the formation of smaller nanoparticles.

The pMAA–PTMP used in this Chapter was synthesized as described previously in Section 2.4.1)[43] using PTMP (pentaerythritol tetrakis(3–mercaptopropionate) as the chain transfer agent and AIBN (2,2'–Azobis(2–methylpropionitrile) as the initiator. The relative amounts of initiator and methacrylic acid monomers was decreased compared to the synthesis described previously. ^{1}H NMR spectroscopy (Figure 4.3) show
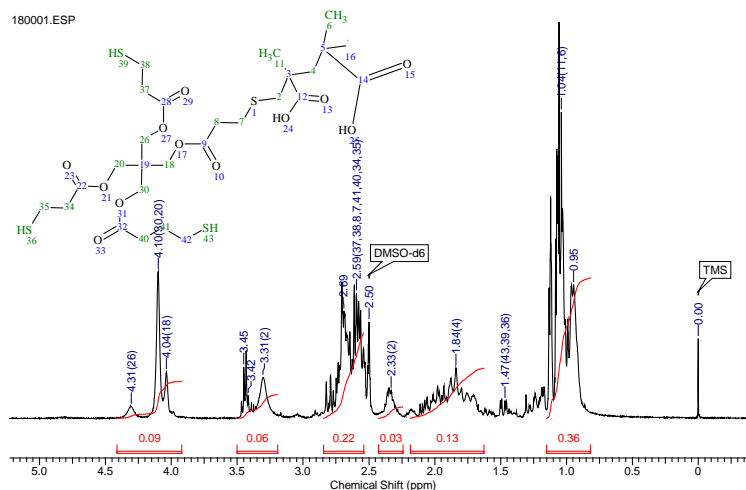
Figure 4.3: ^{1}H NMR spectra of pMAA–PTMP polymeric stabilizer.

the presence of an SH peak at 1.3 ppm, implying that most of the polymeric chains are formed alongside a single thiol on each PTMP unit, as described in Section 2.4.3. [45–47]

Gel permeation chromatography data (Figure 4.2) indicates that the polymer molecular weight is higher than the one used previously in Chapter 2 and that the molecular weight distribution is relatively narrow (M_n = 6359 g/mol, M_w = 7524g/mol and PDI = 1.2). As mentioned in Section 2.4.2, the molecular weight, and thus, the size of the hyhdrophylic polymer main–chain is dependent on the relative ratio of monomers and chain–transfer agent (for a fixed initiator concentration, under similar experimental conditions) used during the chain–transfer polymerization process. For comparison, the polymer prepared using a similar ratio (*i.e.* pMAA–DDT prepared in using 5 mmol of monomer and 1.25 mmol of chain–transfer agent) allowed the preparation of a polymer with and average number molecular weight M_n = 7000 g/mol and weight average molecular weight M_w = 9540. Those data a roughly in accordance with the molecular weight of the polymer described here, and the variations observed between those two polymers can be ascribed to different chain–transfer constant between DDT and PTMP (see Chapter 2 Section 2.4.1).
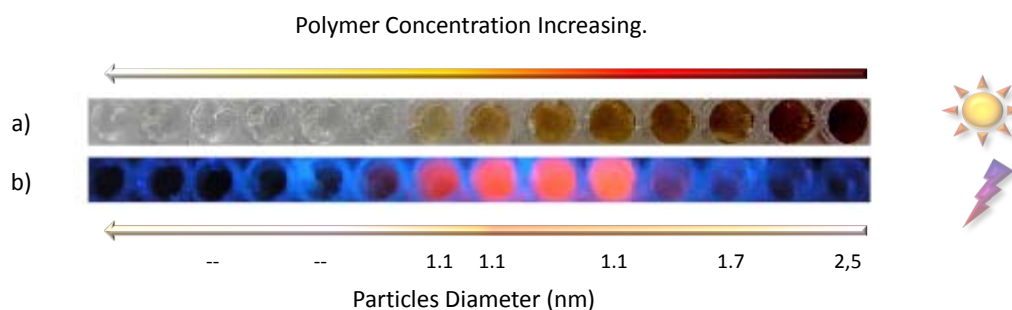
Figure 4.4: Colour image of gold suspensions prepared with a fixed gold concentration (0.5 mM) and various ligand concentration under a) daylight and b) UV visible light (345 nm wavelength).

4.3.2 Formation of gold nanoparticles

This PTMP terminated pMAA was then used as a "multi-dentate" capping agent to control the growth of gold nanoparticles in a manner similar as the one described in Section 3.3.1.4 and different sizes of particles were obtained by varying the polymer/gold ratio in the 0.05 mM to 15 mM range (for a fixed $HAuCl_4$) concentration of 0.5 mM. The so–formed gold suspensions are shown in Figure 4.4a).

When the capping agent / gold ratio is increased, a change of the colour of the nanoparticles solutions from red to yellow is observed for a polymer concentration ranging from 0.05 to approximately 5 mM while keeping the amount of $HAuCl_4$ constant (Figure 4.4a). These observations are in accordance with those described in Chapter 3 and Section 3.3.1.4. This tends to indicate that spectroscopically–distinct particles of different sizes are formed.[19]

However, at polymer concentrations above 5 mM, colourless solutions are observed. The presence of nanoparticles in those samples could not be confirmed, neither ruled out, and those colourless are believed to be due to the formation of very small gold clusters or to gold^{I} complexes.[48]

The size of some of those so–formed particles was studied by TEM and HR–TEM, as depicted in Figure 4.5. Once again, the size of the particles seems to be dependent on the polymeric ligand concentration used during the synthesis, a higher polymer concentration leading to the formation of smaller particles in the 2.5 to 1.1 nm range. This trend is shown in Figure 4.6
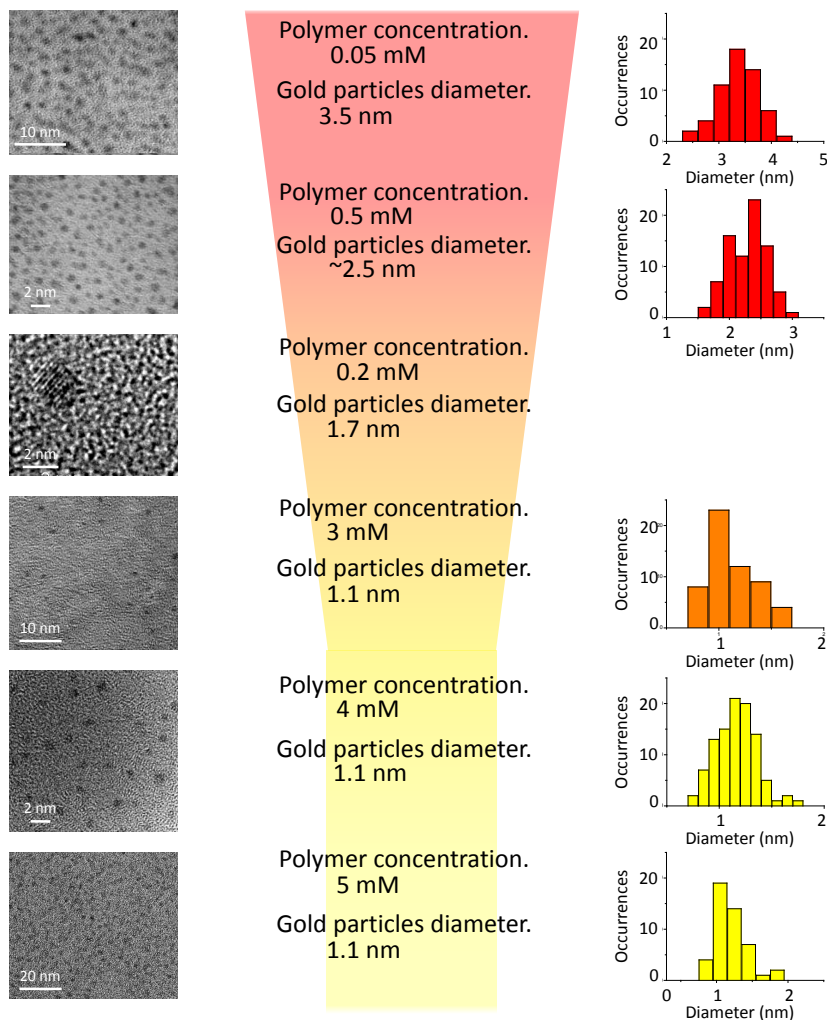
Figure 4.5: TEM, HR–TEM pictures and size distribution histograms of pMAA–PTMP stabilized gold nanoparticles prepared using a 0.5 mM $HAuCl_4$ concentration and various polymer concentrations.

The sizes of the gold particles determined by HR–TEM are roughly in accordance with the data presented in Section 3.3.1.4 and Figure 3.26. The slight increase in the particles size distribution observed between the two sets of experiments (in using a $M_n = 1988$ g/mol pMAA–PTMP in Chapter 2 and a $M_n = 6359$ g/mol pMAA–PTMP herein) corroborates the previous observations describing the influence of the polymeric stabilizer molecular weight on the gold nanoparticles average size, a longer polymeric chain leading to the formation of particles slightly larger (see Section 3.3.1.2).[43]
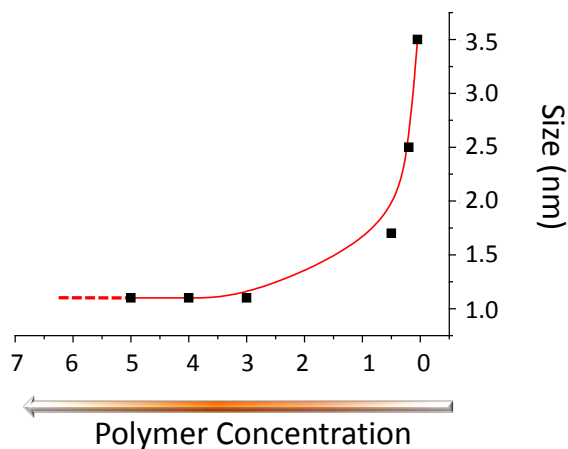
Figure 4.6: Plot of the pMAA–PTMP stabilized particles diameter (determined by TEM) against the polymer concentration used for their synthesis. No particles smaller than 1.1 nm could be observed (preparations using polymer concentrations above 5 mM.
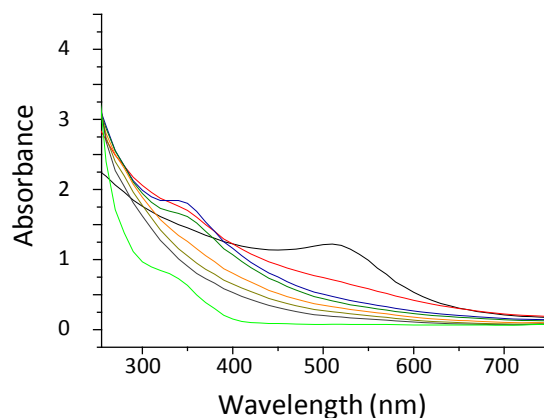
Figure 4.7: UV–Visible extinction spectra of gold suspensions with various ligand concentration; 0.05mM (black line), 0.2mM (blue line), 0.5mM (red line), 1mM (dark green), 2mM (orange line), 3mM (dark yellow line), 4mM (grey line), 6mM (green line).

4.3.3 Gold nanoparticles optical characteristics

The UV visible spectroscopyUV–Visible extinction spectra of the various gold suspensions show that only solutions prepared with a polymer concentration below 0.2 mM (larger nanoparticles) exhibit a weak plasmon band at 510 nm, whereas the solutions
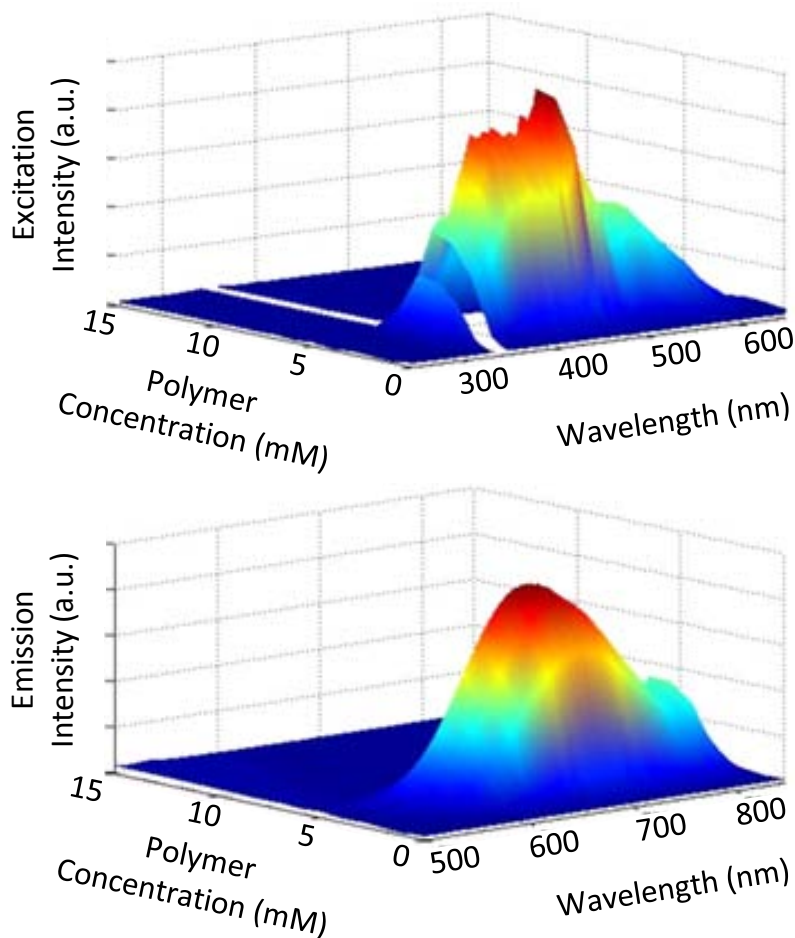
Figure 4.8: Excitation spectra (emission at 695nm) of gold suspensions against ligand concentration (for a fixed concentration of 0.5mM of gold). An experimental artifact due to second order excitation (between 340 and 360nm) was intentionally deleted. Emission spectra (excitation at 450nm) of a gold suspension against ligand concentration (for a fixed concentration of 0.5mM of gold).

prepared using a higher polymer concentration (small nanoparticles) do not show any plasmon band at all (Figure 4.7).

Interestingly, the gold nanoparticles prepared using a polymer / gold ratio between 1/1 and 1/12 (that is a polymer concentration ranging between 0.5 mM and 15 mM, for a fixed gold concentration of 0.5 mM) exhibit a red visible fluorescence when excited
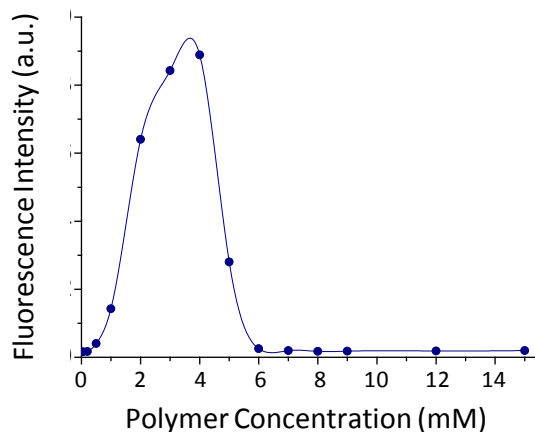
Figure 4.9: Emission intensities at 695 nm as a function of ligand concentration.

under UV–visible light ($\lambda = 345$ nm), as shown in Figure 4.4b). Fluorescence (excitation and emission) spectra were recorded on all samples, revealing a broad excitation band centered at 450 nm and a broad emission band at $700 - 750$ nanometers (Figures 4.8). The magnitudes of the emission and excitation bands are strongly dependent on the polymer concentration with a maximum intensity for a polymer concentration of 4 mM (Figures 4.8 and 4.9).

The excitation spectra exhibit a fine structure and the emission spectra show a sharp secondary peak at 800 nm. These characteristics are reproducibly observed on excitation and emission spectra recorded on batches of gold suspensions obtained in different independent syntheses. The relation between these peaks and the detailed electronic structure remains challenging. However, it has been shown previously that the emission and excitation energies were dependent on the gold clusters size and electronic structure.[28,29] This fine structure (Figure 4.10) can then arguably be assigned to different electronic transitions occurring in small clusters of slightly different sizes, or between different electronic states (see Section 4.4.2.1 for details).[49,50]

4.3.4 Fluorescent particles quantum yield calculations

The quantum yield Θ_f of a fluorescent species is the ratio of photons absorbed to photons emitted through luminescence, and the probability of the excited state being deactivated by fluorescence (or phosphorescence) rather than by another, non–radiative
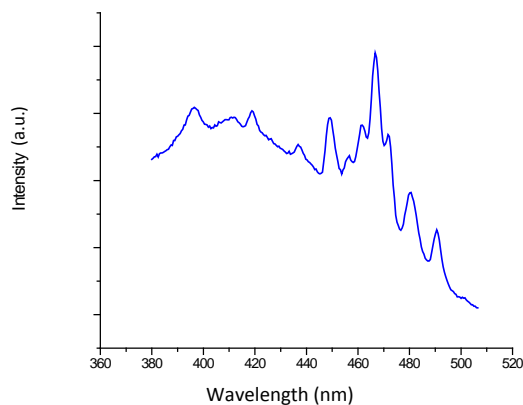
Figure 4.10: Fine structure of excitation spectra of fluorescent gold suspensions (emission at $\lambda = 750$ nm).

mechanism. It is given by Equation 4.1.

$$\Theta = \frac{photons_{em}}{photons_{abs}} \tag{4.1}$$

Herein, the quantum yield of the most fluorescent nanomaterial (prepared using a 0.5 mM HAuCl$_4$ concentration and a 4 mM pMAA–PTMP concentration) was determined using the comparative method of Williams *et al.*,[51] which involves the use of a well characterized standard species with a known quantum yield. Here, tris(bipyridine)ruthenium^{II} chloride was chosen as a standard because it has a similar absorbance than the gold suspension at approximately the same excitation wavelength.[52,53]

Hence, the quantum yields of the gold suspensions and the standard was calculated as the ratio of the integrated fluorescence intensity (between $\lambda = 450$ and 950 nm) to their respective absorbances at their maximum excitation wavelengths (that is, $\lambda = 443$ nm for the standard and $\lambda = 450$ nm for the gold suspensions). This process was repeated at five different concentrations for the standard and the gold suspensions, and the plot of the integrated intensities against the absorbances is shown in Figure 4.11, typical absorption and excitation spectra for the standard and the gold suspensions are depicted in Figure 4.12.

The quantum yield of the gold suspension, Θ_{AuNP} was then calculated in using the
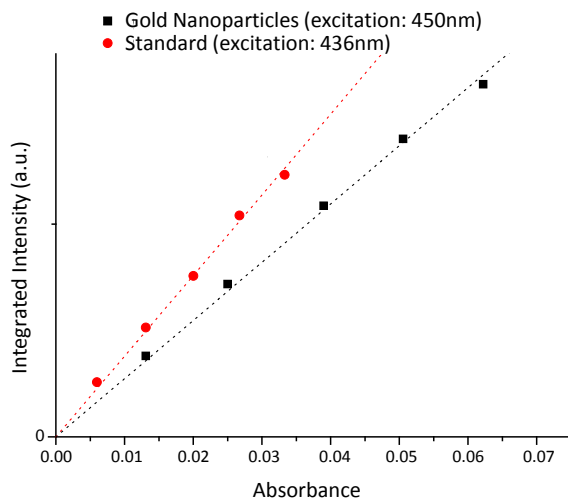
Figure 4.11: Quantum yield of the most fluorescent gold nanoparticles suspension (4 pMAA-PTMP and 0.5 mM HAuCl$_4$) calculated in using Tris(2,2-bipyridyl) ruthenium hexahydrate (II) as a standard.

respective slopes of the two linear fits of the plots shown in Figure 4.11 as:

$$\Theta_{AuNP} = \Theta_{st.} \times \frac{Slope_{AuNP}}{Slope_{St.}} \tag{4.2}$$

with $\Theta_{st.}$ the quantum yield of the standard ($\Theta_{st.} = 4.2\%$),[54] and $Slope_{AuNP}$ and $Slope_{St.}$ the director coefficient of the linear plots of the gold suspensions and the standard respectively. The quantum yield of the fluorescent gold suspension was found to be $\theta = 4.2 \times \frac{2.43}{3.70} = 3\%$.

4.3.5 Purifications and controls

4.3.5.1 Removal of excess unreacted polymeric ligand

Size exclusion chromatography was carried out on the gold suspension samples in order to remove the excess polymer after the synthesis of gold nanoparticles (see Section 4.2.2.3). In order to assess the efficiency of this purification process, an unpurified gold nanoparticles sample synthesized using a 4 mM polymer and 0.5 mM HAuCl$_4$ concentrations was eluted through preparative scale size exclusion chromatography. the sample (15 mL) was first freeze–dried, and resuspended in Milli–Q water (1 mL) No signs of aggregation could be observed when comparing the UV–visisble spectra of the suspensions before and after freeze–drying, no significant difference in their fluorescence
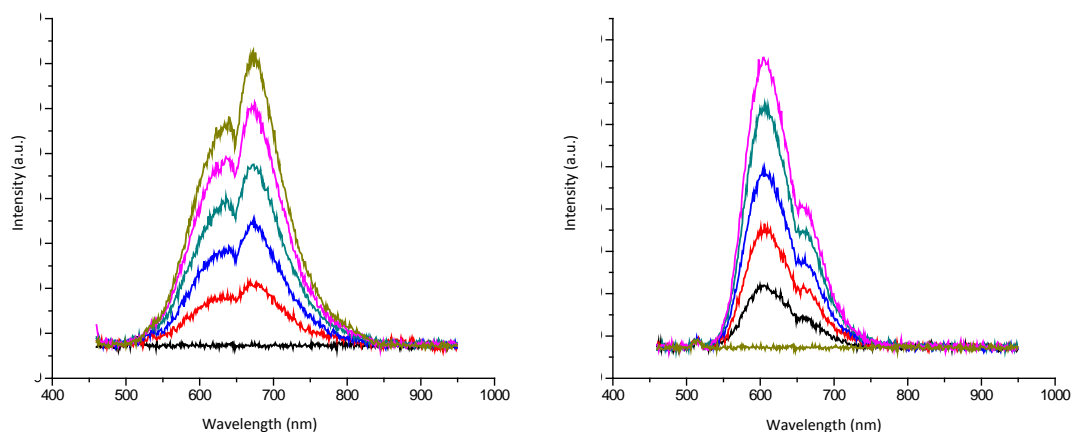
Figure 4.12: Excitation spectra of a) Tris(2,2–bipyridyl) ruthenium and b) the pMAA–PTMP gold suspensions at various low concentrations.

excitation and emission spectra could be noticed either, as shown in Figures 4.13 a) and b).

The output of the column was followed by "online" UV–visible detection (tracking eluted species' absorbance at $\lambda = 208$ nm), and the resulting UV–visible trace is presented in Figure 4.15. The fractions were analyzed by fluorescence spectroscopy and ICP–AES. The setup of this experiment is described in Figure 4.14.

The UV–visible trace show a sharp peak at 9 minutes reduced retention time, and a second broad one at approximately 40 minutes can also be observed. The first peak is related to largest species (shorter elution time) that are yellow upon daylight (gold particles) and fluorescent when excited by UV–Visible radiation ($\lambda = 345$ nm) The second peak is related to smaller (longer elution time) colourless and non–fluorescent species, and is attributed to the excess unreacted polymer.

After elution, the fractions were collected, and their fluorescence intensities recorded, as well as their chemical composition, which was determined by ICP–AES. The results of those controls are shown in Figure 4.16. Once again, the results show a separation of two species. The largest yellow species exhibit a strong fluorescence when excited by UV-visible light (peak at 9 minutes, Figure 4.16a). Elemental analysis of the same fractions showed that the fluorescence is related with the amount of gold. The smallest species on the curve representing the sulphur concentration can be attributed to the

a)

b)
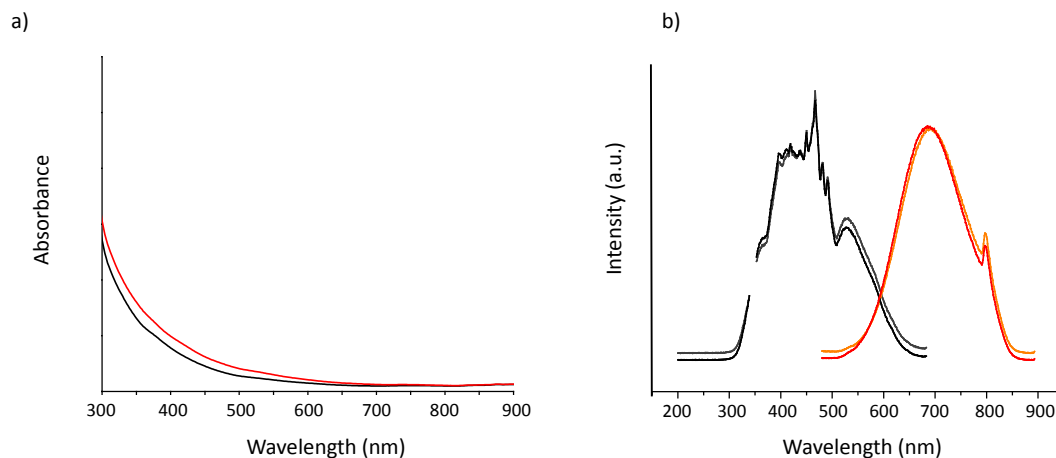
Figure 4.13: a) UV visible spectroscopyUV–Visible absorption spectra of a gold nanoparticles suspension prepared using a 4 mM pMAA–PTMP and a 0.5 mM concentration of $HAuCl_4$ before (black line) and after (red line) freeze–drying. b) Excitation and emission spectra of the same gold suspension before (black and grey lines respectively) and after (red and orange lines respectively) freeze drying. Because the particles have been concentrated, and due to saturation of the detectors (for both UV–Visible and fluorescence spectroscopies), the samples were diluted (in Milli–Q water) prior to analysis, and the spectra shown have been normalized.

excess polymer (peak at 40 minutes (Figure 4.16).

Taken together, these experiments clearly demonstrate that the fluorescence cannot be attributed to the polymer by itself.

4.3.5.2 Oxidation, reduction adducts and Au^I oligomers

To test whether the observed fluorescence could be due to the polymeric species, or a byproduct, excitation and emission spectra were recorded on the polymer itself in aqueous solutions for all the concentrations that were used during the synthesis of the particles (Figure 4.17 a). The same control experiment was repeated on the oxidized form of the polymer (by adding 100 μL of a freshly prepared 50 mM $NaClO_4$ aqueous solution to a 1 mL polymer solution) and its reduced form (by adding 100 μL of a freshly prepared 50 mM $NaBH_4$ aqueous solution to a 1 mL polymer solution). Only a weak emission could be observed on those controls, at $\lambda = 400$ nm; the excitation wavelength could not be detected and is thought to be at a wavelength below 200 nm. The weak fluorescence is observed at high polymer concentrations, at a wavelength different from the one observed for the gold colloids. It is thus unlikely that it is related

125
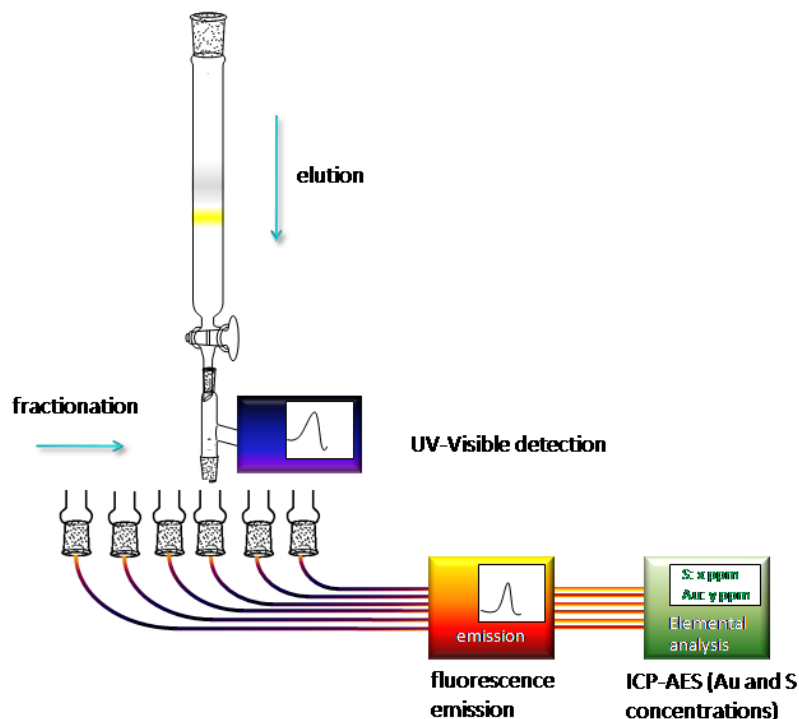
Figure 4.14: Experimental setup of the size exclusion experiment. the output of the column is controlled using a UV–Visible detector ($\lambda = 208$ nm), the fractions are then analyzed by emission spectroscopy and ICP–AES.

to the fluorescence of the gold particles, and is probably due to a weak emission of the polymer itself. (see Figure 4.17 b and c).

The fluorescence of gold^{I} complex has been reported in the literature. [55,56] Therefore, the luminescence of Au^{I} complex that could have been formed during the synthesis was investigated to elucidate if the observed fluorescence could originate from such complexes rather than from Au^{0} clusters. A series of solutions containing pMAA–PTMP and HAuCl$_4$ in different ratios were prepared. These solutions were identical to the one used for nanoparticles synthesis except that no reducing agent (NaBH$_4$ was added. All the solutions were pale yellow after addition of the gold salt and turned rapidly to colourless, indicating that gold^{III} was reduced to gold^{I} by the polymer in solution. [48] Emission and excitation spectra were recorded and no fluorescence could be detected (Figure 4.17 d).

Furthermore, the oxidation state of the gold in some of the fluorescent gold nanoparticles samples was investigated by X–ray photoelectron spectroscopy (XPS) in order to
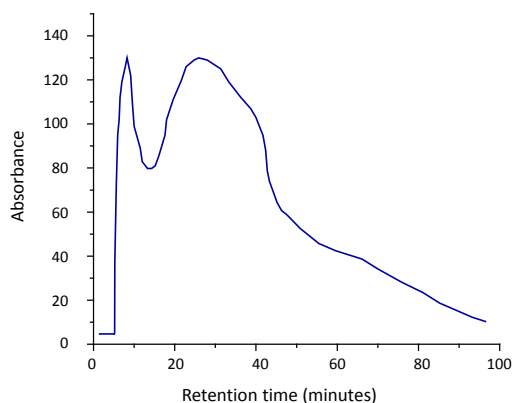
Figure 4.15: UV–visible (λ = 208 nm) detection of size exclusion chromatography elution.

assess the metalic state of the gold clusters. The XPS spectrum exhibits two peaks at 81.83 eV (Au 4f$^{7/2}$) and 85.47 eV (Au 4f$^{5/2}$) that are consistent with the presence of gold^0 nanoparticles (Figure 4.28).[31,34,57] No peak corresponding to the binding energy of gold^I) containing species could be observed.

This set of experiments tends to indicate that the observed fluorescence cannot be attributed to the formation of a gold^I complex. The XPS analysis of the gold suspensions is discussed in details in Section 4.4.1

4.3.6 Photobleaching

In order to confirm the size of the luminescent particles observed by HR–TEM and to relate the fluorescence to the presence of the particles, photothermal spectroscopy coupled to confocal fluorescence spectroscopy was carried out. The former technique allows the detection of single particles by scanning a specific area of a dry film of the sample, the latter can detect small fluorescent dots on the same area. The superposition of two images, the first one showing the position of the particles and the second one showing the presence of fluorescence, would prove that the fluorescence originates from those particles.
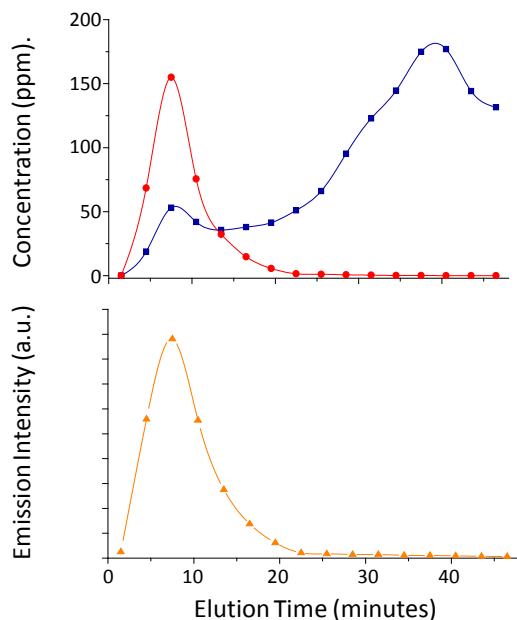
Figure 4.16: Top: Gold (red) and sulphur (blue) concentrations determined by I.C.P.-A.E.S. (Inductively Coupled Plasma - Atomic Emission Spectrometry) of various fractions of an unpurified (unreacted polymer-containing) gold nanoparticles suspension after elution through size exclusion chromatography (Sephadex G25). The sample was prepared using a 4 mM polymer concentration and a 0.5 mM gold concentration. Bottom: Emission intensity of those fractions (excitation and emission wavelength are 485 nm and 645 nm respectively).

4.3.6.1 Photothermal and fluorescence microscopy

Photothermal spectroscopy can detect gold nanoparticles as small as 1.4 nm taking advantage of the large absorption cross section of a nanoparticle that induce a local temperature increase around the particle when illuminated by a laser.[58–60]

Photothermal images of the gold particles prepared using a 4mM pMAA–PTMP and 0.5 mM gold concentrations were taken using the experimental setup presented in Figure 4.18. This setup involves a heating beam absorbed by the particles (green laser, $\lambda = 514$ nm) and a superposed probe beam (red laser, $\lambda = 633$ nm) weakly absorbed, polarized horizontally. An accousto–optical modulator is used to modulate the intensity of the green laser at a frequency Ω . The sample which is mounted onto a piezoscanner and can move along two axes.
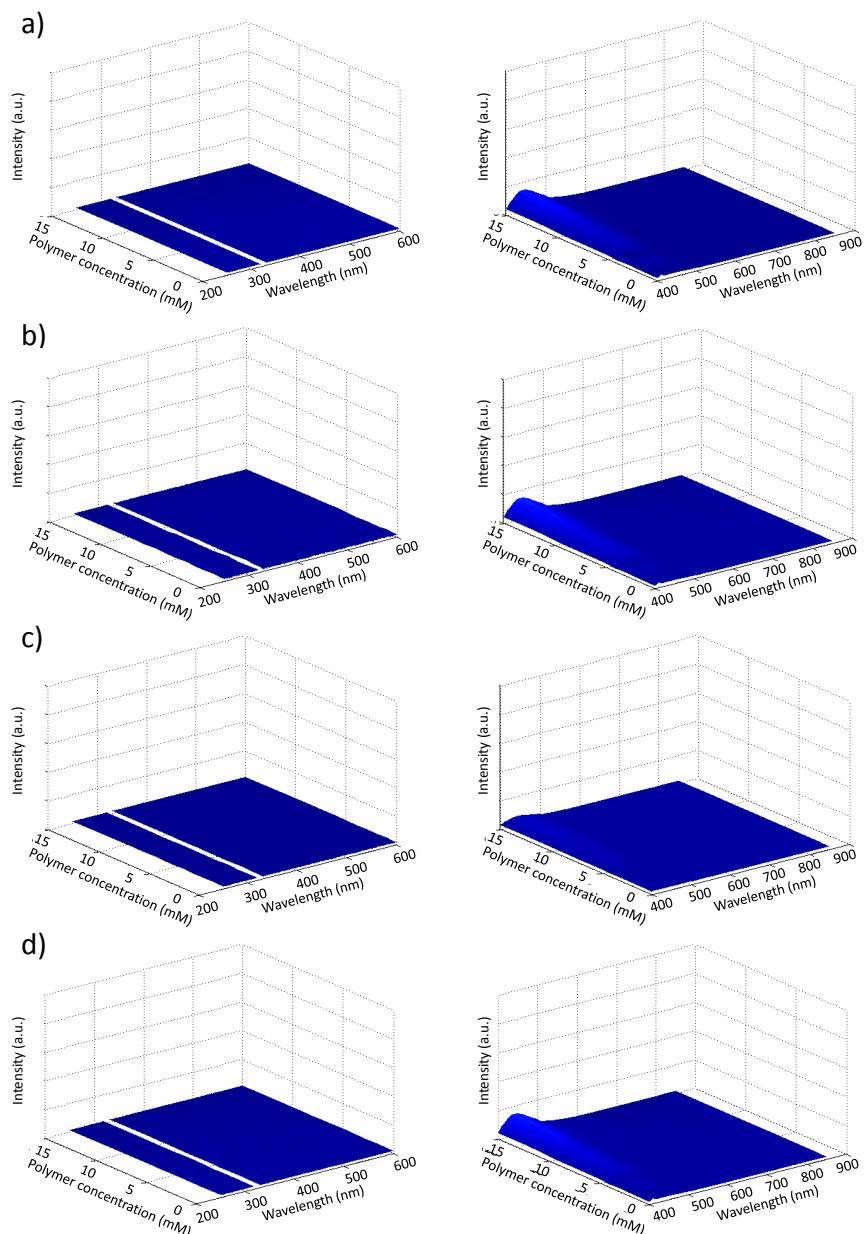
Figure 4.17: Excitation (left) and emission (right) spectra (emission at 695nm) of the polymeric stabilizer (a), the same polymer in the presence of a reducer (b), an oxidant (c) and HAuCl$_4$ at various concentrations. An experimental artifact due to second order excitation (between 340 and 360nm) was intentionally deleted. Emission spectra (excitation at 450nm) of a gold suspension against ligand concentration (for a fixed concentration of 0.5mM of gold).

When a gold nanoparticle is illuminated with an intensity modulated green laser beam, the particle behaves like a heat point source, its heating power being dependent
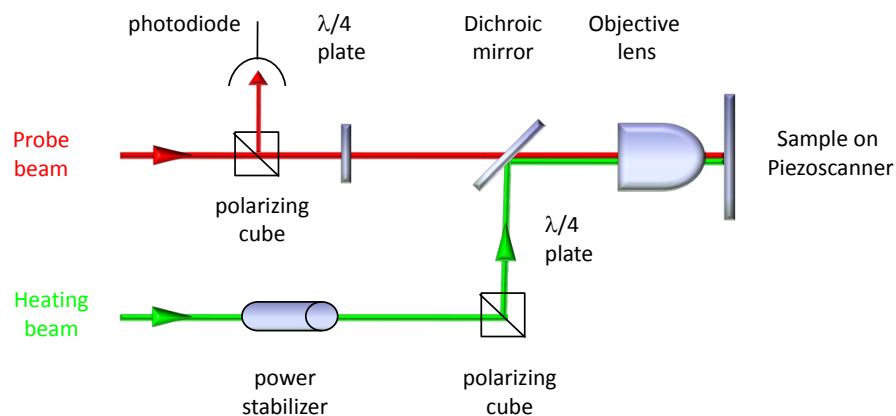
Figure 4.18: Schematic of the photothermal microscope experimental setup. The heating beam intensity is stabilized by an electro-optic modulator. It is overlaid with the probe beam on a broad band dichroic mirror. A combination of a polarizing cube and quarter wave plate is used to extract the reflected probe beam which contains the photothermal signal.

on the laser modulation frequency. The laser absorption by the particle generates a time–modulated index of refraction in the vicinity of the particle. The probe beam interacting with this profile gives rise to a scattered field containing sidebands with frequency shifts ω Interferences between the reference field and the scattered field produces a beatnote at the modulation frequency ω that can be extracted and are recorded for each point of the sample, giving an two dimensional image of the recorded interferences.[58]

A photothermal image taken on a dried film of gold particles (4 mM PTMP p-MAA and 0.5 mM $HAuCl_4$) show the presence of nanoparticles and confirmed an average diameter of approximately 1 to 1.5 nm by comparison with a standard (commercial 2 nm dodecanethiol stabilized colloids). This comparison is built on the relative intensities of the interferences recorded on the pMAA–PTMP coated particles and the commercial sample, and on the fact that those intensities are proportional to the volume of the particles.[59] The photothermal image is presented in Figure 4.19.

4.3.6.2 Confocal fluorescence microscopy

In order to establish a direct link between the presence of a nanoparticle and fluorescence, the photothermal technique was combined with a confocal fluorescence mi-
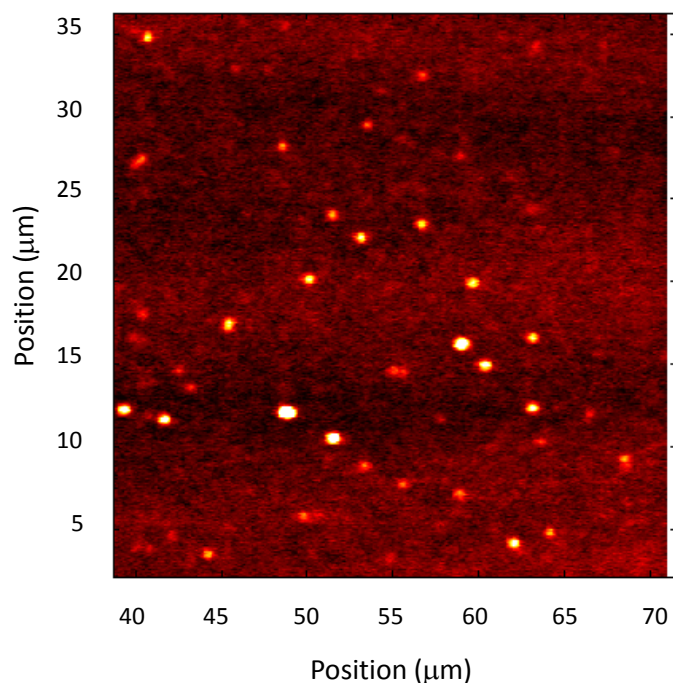
Figure 4.19: Photothermal image of approximately 1 to 2 nm gold nanoparticles in a few tens of nanometers thick polyvinyl alcohol film on a glass substrate. The average heating power was 10 mW.
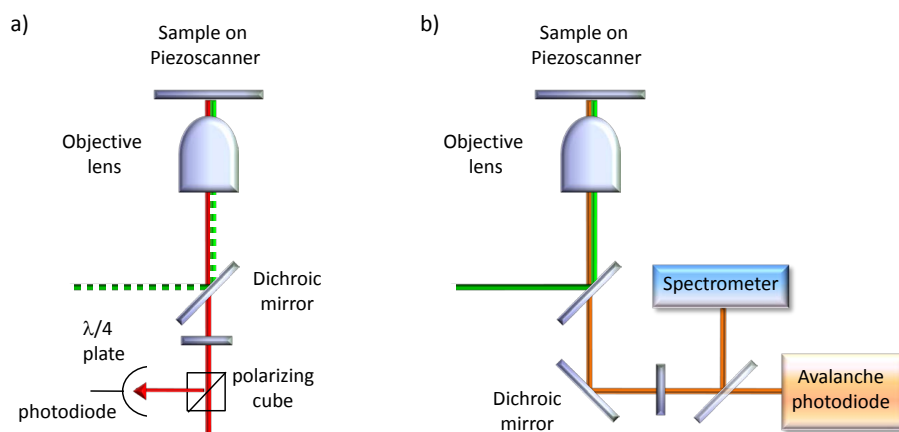
Figure 4.20: Experimental setup of photothermal and fluorescence microscopy.

croscopy setup. The experimental setup is described in Figure 4.20.

This system allow the acquisition of fluorescence images as well as photothermal images of the same sample. The luminescence images were acquired using an excitation laser at a wavelength $\lambda = 540$ nm. The emission signal was detected using a fast

131
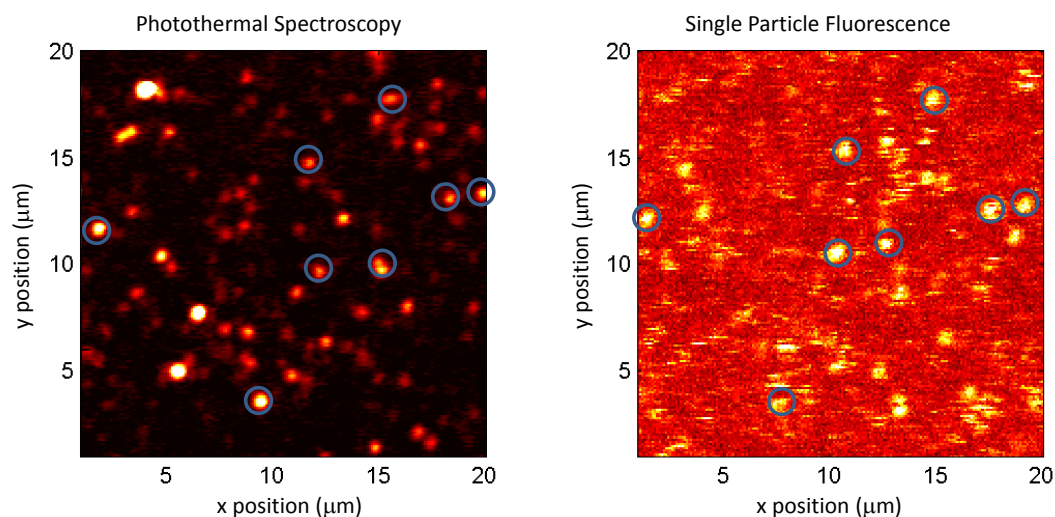
Figure 4.21: Photothermal (a) and fluorescence (b) spectroscopy images of a dried film of fluorescent pMAA–PTMP stabilized gold particles.

photodiode after being filtered through a filter at 600 ± 75 nm.

Figure 4.21 show images taken on a pMAA–PTMP stabilized fluorescent gold particles in "fluorescence" mode (right hand side) and in "photothermal mode" (left hand side).

Even though the correlation between the photothermal and fluorescence images is possible for some spots, the signal to noise ratio in the fluorescence image is relatively high. This effect can be attributed to the relatively low quantum yield of the pMAA–PTMP stabilized particles.

Furthermore, some spots observed on the photothermal image are missing from the fluorescence image. This can be due to the presence of non–fluorescent particles in the sample, or to rapid photobleaching of the particles upon laser excitation. Indeed, photobleaching of the particles could be directly observed during fluorescence images acquisition.

4.3.7 Induced photobleaching

4.3.7.1 Optical microscopy

Photobleaching can be clearly seen on the fluorescent image of a dried film of pMAA–PTMP coated fluorescent nanoparticles (Figure 4.22 and 4.23). The film shown here
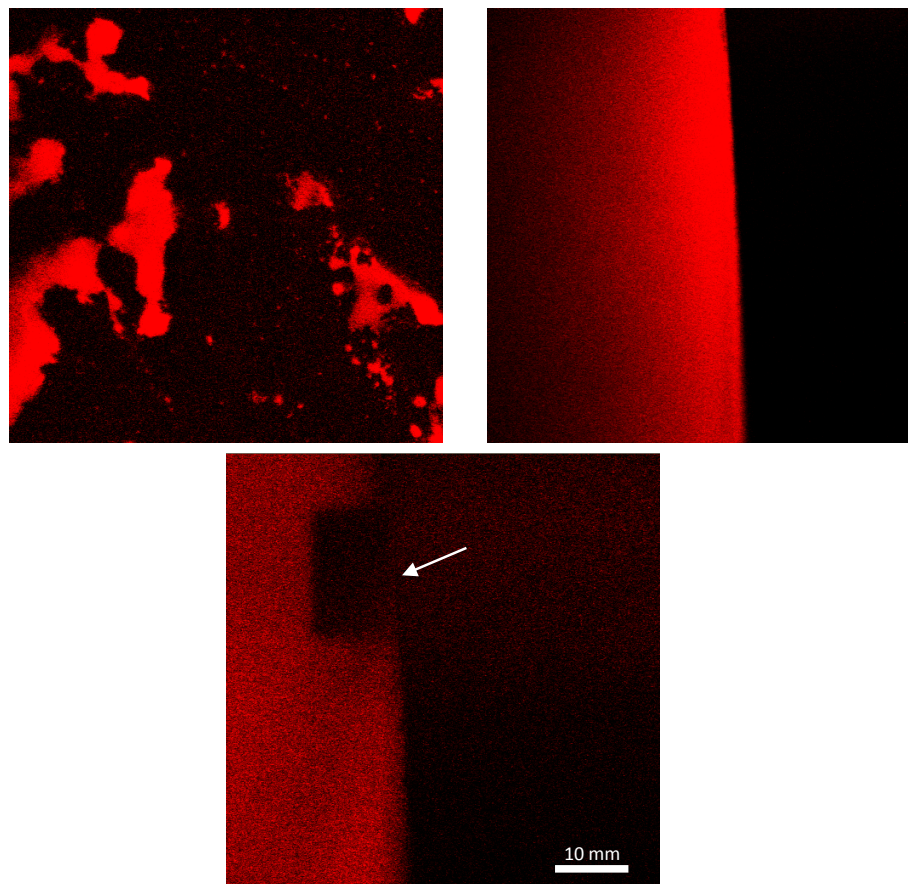
Figure 4.22: Multiphoton microscope image of a dried film of gold nanoparticles (4 mM pMAA-PTMP and 0.5 mM HAuCl$_4$) dried film; the dark area is a part of the droplet that undergo photobleaching after a few seconds upon laser excitation (458 nm, 0.9W).

is simply obtained by drying a droplet of particles suspension on a glass slide. Figure 4.22a shows the aggregated particles after drying at low magnification. Figures 4.22b and c show the edge of one of those aggregates, the red colour being due to the nanoparticles emission. The dark square on Figure 4.22 ccorresponds to an area that has been scanned several times at 458 nm, resulting in the desactivation of the gold nanoparticles fluorescence. To our knowledge, it is the first time that photobleaching of gold nanoparticle has been reported, and this phenomena could be due, for example, to heat induced structural changes in the particles. Gold nanoparticles with diameters less than 5 nm have melting temperatures that are much lower than bulk gold (300 – 500°C *versus* 1063°C), this properties have been used for laser curing of printed gold nanoparticle inks.[61] This differences in melting points are due to the surface atoms

133
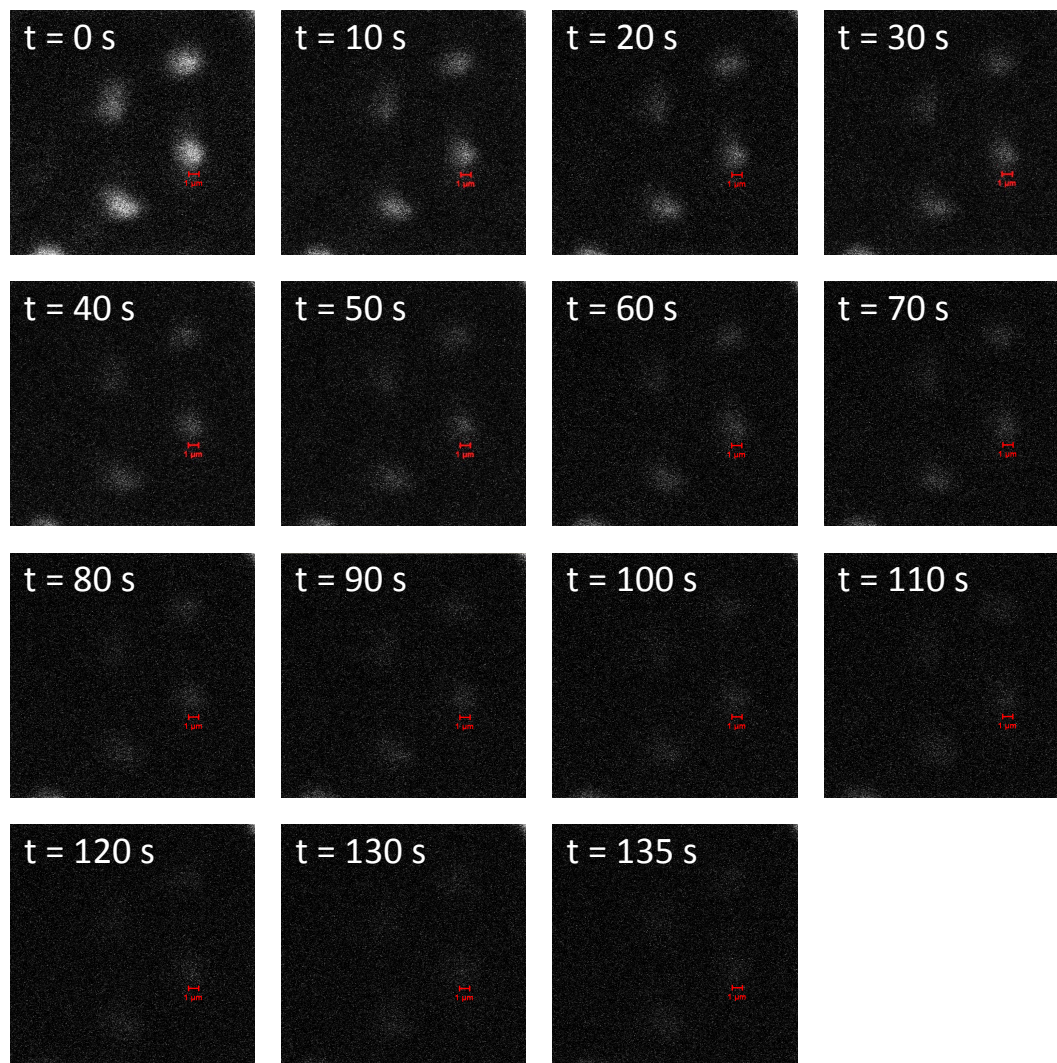
Figure 4.23: Evolution of photobleaching of dried aggregates of fluorescent particles with laser illumination time.

that tend to be coordinatively unsaturated at such a size scale.[62] Photobleaching can also be ascribed to morphological changes under laser irradiation (fragmentation and photofusion); such processes have been reported previously.[63–71]

4.3.7.2   Fluorescence recovery after photobleaching

Building on this observation, fluorescence recovery after photobleaching (FRAP) in a capillary was used to measure the hydrodynamic radius of the fluorescent species. In this case, dynamic light scattering (DLS) was not used to assess the hydrodynamic radius of the particles, due to their emission wavelength that slightly overlaps the

134
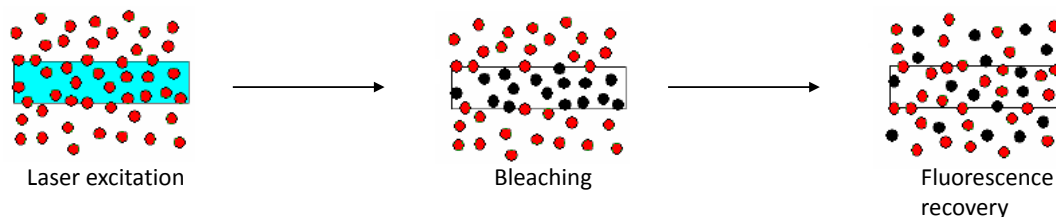
Figure 4.24: Schematic representation of the fluorescence recovery after photobleaching process.

wavelength of the DLS laser ($\lambda = 532$ nm).

Fluorescence recovery after photobleaching allows the measurement the diffusion coefficient of fluorescent colloids in a solvent.[72] In practice, the FRAP experiment consists in a local photobleaching by laser illumination. Fluorescence recovery results from the movement of unbleached particles from the surrounding zone into the bleached area due to Brownian motion, as shown in Figure 4.24. The fluorescence recovery is time dependent and follows a Gaussian profile (see Figure 4.25) The evolution of this Gaussian profile is described by:

$$I(z,t) = I_0 \sqrt{\frac{\frac{\omega_0^2}{2}}{4Dt + \frac{\omega_0^2}{2}}} \left(-\frac{z^2}{4Dt + \frac{\omega^2}{2}}\right) = I_0 \sqrt{\frac{\frac{\omega_0^2}{2}}{\frac{\omega^2}{2}}} \left(-\frac{z^2}{\frac{\omega^2}{2}}\right) \tag{4.3}$$

with ω the width of the Gaussian (and ω_0 the width at t = 0), I it's intensity and D the diffusion coefficient of the colloids in suspension. The diffusion coefficient of those colloids is sensitive to the temperature and solvent viscosity, thus, the D value calculated from equation 4.3 is normalized using the relation:

$$D(20^oC) = D \times \frac{\eta(T) \times T_0}{\eta(T_0) \times T} \tag{4.4}$$

From the values of the diffusion coefficient calculated using equations 4.3 and 4.4, the hydrodynamic radius of the same sample is then calculated applying the Stokes–Einstein equation (equation 4.5, where k is the Boltzman constant ($k = 1.38 \times 10^{-23}$).

$$D = \frac{(k \times T)}{6 \times \pi \times \eta \times R} \tag{4.5}$$

135
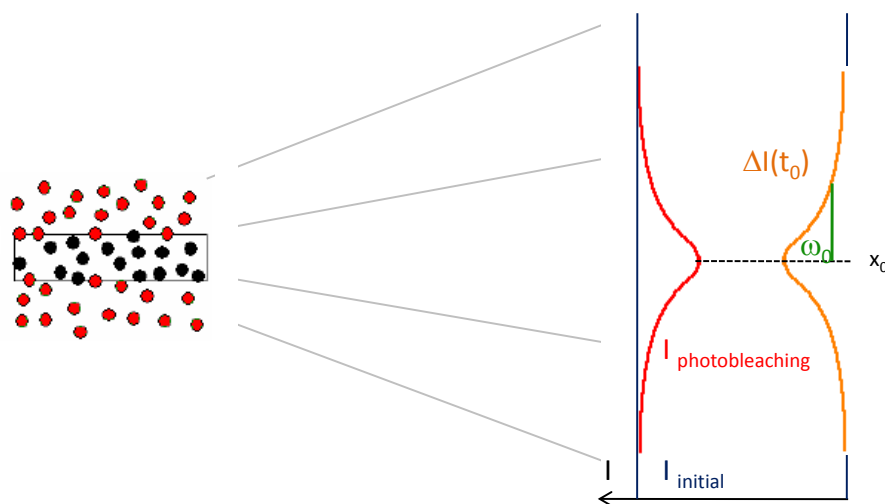
Figure 4.25: Schematic representation of the gaussian profile of the bleaching area of the particles during the FRAP experiment.

FRAP measurements were carried out in a 1mm wide capillary on a nanoparticles suspension(4 mM PTMP p-MAA and 0.5 mM $HAuCl_4$). The sample was scanned 50 times over seven days, the calculated values of D are reported in Figure 4.26. No sign of aggregation could be observed over those measurements after a week; the diffusion constant distribution from those measurements are presented in Figure 4.27 and the corrected average D value was found to be on average $62.3 \, \mathrm{m.s^{-1}}$. It is related, according to equation 4.5, to the presence of 6.9 nm hydrodynamic diameter gold particles.

4.4 Discussion

4.4.1 X–ray photoelectron spectroscopy

X–ray photoelectron spectroscopy was used to investigate the overall charge states of the gold nanoparticles, as mentioned in Section 4.3.5.2. Since the number of the free electrons in the metal nanoparticles is strongly dependent on the charge states of its constituent metal atoms, XPS technique was employed to measure the binding energies of core electrons and considered as being indicative of the overall charge states of gold atoms in some of the luminescent and non–luminescent pMAA–PTMP coated gold nanoparticles. Au $4f^{7/2}$ and $4f^{5/2}$ binding energies in the luminescent and non–luminescent gold nanoparticles were investigated and XP spectra of various gold

136
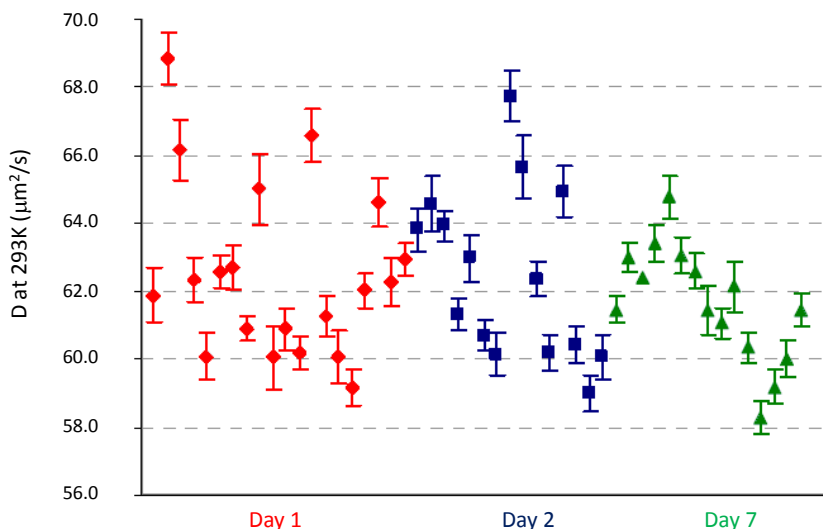
Figure 4.26: Evolution of the diffusion constant D after 50 FRAP measurements with time.
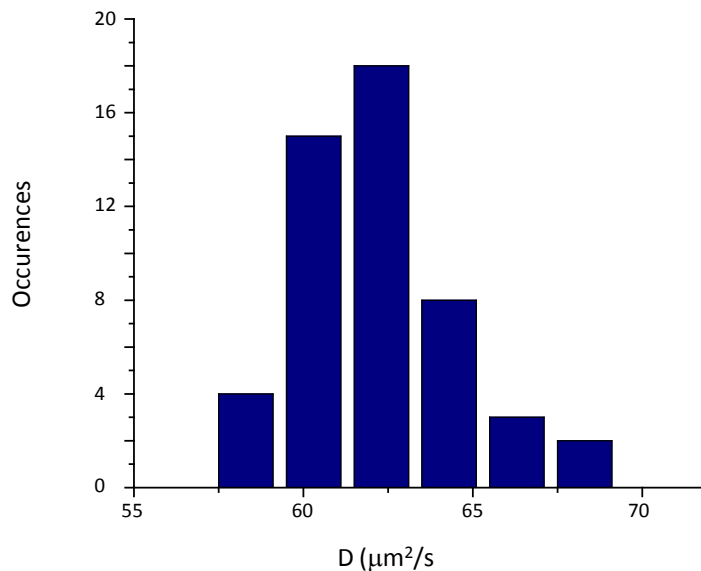
Figure 4.27: FRAP (Fluorescence recovery after photobleaching) histogram. The mean diffusion constant of a nanoparticles suspension prepared using a 4 mM polymer and 0.5 mM gold concentrations is 62.3 mm/s (standard deviation = 2.3 m.s-1) corresponding to a 3.45 nm hydrodynamic radius species (standard deviation = 0.1nm).

suspensions are depicted in Figure 4.28 with XP spectra of standard commercial gold compounds (*i.e.* Au_2O_3, $AuClPPh_3$ and gold foil) for comparison.
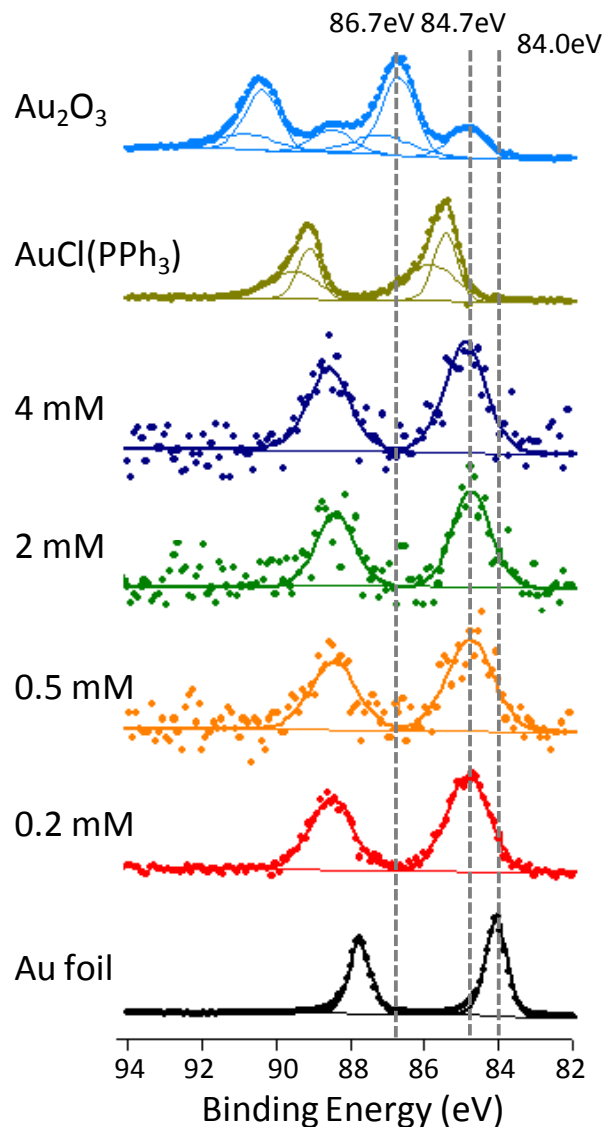
Figure 4.28: X–ray photo-electron spectra of AuNP of various sizes and gold containing references.

Samples were prepared for XPS by pipetting solutions of the polymer capped Au nanoparticles onto adhesive carbon discs. Solvent was allowed to evaporate off under ambient conditions to leave a waxy film. Au foil, Au_2O_3 and $AuClPPh_3$ were mounted directly on the adhesive carbon discs.

X–ray photoelectron spectra were collected on a Kratos Axis Ultra X–ray photo-electron spectrometer with monochromatic Al–Kα radiation and charge neutralization. High resolution scans of the C^{1s} region were acquired for calibration ($C^{1s} = 285.0$ eV

Sample	BE calibration to	BE Au 4f$^{7/2}$ [eV]	FWHM [eV]
Au foil	C 1s 285.0 eV	84	0.74
0.2 mmol	C 1s C=0 289.33 eV	84.8	1.37
0.5 mmol	C 1s C=0 289.33 eV	84.7	1.49
2 mmol	C 1s C=0 289.33 eV	84.7	1.21
4 mmol	C 1s C=0 289.33 eV	84.9	1.33
AuCl(PPh$_3$)	C 1s 285.0 eV	85.4	0.74
		85.8	1.65
Au$_2$O$_3$	C 1s 285.0 eV	84.8	1.23
		86.7	1.06
		87	1.99

Table 4.1: X–Ray photoelectron data acquired on various pMAA–PTMP coated gold particles, and standards.

for carbon, and C^{1s} = 285.0 for $C = O$ groups). The values of the Au^{4f} bonding energy after calibrations are summarized in Table 4.1.

The Au^{4f} emission lines (Figure 4.28) have symmetric peak shapes. They are broadened and shifted in binding energy (BE) by approximately +0.7 eV relative to bulk metallic gold (compared to Au foil). This indicates that the gold samples are electronically different from bulk metallic gold. The Au^{I} reference sample (AuCl(PPh$_3$), exhibits slightly larger BE shift. Assuming a linear relationship between the Au^{4f} binding energy and Au valency in bulk compounds,[73] one may, on first sight, conclude that the photoelectron spectra are associated with Au species with an oxidation state close to +1. Indeed, binding energies similar to those of fluorescent gold suspensions shifts are have previously been observed for polymeric Au^{I} complexes.[74]

However, such BE shifts also occur in small, essentially metallic gold nanoparticles such as those in the pMAA–PTMP coated particles samples.[75] The origin of these shifts is ascribed to a retardation of the emitted photoelectron, either by less efficient screening of the core hole created during the photoemission process, or due to Coulomb retardation, *i.e.* accumulation of charges on metallic particles in an electrically insulating matrix. Superpositions of these effects are likely and it is not possible to disentangle their effects. However, it can be noted the lower BE component visible in the Au^{4f}

emission of the polycrystalline Au_2O_3 reference sample (Figure 4.28), which is due to small metallic gold particles formed by slow photo–induced decomposition processes at room temperature.[76]

It should also be noted that the full width at half maximum (FWHM, see Table 4.1) and the binding energy shift of the Au_2O_3 standard are of similar magnitude, namely 1.23 eV and +0.8 eV respectively as for the gold component in the pMAA–PTMP stabilized gold samples.

Interestingly, no difference can be detected between the XP spectra of the highly fluorescent sample (4 mM pMAA–PTMP) and the less fluorescent sample (0.2 mM pMAA–PTMP) within the signal–to–noise limits of the XP measurements, indicating that the variations in fluorescence behavior could be caused by the interaction with the polymer matrix (see Sections 4.4.2.2 and 4.4.2.3).

4.4.2 Origin of photoluminescence.

4.4.2.1 Electronic transitions

The photoluminescence of small gold clusters have been investigated previousely, and even if the exact photochemical process leading to this phenomena is not yet completely understood, rationalizations of such effect have been attempted. A theoretical study from Apell *et al.* relates the observed luminescence of gold (and other noble metal) clusters to electronic transitions between the occupied *d* bands and the energetic states above the Fermi level (Figure 4.29 a).[29] In a similar manner, Link *et al.* attribute the near infrared luminescence of small glutathione stabilized Au_{28} clusters to the same radiative electronic recombination.[77] However, this second study infers that the luminescence can also be attributed to a radiative interband treansition within the sp bands across the HOMO–LUMO energy gap (Figure 4.29b).

Furthermore, Wang *et al.*, and Huang *et al.* attribute the luminescence not only to HOMO–LUMO interband transitions, but also to localized core–surface states of size–independent energetics.[30,39]

The two possible radiative electronic desexcitation that could lead to fluorescence emission are schematized in Figure 4.29.

Herein, it is evident that the observed fluorescence intensity is dependent on the
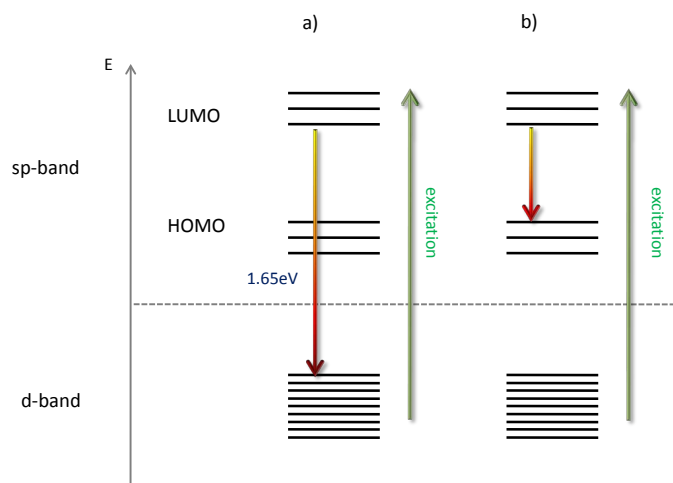
Figure 4.29: Proposed solid state model for the origin of luminescence by a) radiative inter–band transition within the sp band across the HOMO LUMO gap and/or b) by radiative recombination between the *sp* band and the *d* band.

polymer concentration used during the synthesis, and thus to the size of the so–formed clusters. However, no significant shift in the excitation or emission spectra could be observed for samples prepared using various polymer concentrations. A decrease in the cluster size would, in theory, lead to an increase of the HOMO–LUMO energy band gap of the clusters, thus a shift in the luminescence spectra would be observed.[78] Thereby, the red fluorescence cannot be ascribed to an HOMO–LUMO band gap electronic recombination, but is more consistent with an *sp* to *d* energy states recombination. Furthermore, the energy of the observed desescitation (1.65 eV) is consistent with previous studies for the same type of electronic transitions.[77]

Herein, the variations of fluorescence intensity with the variations of polymer concentrations used for the preparation of the gold clusters can be explained with the formation of clusters with a size distribution, a single gold–containing species leading to fluorescence. For example, the relatively low fluorescence intensity observed when using a 1 mM pMAA–PTMP concentration can be ascribed to the formation of a small fraction of fluorescent clusters and a higher ratio of larger gold structures, and the higher fluorescence intensity observed when using a 4 mM pMAA–PTMP concentration ascribed to the formation of a higher number of fluorescent gold species relatively to larger structures or gold species.
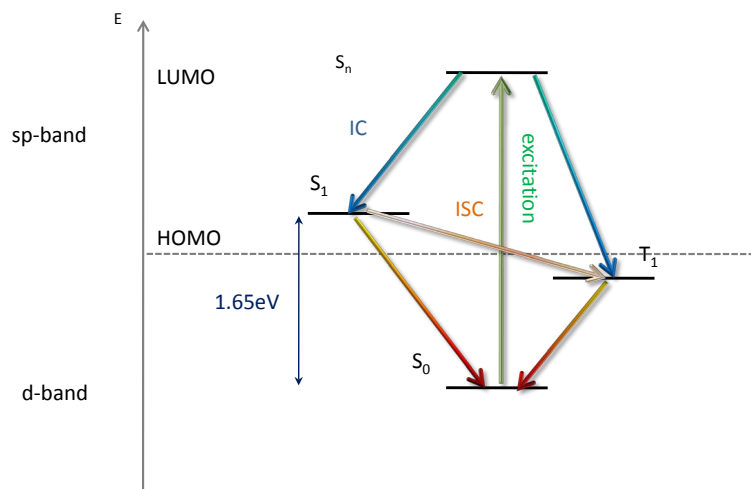
Figure 4.30: Molecular model for the origin of the two possible luminescence origin. Excitation to higher energy (S_n)is followed by relaxation (internal conversion, IC) to the lowest excited singlet state (S_1). Fluorescence can occur by radiative recombination with the ground state (S_0). Inter–system crossing (ISC) to the lowest triplet state (T_1)and subsequent radiative relaxation to the ground state (S_0) involves a forbidden transition (T_1 S_0) and causes phosphorescence.

Figure 4.29 refers to the electronic structure of the gold suspensions considered as clusters. However, clusters in this size range have only a few number of gold core atoms, most of the gold atoms being on the surface of the cluster.[79] Thus, the energetics of those clusters can also be described using a molecular model. Such representation is proposed in Figure 4.30. This model describes the two radiative electronic recombinations processes in the case of molecule–like structures.[80]

The transition from the lowest excited singlet state (S_1) or from the lowest triplet state (T_1) to the ground level (S_0) leads to fluorescence through internal conversion (IC) or to phosphorescence through the "forbidden" transition (inter system crossing, ISC) respectively. Herein, the sp–d inter–band transition described in the previous model is consistent with the internal conversion process. However, no luminescence life time could be recorded on the fluorescent suspensions, and the desexcitation process through ISC and the presence of phosphorescence could neither be confirmed nor ruled out.
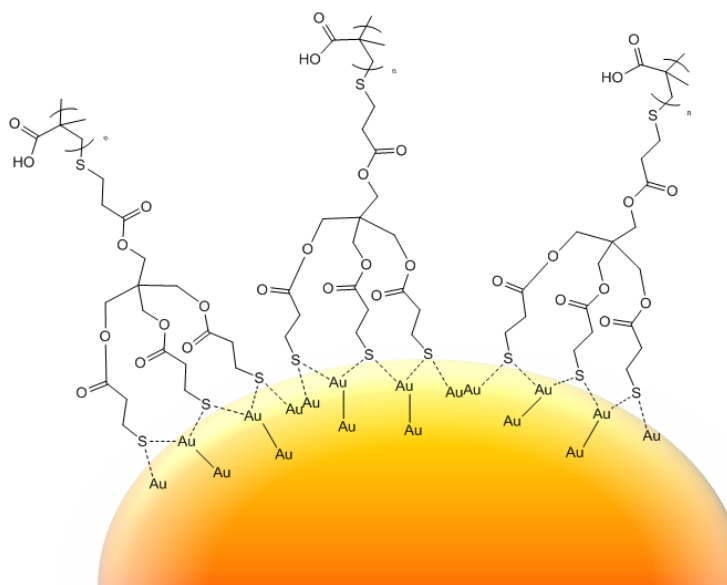
Figure 4.31: Schematic of the possible sulphur–gold bonding leading to a ligand to metal, or ligand to metal–metal charge transfer.

4.4.2.2 Charge transfer

Fluorescence from alkenethiols / gold structures has also been argued to stem from ligand to metal charge transfer (LMCT) [78] or from ligand to metal–metal charge transfer (LMMCT). [81,82] In both cases, such effect appears when in the presence of oligomeric gold(I) complexes, when two gold atoms are adjacent and their distance is less then 3.6Å, [83] and their bonding forces are in the 30 to 45 kJ/mol, comparable to hydrogen bonding forces. [84]

Herein, the direct observation of gold structures by HR–TEM in the fluorescent samples in Figure 4.5 and not in the case of colourless suspensions (for higher polymer concentrations), the size exclusion chromatography experiment (Section 4.3.5.1) and the XPS data (Figure 4.28 and Table 4.1) tend to rule out the presence of exclusively gold(I) complexes or oligomers within the fluorescent suspensions. However, such effect can arguably happen in the case of small clusters, depending on the gold / thiolate bonding nature, as described in Figure 4.31.
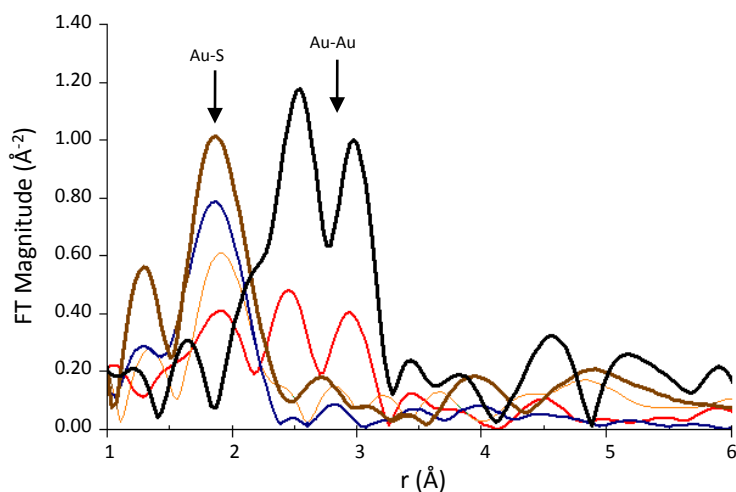
Figure 4.32: FT–EXAFS spectra of the gold nanoparticles prepared using 0.2 mM (red line), 0.5 mM (orange line), 4 mM (blue line) and 15 mM (brown line) polymer concentrations for a 0.5mM gold concentration. The black line corresponds to metallic gold (gold foil).

4.4.2.3 Extended X–ray absorption fine structure

In an attempt to get a better understanding of the structure of the gold / sulphur layer on the surface of the fluorescent particles, and to corroborate the presence of Au^0 in the sample, extended X–ray absorption fine structure (EXAFS) was carried out on various samples of fluorescent and non fluorescent species. The results are depicted in Figure 4.32.

EXAFS spectra arise from the oscillations in the photoelectron cross section because of the scattering of the ejected potoelectron by atoms in the vicinity of the absorbing atom (see Chapter 1, Section 1.8.7).[85]

This set of data (Figure 4.32) show that the Au–S contributions (Au–S $\simeq$ 2 Å) to the Fourrier transformed EXAFS are visible in all samples regardless of fluorescent activity and their intensity is directly proportional to polymer concentration (relative to a fixed Au concentration of 0.5 mmol). Thus, one can conclude that the Au–S contributions are probably not associated with the Au species responsible for the fluorescent activity since they are visible in both fluorescent and non-fluorescent samples. Rather they represent the presence of an Au–S polymeric structure. Those contributions are present on all samples, even after extensive purification by size exclusion chromatography. Thus, they

cannot be ascribed to the presence of loosely bound polymers around the particles, or any other synthesis byproduct.[86] However, they can arguably be ascribed to the formation of S–Au–S structures onto the particle surface, as described in Figure 4.31. The possibility of the fluorescence being related to LMMCT becomes then possible under those conditions (see Section 4.4.2.2). Those conclusions are in accordance with the luminescence originating from the stabilized–particles, as mentioned in Sections and 4.3.5.1 and 4.3.6.2 and Figures 4.16 and 4.3.6.2

It is unclear why the Au–Au contribution at 2.9 and 3.2 are weakly visible, or completely absent for samples prepared using polymer concentrations between 0.2 to 4 mM. However, it can be ascribed to an experimental artifact, since HR–TEM pictures show the presence of "crystalline" gold (for particles prepared using a 0.5mM pMAA–PTMP concentration, see Figure 4.5) and no Au–Au contribution is visible on the EXAFS spectra.[87]

Overall, the observed photoluminescence can be ascribed to one of those two processes, a radiative electronic recombination between the *sp* and *d* energy levels, or to a metal–metal ligand charge transfer. However, none of these processes could be clearly confirmed or ruled out.

4.4.3 Proposed model of the fluorescent material

A simple model of the core shell nanoparticle can be inferred from the analytical data; electron microscopy images show the presence of 1.1 nm nanoparticles, and FRAP data indicate the presence of a 6.9 nm hydrodynamic diameter species. Moreover, ICP–AES carried on an extensively purified nanoparticles solution (4 mM PTMP p-MAA and 0.5 mM HAuCl4) indicate a polymer/gold ratio of 5/41. It has been reported previously that a gold core of 1.1 nm is likely to be made up of 38 atoms of metallic gold.[79,88] Building on this information, it can be deduced that each gold core is surrounded by, on average four or five polymer chains. Thus, a molecular model of the core–shell nanoparticle is proposed. Four or five pMAA–PTMP chains were "attached" to a 38 atoms gold core through the three thiol end-groups, with the polymeric chains evenly spaced onto the gold surface (Figure 4.33 a and c respectively). The polymer chains were then allowed to relax and coil around the particles (Figure 4.33 b and d respectively).
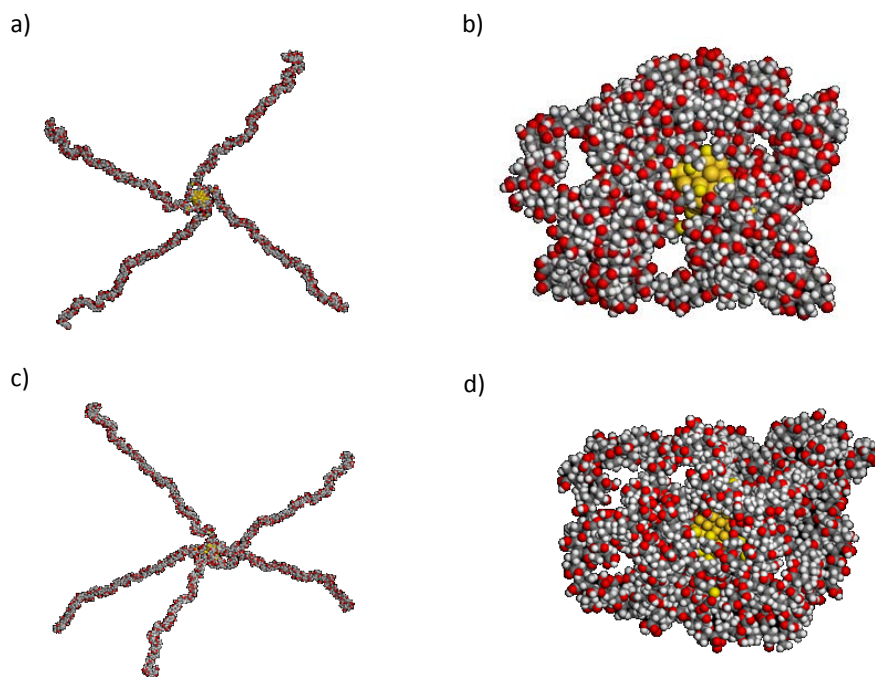
Figure 4.33: Simulation of the core–shell structure of the most fluorescent material consisting of a 1.1 nm gold cluster (38 gold atoms) surrounded by 4 (a and b) and 5 (c and d) pMAA–PTMP chains before (a and c) and after (b and d) allowing the polymer to relax around the gold core.

The proposed model is a 6.3 nm diameter core–shell system, which is consistent with the experimental data.

This model confirms that a system made up of a 1.1 nm gold core surrounded by five polymeric chains is sterically possible in theory, and that all fifteen thiols and five thioethers can bound to the gold surface.

4.5   Summary

The simple protocol reported here for the synthesis of fluorescent nanoparticles opens a wide field of investigations. The photophysical properties of these nanoparticles could be further improved by optimizing the structure of the polymer layer and the synthesis conditions. Indeed fluorescence is very sensitive to the structure of the polymer. Preliminary results indicate a complete loss of fluorescence upon a small change of the

polymer structure: no fluorescence is observed when PTMP p-MAA is replaced by PTMP p-AA (Pentaerythritol tetrakis(3-mercaptopropionate)-terminated polyacrylic acid), a polymer which has the same terminal group but lack an additional methyl group on the monomer unit.

4.6 Bibliography

1. R.C. Mucic R.L. Lestinger C.A. Mirkin R. Elghanian, J.J. Storhoff. *Science*, 277:1078, 1997.

2. R.C. Doty I. Hussain R.J. Nichols D.J. Schiffrin M. Brust D.G. Fernig R. Levy, N.T.K. Nguyen. *J. Am. Chem. Soc.*, 126:10076, 2004.

3. D. Astruc M.C. Daniel. *Chem. Rev.*, 104:293, 2004.

4. L.M. Liz-Marzan. *Langmuir*, 22:32, 2006.

5. J.M. Kohler W. Fritzsche J. Reichert, A. Csaki. *Anal. Chem.*, 72:6025, 2000.

6. P.A. Alivisatos. *Science*, 271:933, 1996.

7. R.L. Letsinger A.T. Taton, C.A. Mirkin. *Science*, 289:1757, 2000.

8. E.R. Goldman G.P. Anderson V.C. Sundar F.V. Mikulec M.G. Bawendi H. Mattoussi, M.J. Mauro. *J. Am. Chem. Soc.*, 122:12142, 2000.

9. S. Koester E. Matijevic I. Sondi, O. Siiman. *Langmuir*, 16:3107, 2000.

10. L. Duchesne C.R. Doty A.I. Cooper M. Brust D.G. Fernig R. Lévy, Z. Wang. *Chem. Biochem.*, 7:592, 2006.

11. E.H. Hu P.F. Barbara A.M. Belcher S.R. Whaley, D.S. English. *Nature*, 405:665, 2000.

12. P. Gin S. Weiss P.A. Alivisatos M. Bruchez Jr., M. Moronne. *Science*, 281:2013, 1998.

13. S. Nie W.C.W. Chan. *Science*, 281:2016, 1998.

14. R.L. Letsinger G.P. Mitchell, C.A. Mirkin. *J. Am. Chem. Soc.*, 121:8122, 1999.

15. *J. Am. Chem. Soc.*, 123:4103.

16. L.E. Brus. *J. Chem. Phys.*, 80:4403, 1984.

17. G. Schmid. *Chem. Rev.*, 92:1709, 1992.

18. L. Brus M. Nirmal. *Acc. Chem. Res.*, 32:407, 1998.

19. A. Henglein. *Chem. Rev.*, 89:1861, 1989.

20. R.W. Murray A.C. Templeton, D.E. Cliffel. *J. Am. Chem. Soc*, 121:7081, 1999.

21. J.A. Preece J.F. Stoddart S. Wenger N. Zaccheroni D. Fitzmaurice, S.N. Rao. *Angew. Chem. Int. Ed.*, 38:1147, 1999.

22. H. Miyoshi J.R. Norris Jr O.V. Makarova, A.E. Ostafin. *J. Phys. Chem. B*, 103:9080, 1999.

23. G. Decher G. Schneider. *Nano. Lett.*, 6:530, 2006.

24. M. Charlot M. Blanchard-Desce N. Nerambourg, M.H.V. Werts. *Langmuir*, 23:5563, 2007.

25. P.V. Kamat. *J. Phys. Chem. B*, 106:7729, 2002.

26. Z. Gaburro D.L. Andrews. *Frontiers in Surface Nanophotonics.* Springer, 2006.

27. A. Mooradian. *Phys. Rev. Lett.*, 22:185, 1968.

28. F. Parsapour B. Wiedenman-D.F. Kelley J.P. Wilcoxon, J.E. Martin. *J. Chem. Phys.*, 108:9137, 1998.

29. S. Lundqvist P. Apell, R. Monreal. *Phys. Scr.*, 38:174, 1988.

30. R.W. Murray T. Huang. *J. Phys. Chem. B*, 105:12498, 2001.

31. T. Tsukuda Y. Negishi, K. Nobusada. *J. Am. Chem. Soc.*, 127:5261, 2005.

32. S. Sato H. Yao-K. Kimura T. Tsukuda Y. Negishi, Y. Takasugi. *J. Am. Chem. Soc.*, 126:6518, 2004.

33. G. Kalyuzhny J.-P. Choi R.W. Murray G. Wang, R. Guo. *J. Phys. Chem. B*, 110:20282, 2006.

34. I. Gerhards D. Mathys P. Oelhafen M. Buttner, H. Kroger. *Thin Solid Films*, 495:180, 2005.

35. *J. Chem. Phys.*, 108:174.

36. S.J. Nie H. Duan. *J. Am. Chem. Soc*, 129:2412, 2007.

37. C.-H. Lee S.H. Huang R.A. Sperling M. Zanella J.K. Li J.-L. Shen H.-H. Wang H.-I Yeh W.J. Parak W.H. Chang C.-A.J. Lin, T.-Y. Yang. *ACS Nano*, 3:395, 2009.

38. O. Dag T.P. Bigioni, R.L. Whetten. *J. Phys. Chem. B*, 104:6983, 2000.

39. R.W. Murray L. Menard R.G. Nuzzo G. Wang, T. Huang. *J. Am. Chem. Soc.*, 127:812, 2004.

40. R.M. Dickson J. Zheng, J.T. Petty. *J. Am. Chem. Soc.*, 125:7780, 2003.

41. A.J. Bard W.I. Lee, Y. Bae. *J. Am. Chem. Soc.*, 126:8358, 2004.

42. K. Sun K.W. Janczak X. Shi J.R. Baker Jr L.P. Balogh W. Lesniak, A.U. Bielinska. *Nano Lett.*, 5:2123, 2005.

43. I. Hussain N. Schaeffer M.F. Wyatt M. Brust A.I. Cooper Z. Wang, B. Tan. *Langmuir*, 23:885, 2007.

44. Z.X. Wang B. Tan D.C. Sherrington S.P. Rannard A.I. Cooper M. Brust I. Hussain, S. Graham. *J. Am. Chem. Soc.*, 127:16398, 2005.

45. C. Dickinson M.J. Rossensky A. Laromaine D.W. McComb M.M. Stevens Y. Wang L. Petit-C. Barentin D.G. Spiller A.I. Cooper-R. Levy N. Schaeffer, B. Tan. *Chem. Commun.*, 34:3986, 2008.

46. B. Tan A.I. Cooper M.F. Wyatt, N. Schaeffer. *J. Am. Soc. Mass Spectrom.*, 18:1507, 2007.

47. V.P. Balagangadharan C.P. Reghunadhan Nair, P. Sivadasan. *J. Macromol. Sci. A*, 36:51, 1999.

48. D.G. Georganopoulou R.J. White A.S. Harper A.J. Mills D. Lee R.W. Murray D. Jim, V.L. Genez. *Langmuir*, 20:6864, 2004.

49. C.N.R. Rao P.P. Edwards, R.L Jonston. *Metal Clusters in Chemistry*. Wiley VCH Weinheim, 1999.

50. G. Schmid. *Clusters and Colloids*. VCH Weinheim, 1994.

51. J.N. Miller A.T.R. Williams, S.A. Winfield. *Analyst*, 108:1067, 1983.

52. R.J. Watts J. Van Houten. *J. Am. Chem. Soc*, 98:4853, 1975.

53. S.I. Wawilow. *Z. Physik*, 42:311, 1927.

54. D.F. Eaton. *Pure & Appl. chem.*, 60:1107, 1988.

55. K.K.-M. Lo. V.W.-W.Yam. *Chem. Soc. Rev.*, 28:323, 1999.

56. R.J. Puddephatt. *Coord. Chem. Rev.*, 216–217:313, 2001.

57. P. Zhang T.K. Sham, P.-S.G. Kim. *Solid State Commun.*, 138:553, 2006.

58. G.A. Blab B. Lounis S. Berciaud, L. Cognet. *Phys. Rev. Lett.*, 95:257402, 2004.

59. A. Maali B. Lounis M. Orrit P. Boyer, P. Tamarat. *Science*, 297:1160, 2007.

60. L. Duchesne D. Lasne N. Schaeffer D.G. Fernig B. Lounis V. Octeau, L. Cognet. *ACS Nano*, 3:345, 2009.

61. N.R. Bieri C.P. Grigoropoulos D. Poulikakos J. Chung, S. Ko. *Appl. Phys. Lett.*, 84:801, 2004.

62. K.J. Klabunde. *Nanoscale Materials in Chemistry*. Wiley Interscience, 2001.

63. P.V. Kamat H. Fujiwara, S. Yanagida. *J. Phys. Chem. B*, 103:2589, 1999.

64. G. Hartland P.V. Kamat, M. Flumiani. *J. Phys. Chem. B 1998*, 102:3123, 1998.

65. T. Sato S. Yamada Y. Niidome, A. Hori. *Chem. Let.*, page 310, 2000.

66. Y. Sawai Y. Nakato K. Murakoshi, H. Tanaka. *J. Phys. Chem. B*, 106:3041, 2002.

67. M.B. Mohamed B. Nikoobakht M.A. El-Sayed S. Link, C. Burda. *J. Phys. Chem. A*, 103:1165, 1999.

68. M.A. El-Sayed S. Link, Z.L. Wang. . *J. Phys. Chem. B*, 104:6767, 2000.

69. P.V. Kamat A. Dawson. *J. Phys. Chem. B*, 105:960, 2001.

70. K. Nakano-S. Koda A. Takami, H. Yamada. *Jpn. J. Appl. Phys.*, 35:L781, 1996.

71. C.A. Mirkin-K.L. Kelly G.C. Schatz-J.G. Zheng R.C. Jin, Y.W. Cao. *Science*, 294:1901, 2001.

72. M. Hoppert. *Microscopic Techniques in Biotechnology.* Wiley VCH, 2003.

73. H. Overhof-F. Hensel J. Knecht, R. Fischer. *Chem. Commun.*, 21:905, 1978.

74. W.E. Smith-M. Gibson L. Watson A. McNeillie, D.H. Brown. *Dalton Trans.*, 5:767, 1980.

75. D. Rosenthal-H. Bluhm M. Havecker-E. Kleimenov A. Knop-Gericke R. Schlogl S.L.M. Schroeder E.A. Willneff, S. Braun. *J. Am. Chem. Soc.*, 128:12052, 2006.

76. C. Wilderotter G. Kästle P. Ziemann R. Wahrenberg P. Oelhafen B. Koslowski, H. G. Boyen. *Surf. Sc.*, 475:1, 2001.

77. S. Fitzgerald M.A. El-Sayed T.G. Schaaf R.L. Whetten S. Link, A. Beeby. *J. Phys. Chem. B*, 106:3410, 2002.

78. K.-H. Lee-H.-T. Chang C.-C. Huang, Z. Yang. *Angew. Chem. Int. Ed.*, 46:6824, 2007.

79. C.J. Zhong-J.E. Harris-R.W. Vachet M.R. Clak J.D. Londono S.J. Green J.J. Stokes G.D. Wignall G.L. Glish M.D. Porter-N.D. Evans R.W. Murray M.J. Hostetler, J.E. Wingate. *Langmuir*, 14:17, 1998.

80. D. Felder-J.-F. Nicoud N. Armaroli G. Marconi V. Vicinelli C. Boudon J.-P.l Gisselbrecht M. Gross-G. Hadziioannou V. Krasnikov L. Ouali L. Echegoyen S.G. Liu J.-F. Nierengarten, J.-F. Eckert. *Carbon*, 38:1587, 2008.

81. K.-H. Kim-J.-C. Lee S.-H. Cha, J.-U. Kim. *Chem. Mater.*, 19:6297, 2007.

82. H. Schmidbaur. *Gold Bull.*, 23:11.

83. A.L. Balch R.L. White-Morris, M.M. Olmstead. *Inorg. Chem.*, 42:6741, 2003.

84. P. Pyykko. *Angew. Chem. Int. Ed.*, 43:4412, 2004.

85. P. Picozzi A. Reale S. Santucci A. Balerna, E. Bernieri. *Surf. Sc.*, 156:206, 1985.

86. F.G. Requejo S.R. Isaacs Y.S. Shon M. Salmeron J.M. Ramallo-Lopez, L.J. Giovanetti. *Phys. Rev. B*, 74:073410, 2006.

87. R. Litran D. Martínez-Martínez J. M. de la Fuente S. Penades A. Fernandez C. Lopez-Cartes, T. C. Rojas. *J. Phys. Chem. B*, 109:8761, 2005.

88. R.W. Murray R.L. Donkers, D. Lee. *Langmuir*, 20:1945, 2004.

Chapter 5

Conclusions and Perspectives

5.1   General conclusions

In the first Chapter of this thesis, the systematic synthesis and characterization of series of potential gold nanoparticles polymeric stabilizers is reported. Several parameters were varied; those are related to the main chain structure of the polymeric species (through the synthesis of polymers of various main chain nature, and of polymethacrylic acid chains of various chain sizes), and to the end– functionality of the polymers (through the preparation of polymethacrylic acid chains containing end–groups of increasing hydrophobicity, and polymer chains functionalized with multiple thiols and/or thioethers end–groups). Those polymeric species were synthesized by chain transfer polymerization; this method is relatively straightforward, fast and cost–effective. It allows the production of polymers with a desired functionality (here, a thiol or thioeteher containing end–group) of low molecular weight, polymeric species monodisperse in size. The chain transfer polymerization can be applied to a wide range of water soluble (and organic soluble) monomers, beyond the ones used in this study.[1,2]

The second Chapter describes a new and simple method for the preparation of gold nanoparticles in the *ca.* 1 to 5 nm diameter range using the polymeric stabilizers described in Chapter 2. This method can easily be scaled up to the gram range and does not involve multiple preparative steps, or cumbersome purification procedures that would lower the yield of the as–produced gold particles, and not necessarily compel to particles monodisperse in size, even after fractionation and size segregation. The effect of the various polymer properties (in terms of main chain structure and end group functionality) on the growth process and stabilization of the particles was investigated.

Overall, the acrylic acid and methacrylic acid based dodecanethioether end–terminated polymers gave rise to the formation of particles between 2 to 5 nanometers in diameter, the size of the so–formed particles being controlled by the polymer to gold relative concentrations. More importantly, the dispersion in size of the particles have been improved compared to previous studies. The influence of the polymeric stabilizer molecular weight on the formation of gold particles have also been investigated in the case of dodecanethioether end–functionalized polymethacrylic acid, and it was found that, even though the effect of the polymer chain size on the particles size is relatively low, particles formed using longer polymeric stabilizers are slightly smaller over the range of polymer concentrations studied. The effect of the polymer end–group hydrophobicity, for polymethacrylic acid chains of similar sizes was found to be more important than the stabilizer molecular weight, with the so–formed gold particles being slightly smaller and more monodisperse in size for relatively hydrophobic end–groups. Finally, the presence of free thiols on the polymer end–group has led to a further increase in the particles dispersion in size, with the particles getting smaller. Unprecedented size and size dispersion was achieved in the case of particles stabilized using pMAA–PTMP. This polymer, and the particles formed using it as a stabilizing agent were analyzed by matrix assisted laser desorption ionization time of flight spectrometry, and a new strategy for the analyte preparation that leads to an improvement of the signal to noise ratio of the mass spectra have been developed for those two structures.[1,2]

By increasing the size of the pMAA–PTMP used in Chapter 3, the solubility of the polymer in water was increased, allowing the formation of smaller, and still monodisperse gold clusters which exhibits a strong size dependent red visible fluorescence. The quantum yield of this nanomaterial was found to be 3%, that is 10 to 100 times higher than the values reported in the litterature for this kind of compounds. Extensive characterization of this fluorescent nanomaterial clearly shows that the observed luminescence stems from the gold particles / polymers structures as a whole, and is not due to the presence of a byproduct, an oligomeric gold / polymer species or to the polymer itself. This luminescence is thought to originate from a radiative electronic recombination between the gold cluster's sp and d energy level , or from a metal to ligand charge transfer. Rapid photobleaching of those cluster has also been observed upon intense

illumination. To the best of our knowledge, it is the first time that photobleaching of fluorescent gold clusters is reported. The origin of this effect can arguably be ascribed to structural changes in the polymer layer surrounding the gold cluster and/or the gold cluster itself. Finally, a simple core/shell model for this fluorescent material is proposed.[3]

5.2 Perspectives and suggestions for future work

Beyond the possible use of small monodisperse gold nanoparticles in various scientific areas, such as materials chemistry, biosciences, nanoelectronics devices manufacture, catalysis and optics, and the ability to use routinely a one–step rapid and cost–effective preparative method for the production of those nanoparticles at the gram scale, the so–formed particles are interesting candidates for self–assembly experiments. Indeed, the particle surface properties are mostly dependent on the nature of their polymeric shell. Thus, taking advantage of the intrinsic properties of various polymers to self–assemble, one can imagine various possibilities of using those particles as building blocks for the formation of larger structures, such as multi–dimensional networks, amphiphilic structures, micelles, *etc...* [4]

Such assemblies could, in theory, be achieved either by reacting the hydrophylic polymer coated nanoparticles with hydrophobic polymer structures to induce phase separation, or by taking advantage of the potential reactions that can occur between two sets of particles coated with different polymers. The synthesis of particles embedded in a mixed polymer shell and their ability to self–assemble could also be investigated.[5–10]

In this regard, the development of a method for the solid–phase preparation of mono-functionalized amphiphilic gold nanoparticles (*i.e.* hydrophobic nanoparticles bearing a single thiol terminated hydrophylic poly(2–(dimethylamino)ethyl methacrylate attached to each particle was attempted. This method relies on electrostatically binding thiol–terminated polymer chains onto a silica surface whilst keeping the grafting density relatively low so as to avoid overlapping of polymer chains and thiols.[11,12] The function-nalized silica is then incubated with butanethiol stabilized gold nanoparticles so as to allow ligand place exchange reaction between the butanethiols and the thiol–terminated pDMAEMA chains.[13,14] Finally, the polymer / gold nanoparticles are desorbed from
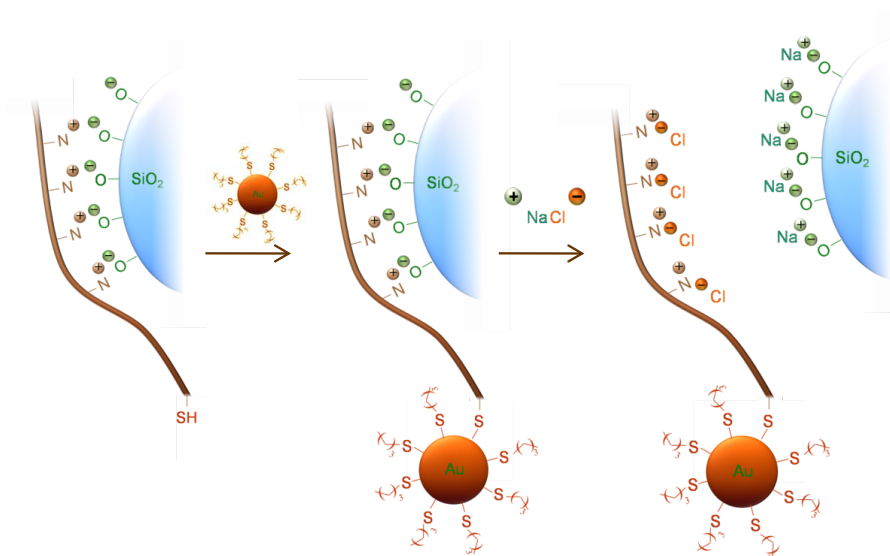
Figure 5.1: Scheme for the preparation of pDMAEMA mono–functionalized gold nanoparticles.

the silica (see Figure 5.1).[12,15]

The study the adsorption of different pDMAEMA polyelectrolytes onto a silica surface and the demonstration that the subsequent bonding of butanethiol stabilized gold particles onto the so–formed polymer / silica structures occurs through ligand place exchange reaction between the gold particles butanethiol layer and the thiol end–group from the polymers, and is not due to non–specific interactions between the silica surface and / or any other chemical function present onto the polymeric chains (amines, carbonyls) was carried out using five different pDMAEMA chains. Those polymer chains were synthesized by atom transfer radical polymerization, free radical polymerization and chain transfer polymerization.[16–18] Those polymerization processes allowed the formation of pDMAEMA chains end–functionalized with a thiol–containing, thioether–containing or "blank" end–group, or containing a central disulfide bond.[19,20] Figure 5.2a shows that the adsorption of butanethiol stabilized particles occurs onto silica particles functionalized with thiol–containing pDMAEMA, and not onto the silica functionalized with the control polymers. Figure 5.2b infers that the desorption of the particles after adsorption onto the silica is possible. However, quantitative measurements of the amount of functionalized particles and adsorbed polymer, and complete characteriza-

156
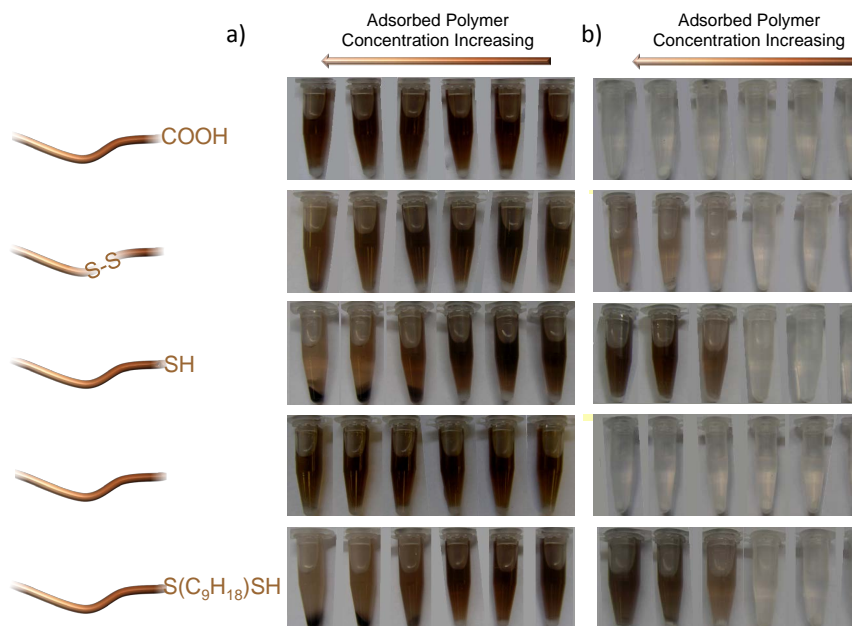
Figure 5.2: a) Adsorption and b) desorption of butanethiol stabilized gold nanoparticles on silica particles functionalized with various end–group terminated pDMAEMA.

tion of the pDMAEMA–gold particles amphiphilic structures characterization is still under investigation.

Fluorescent pMAA–PTMP passivated gold clusters can find applications as biological markers. Such application would involve their functionalization with appropriate receptors and/or drugs that can interact in a specific biological environment. Post functionalization of the fluorescent clusters (*i.e.* substitution of the polymeric chains by a suitable bio–organic molecule after formation of the clusters through ligand place exchange), could be seen as a strategy; however, this route might be quite challenging due to of the difficulty to displace the polymer chains that are bound to the gold through three thiols and one thioether. Cross–linking reactions between the polymeric shell and a bio–organic molecule could be seen as a more realistic approach.

5.3 Bibliography

1. I. Hussain N. Schaeffer M.F. Wyatt M. Brust A.I. Cooper Z. Wang, B. Tan. *Langmuir*, 23:885, 2007.

2. B. Tan A.I. Cooper M.F. Wyatt, N. Schaeffer. *J. Am. Soc. Mass Spectrom.*, 18:1507,

2007.

3. C. Dickinson M.J. Rossensky A. Laromaine D.W. McComb M.M. Stevens Y. Wang L. Petit C. Barentin D.G. Spiller A.I. Cooper R. Levy N. Schaeffer, B. Tan. *Chem. Commun.*, 34:3986, 2008.

4. J.C. Gielen P.C. M. Christianen S.C.J. Meskers A.P.H.J. Schenning R.T.M. Jakobs, J. van Herrikhuyzen. *J. Mater. Chem.*, 18:3438, 2008.

5. D. Astruc M.C. Daniel. *Chem. Rev.*, 104:293, 2004.

6. C.M. Niemeyer. *Angew. Chem. Int. Ed.*, 40:4128, 2001.

7. M. Gratzel A. Hagfeldt. *Acc. Chem. Res.*, 33:269, 2000.

8. P. Gin S. Weiss P.A. Alivisatos M. Bruchez Jr., M. Moronne. *Science*, 281:2013, 1998.

9. S. Nie W.C.W. Chan. *Science*, 281:2016, 1998.

10. C. Plank 16 R9-R25 (2005). W.J. Parak, T. Pellegrino. *Nanotechnology*, 16:R9, 2005.

11. M.M. Santore Y. Shin, J.E. Roberts. *J. Coll. & Int. Sc.*, 247:22, 2002.

12. R. Jerome G. Pfutze M. Stamm R. Mahltig, J.-F. Gohy. *J. Pol. Res.*, 10:69, 2003.

13. R.W. Richards R.A.L. Jones. *Polymers at Surfaces and Interfaces*. Cambridge University press, 1999.

14. M. Muller R. Jerome M. Stamm B. Mahltig, C. Werner. *J. Biomater. Sci. Polymer Edn.*, 12:995, 2001.

15. M.M. Santore N. Hansupalak. *Langmuir*, 19:7423, 2003.

16. M. Kamigaito M. Sawamoto. *Trends Polym. Sci.*, 4:371, 1996.

17. J. Xia K. Matyjaszewski. *Chem. Rev.*, 101:2921, 2001.

18. M. Sawamoto M. Kamigaito, T. Ando. *Chem. Rev.*, 101:3689, 2001.

19. W. Steglich B. Neises. *Angew. Chem. Int. Ed.*, 17:522, 1997.

20. G.E. Keck E.P. Boden. *J. Org. Chem.*, 50:2395, 1985.

Index